Plant Stress Responses: Autophagy and Senescence

by

Nicola Jane Harrison-Lowe

A dissertation submitted in partial fulfillment
of the requirements for the degree of
Doctor of Philosophy
(Molecular, Cellular and Developmental Biology)
in The University of Michigan
2009

Doctoral Committee:

Associate Professor Laura J. Olsen, Chair
Professor Steven E. Clark
Professor Daniel J. Klionsky
Assistant Professor Yin-Long Qiu
Associate Professor Marianne M. Laporte, Eastern Michigan University

Dedicated to those who always store

their lentils on top of the coffee.

Acknowledgements

This thesis represents the culmination of my academic career to date. Over the years, I have “progressed” from making anatomically creative 3D-fish sculptures, to carefully avoiding invisible pellets in tiny plastic tubes “as seen on TV”. Throughout it all, “standing, sitting, and bending” beside me, my family and friends have rallied around, strengthening, revitalizing, and inspiring me. While there is just one name embossed on the spine of volume, without the love and support of these truly exceptional and unique individuals, none of this would have been possible. Now is my opportunity to thank each and everyone, a serious challenge in just a few pages.

First, thanks to my “boss” who, while allowing me to forge onward into the ever scary and turbulent unknown, never allowed me enough rope to completely hang myself. Laura, for all your advice, both personal and professional, I thank you. My earnest thanks also go to her quilting partner, for helping Laura maintain her sanity through all the ups and downs, explosions and implosions, and for providing the lab with an endless variety of baked treats. Thanks go to my current and former lab mates who, apart from eating the aforementioned baked treats, made the lab a great place to be. I would especially like to thank the lab genie, not only for her assistance with the merciless assault of innocent tobacco, but also for smiling, even when it is raining indoors.

I extend my sincere appreciation to the members of my thesis committee, Steve, Marianne, Yin-Long and Dan, who have advised and guided my science throughout my graduate school career. Thank you for challenging me and for helping me to maintain my sense of humor. I particularly remember one meeting when Dan pointed out that as a quasi-pollen biologist I had spent two years studying the plant equivalent of yeast: single-celled, haploid and completely

devoid of chloroplasts. Thanks also to those faculty members who kindly opened their office doors, and later their supply cupboards, allowing me to complete this thesis. I would like to thank my collaborators at MSU, Joanne for her help with the microscopy and Sigrun for all her help and advice.

I thank the fabulous girls (and boys) of the plant group, past and present, who congratulated me whenever I came running from the lab heralding news of a successful import, and later commiserated with me, over a beer, when the next experiment went belly-up in splendid fashion. Thanks to the self-proclaimed “gang of five”, for teaching me how not to kill my plants, and for divvying-up the figures in journal club. Thanks to the roaming gnome for telling me that I should go for what I want, and standing by me when I did. Thanks to my lunch-buddies, we are a rare breed of hookers and needlers, “fearless” beer drinkers, and east coast “wet wedding-ers”. Together, you have made my maize and blue years so much more than simply do-able, rather truly memorable. Keep planting, I expect great things.

Thanks, to the members of my graduate school class, we are the proud, the strong, the “on to the next step”-pers. To my CBTP comrades, who broadened my mind with talk of oxygen gradients and micro-fluidic chips. To my fellow grad-student instructors, for sharing the highs and lows of teaching and offering some great advice, including how to remove gum from your hair. To my bus-buddy of the “racing-type”, for reminding me that girls and ball-tip joints are a wonderful combination. To my oldest friend, of the welsh persuasion, who despite the thousands of miles between us still manages to remember my Birthday. I would like to thank the fairy-lit late-night folk of the scatter-flake crew. Those evenings spent covered in hairspray were a diversion I needed, and truly relished. Thanks to my dear friend in the cherry-picker whose “sees” things, connected things. Your honest and insightful words inspired me to navigate the difficult times and persevere through to the “good-stuff”.

Thank to my family “back home” for supplying me with British goodies, and understanding when my mum reported that Nicola was still in school. Thanks to

my Nana, who taught me how to grow potatoes even though I despise them. Thanks to my little sister, to whom I am truly grateful. Thank you for listening to me, making your point by shouting at me when necessary, and above all, sticking around no matter what, even when we ran out of chocolate. Thank you to parental units one and two. Mum, Dad, I cannot begin to describe how profound an impact you have had on my life. Whether it was a chemistry set, riding hat or brill boys BMX bike, you have been there throughout it all, reinforcing the importance of following my own path and tackling obstacles along the way. You've always been ready to pick up the pieces and stick them back together again with plasters. Thank you, for your unwavering faith in me, your unconditional love, and seemingly endless encouragement and support.

To my fellow penguinier, my coaster-buddy, my partner in tofu-eating bliss, people say that anything is possible, every morning you make me believe it.

Table of Contents

List of Figures

List of Tables

List of Abbreviations

ATG6	Autophagy Protein 6
Vps30	Vacuolar protein sorting 30
Vps34	Vacuolar protein sorting 34, Phophatidylinositol-3-kinase
Vps27	Vacuolar protein sorting 27
PI3K	Phophatidylinositol-3-kinase
PI3P	Phosphatidylinositol-3-phosphate
vac8	Vacuolar protein 8
APE1	Aminopeptidase I
FDC	FYVE Domain Containing (protein)
GLO	Glycolate Oxidase
PTS1	Peroxisomal targeting signal 1
PTS2	Peroxisomal targeting signal 2
PEX5	Peroxin 5, the PTS1 receptor
PEX7	Peroxin 7, the PTS2 receptor
qrt-1	Quartet-1 mutant
grl-2	Glabra 2 mutant
Col-0	Columbia ecotype O
LAT52	Pollen-specific gene
35S	Cauliflower mosaic virus promoter
GUS	β-glucoronidase reporter

Abstract

Plant stress responses: Autophagy and Senescence

by

Nicola Jane Harrison-Lowe

Chair: Laura J. Olsen

In plants, the process of senescence advances an individual cell, organ, or plant toward developmentally programmed, or environmentally induced, death. This requires the coordination of distinct, but functionally related, pathways that integrate external cues from biotic and abiotic stress factors with internal age-related cues. This allows for drastic alteration of cellular metabolism and organelle functions. Once initiated, senescence allows for degradation of intracellular components and nutrient recycling to healthy developing areas of the plant. The stress-related autophagy pathway is active during senescence, and mediates cellular degradation by delivering selective and non-selective cargo to the vacuole for hydrolysis. Through the study of three proteins, AtATG6, AtFDC, and AtNHL57, my research provides an integrated perspective on plant stress biology.

Examination of *Arabidopsis* Autophagy-related Protein 6 (AtATG6) established a link between autophagy and reproductive development. Homozygous *atg6* plants were never recovered, suggesting a gamete transmission defect. Pollen test crosses determined that a male gametophyte defect was responsible and germination assays revealed that *atg6(-)* pollen

grains germinated at very low efficiencies *in vitro*. This highlighted a new role for AtATG6 during pollen germination.

Our understanding of AtATG6 function was broadened through characterization of a novel interacting partner, a FYVE-domain-containing protein (AtFDC). AtFDC bound AtATG6 directly, was zinc coordinated, and peripherally associated with a punctate membrane structure. These traits are all consistent with its putative role as PI3P-binding protein. AtFDC is the first of the non-PRAF *Arabidopsis* FYVE-domain proteins to be characterized, and the first novel ATG6 interaction partner identified in plants.

Finally, we identified AtNHL57, a senescence-associated protein with a novel Peroxisomal Targeting Signal 1 (PTS1), an SFL tripeptide. NHL57 localized to peroxisomes, and *in vitro* protein import experiments revealed that the SFL tripeptide was necessary, but not sufficient, for targeting. In addition, *nhl57* homozygous mutant plants exhibited retarded degradation of chlorophyll during dark-induced senescence. This furthered our knowledge of PTS1 tripeptides and provided an intriguing link between chlorophyll degradation and peroxisomes during senescence.

In conclusion, these data provide a unique perspective on plant stress biology and provide a foundation for future work in pollen biology, lipid signaling and the physiology of senescent peroxisomes.

Chapter 1

Introduction

Plant Stress Responses: Autophagy and Senescence

Plants are non-motile, photosynthetic, eukaryotic organisms. When it comes to stress exposure, the term non-motile is of particular significance. While plants can produce and disperse their seed in the hopes that their offspring will encounter more favorable growth conditions, the parent organism must be able to adequately respond to environmental changes *in situ*. Consequently, plants are able to respond to a wide variety of biotic and abiotic stress factors, including macro- and micro-nutrient deficiency, excessive irradiation, and phytotoxins such as heavy metals. In addition, plants must respond to attack by a variety of pathogens, including viruses, bacteria, and fungi, as well as to tissue destruction due to insect and animal herbivory.

Plants coordinate a series of distinct, but functionally related pathways to mediate their responses to these factors (Figure 1.1). While the systemic acquired resistance pathway (SAR) and hypersensitive response (HR) primarily work to limit pathogen infection, the autophagy pathway and the process of senescence regulate the response to a variety of abiotic and biotic factors. Response to nutrient limitation is predominantly mediated by the autophagy pathway, which regulates nutrient levels through the targeted degradation of cytosolic components. In addition, autophagy works to maintain cell homeostasis through the degradation of oxidized and misfolded protein aggregates, disposal of excess or unneeded proteins and lipids, and the identification and removal of aberrant organelles. Finally, the process of senescence, which occurs naturally at the end of the plant's lifecycle or in response to a variety of stress factors,

regulates both autophagic and non-autophagic degradation as the cell progresses toward, and enters into, the programmed cell death pathway. Here I will discuss the integrated roles that the autophagy pathway and the process of senescence play during plant stress response.

Autophagy – Recycle and Reuse

Autophagy is a highly conserved intracellular process that allows eukaryotic cells to prolong their survival under hostile conditions. Since it was first observed in the mid 1950s [1], the autophagy pathway has been intensively studied in yeast and mammalian systems, and more recently in plants [2,3]. Autophagy is most well known for its important role in response to nutrient deprivation [4]. In yeast exposed to nitrogen limiting conditions, the autophagy pathway is responsible for the targeted sequestration, transportation, and degradation of superfluous or damaged intracellular components [5]. Through the breakdown, assimilation and recycling of the resulting macromolecules, cells increase the likelihood they will be viable should conditions become more favorable. In contrast to the degradation activity of the ubiquitin proteasome machinery [6], which predominantly degrades short-lived proteins, upon induction the autophagy pathway targets long-lived proteins, cytoplasmic components, and entire organelles to the vacuole for degradation [2,4]. This is strikingly observed in the methylotrophic yeast *Pichia pastoris*, which selectively degrades their alcohol oxidase-rich peroxisomes when their carbon source is switched from methanol to glucose [7]. As one would anticipate, autophagy is a tightly regulated process whose function relies upon continual inductive feedback from the environment [8]. If the hostile environment alters in the organism's favor, the autophagy pathway returns to a basal level of activity, removing damaged or aberrant proteins. Alternatively if conditions do not change, the cell progresses toward death [9].

In addition to its well studied role during starvation, the autophagy pathway has been implicated in a wide variety of cellular and developmental processes, including apoptosis and necrotic cell death [10]. Autophagy is

required for dauer development and life span extension in *C. elegans* [11], tissue remodeling in *Drosophila* [12], neuronal and embryonic development in mice [13,14], and is essential for fruiting body formation *in Dictyostelium* [15]. Particular attention has also been paid to the role of autophagy in various human disease pathologies [16]. Autophagy suppresses tumor formation [17], limits bacterial and viral pathogen infection [18], and is implicated in the clearing of amyloids related to neurodegenerative diseases, including Alzheimer's and Parkinson's [19]. In *N. tobacum,* autophagy plays important roles in the regulation of programmed cell death following the hypersensitive response [20,21], and is implicated in pollen germination in *Arabidopsis* [22-24].

Two types of non-selective autophagy

Regardless of the specific environmental or developmental cues, once initiated non-selective autophagy can occur in one of two manners, termed micro- and macroautophagy [5]. These two "types" are morphologically distinguishable using electron microscopy, and while both involve the sequestration of cytoplasmic components, they differ in the site of sequestration. As seen in Figure 1.2, microautophagy occurs when the tonoplast or lysosomal membrane invaginates or protrudes, resulting in direct uptake of cytosolic components. This can include the direct uptake of organelles that lie adjacent to the vacuole. In plants, microautophagy has been described in the cotyledons of germinating seedlings and in senescent leaves [25,26]. Small ER-derived vesicles containing proteases have also been seen, in senescing tissues, being directly engulfed by the vacuole [27]. These vesicles serve as an alternative mechanism for delivery to the plant vacuole for a variety of cargo, including wheat gliadin endosperm, oil bodies, and rubber particles. In addition, entire amyloplasts (starch-containing granules) have been observed surrounded by tonoplast protrusions, possibly indicating that microautophagy is occurring [28,29].

In contrast, macroautophagy (Figure 1.2) involves the sequestration of cytoplasmic components into double-membrane vesicles called autophagosomes [30]. Macroautophagy has been observed in tobacco cells in response to sucrose

starvation and is characterized by the formation of acidic vesicles in the cytosol [31]. In yeast, these vesicles are nucleated and form at the phagophore assembly site (PAS) which is located on the vacuolar membrane [32]. This structure is characterized by the co-localization of a large number of autophagy proteins to a single punctate site [33]. Despite morphological similarities between yeast and plant autophagy, to date, no one has identified the PAS in plants. Rather it is currently hypothesized that provacuoles, small vesicles of *trans*-Golgi network or endoplasmic reticulum origin, form the tubular structures initially observed at the sequestration site [34-36]. These tubular structures expand as membrane is delivered to the sequestration site, ultimately fusing to form a vesicle [2]. There has been a great deal of investigation regarding the origin of the sequestrating membrane; current data suggest that the mitochondria, *trans*-Golgi network, and endoplasmic reticulum all contribute to the process [37]. The plasma membrane and central vacuole have also been suggested as sources of membrane in plants [38]. After formation, autophagosomes traffic through the cytosol and dock at lysosomal or vacuolar membranes [4]. The outer membrane of the autophagosome then fuses with the vacuolar membrane. This releases a single-membrane bound autophagic body into the vacuole for lysis and subsequent degradation by the resident hydrolases [39].

Selective autophagy

While both micro- and macroautophagy are thought to be largely non-specific regarding the degradation of cytoplasmic components, organelles are degraded in a selective manner. Termed pexophagy or mitophagy, when the cargo is peroxisomes or mitochondria, respectively, these specialized forms of autophagy are induced by different stimuli than the bulk degradation pathway [7]. These pathways remove damaged or aberrant organelles and in addition, allow for the targeted removal of organelles whose primary metabolic function has become redundant [40]. While they share many molecular components with the non-selective autophagy pathways, additional proteins are required for cargo recognition, including certain peroxisome biogenesis proteins such as PEX14 [7].

In addition to the selective micro and macroautophagy pathways, the selective Chaperone Mediated Autophagy pathway (CMA), functions in mammalian cells to deliver unfolded proteins directly into the lysosome [41]. However, evidence for the conservation of this pathway in plants has not been forthcoming. In mammals, CMA is mediated by the cytosolic chaperone hsc70 and the lysosome-associated membrane protein type 2A (LAMP-2A) [5]. Together, they target cytosolic forms of secretory proteins, transcriptions factors, protease subunits, and calcium-binding proteins to the lysosome for degradation.

Increasing complexity - the molecular machinery

Autophagy shares protein components with the morphologically similar endomembrane vesicular trafficking pathways, including the yeast cytoplasm-to-vacuole targeting (CVT) pathway and the vacuolar protein-sorting (VPS) pathway [42]. Extensive genetic analysis using yeast mutants has allowed for the identification of 31 AuTophaGy-related (ATG) genes [5]. Consequently, research in this system allows us to understand the molecular mechanisms that control the induction and regulation of the autophagy pathway. Additional research in mammals and plants has highlighted the congruency and disparity between the molecular mechanisms in different organisms. Regardless of the system studied, the process can be separated into several distinct stages: induction and regulation, autophagosome formation and, finally, trafficking and degradation.

Induction and regulation: The autophagy pathway is negatively regulated by the Target Of Rapamycin (TOR) kinase [43], which hyperphosphorylates Atg13, an activating component of the ATG1 kinase complex (Figure 1.3a) [44]. Under nutrient-limiting conditions, this phosphorylation is inhibited, allowing for formation of the Atg1 kinase complex [45]. This complex contains Atg1, Atg13, and Atg17, though recent data suggest that Atg11, Atg20, Atg24, Atg29, Atg31 are also present [46]. Of these only Atg1, Atg13 and Atg20 appear to have sequence-based homologs in plants [8]. Concurrently, the induction of autophagy also requires activation of the class III phosphatidylinositol-3-kinase (PI3K)

complex, which is involved both in regulating TOR activity, and in autophagosome formation [47]. Interestingly, the placement of the PI3K complex in the induction pathway varies. In mammalian cells, the class I and class III PI3K complexes have been reported to work upstream of TOR to transduce nutrient signals[8]; however recent data suggest TOR functions independently of class III PI3K signaling in *Drosophila* [48]. In both systems, experiments using the PI3K inhibitors wortmannin and 3-methyladenine revealed that class III PI3K activity is also required for the induction of autophagosome formation [47,49,50].

Regardless of the organism, the PI3K complex is composed of three conserved subunits, the PI3K catalytic subunit, Vps34, an activating kinase Vps15, that anchors the complex to the membrane, and ATG6 (Figure 1.3b). In yeast, a fourth subunit, Atg14, is also present [51]. The PI3K enriches the sequestration membrane with phosphatidylinositol-3-phosphate (PI3P). These PI3P-rich membranes have been shown to directly traffic to the vacuole in both yeast and plants [52-54]. Addition of the PI3P lipid moiety to the autophagosome membrane leads to the recruitment and membrane association of additional autophagy proteins, including the Atg18-Atg2 complex [55]. Following recruitment, the Atg18- Atg2 complex functions, in conjunction with the Atg1 kinase complex, to regulate the cycling of the integral membrane protein Atg9 between intracellular compartments, including mitochondria, during vesicle formation [56]. Current data suggest that as Atg9 cycles between compartments, it delivers membrane to the growing autophagosome. Recently an association between Atg9 and Arp2 has been reported, which suggests that the actin cytoskeleton is required for Atg9 cycling [57].

Autophagosome formation: Following vesicle nucleation, two ubiquitin-like conjugation systems are responsible for the assembly of two protein complexes essential for vesicle formation. Both conjugation systems are conserved in yeast, plants, and mammals [2,5,36,58]. Based upon the phenotypes of deletion mutants, these complexes regulate the size, rate of expansion, and curvature of the growing autophagosome.

Assembly of the Atg12-Atg5 complex begins with the conjugation of the C-terminal glycine of Atg12 to an internal cysteine of the E1-activating enzyme Atg7 via a thioester bond [4]. Atg12 is subsequently transferred to an internal cysteine of the E2-conjugating enzyme Atg10, and then forms an amide bond with Atg5 (Figure 1.3d) [46,59]. Following this conjugation, a large hetero-octomeric complex composed of Atg12, Atg5, and Atg16 is formed [5]. This complex associates with the growing autophagosomal membrane (phagophore) and is thought to aid in the expansion and curvature of the membrane [5]. This complex is also required for recruitment of Atg8 to the forming autophagosome.

ATG8 is the only autophagy protein present in the completed autophagosome (aside from the prAPEI receptor Atg19) and is associated with both the inner and outer membrane. A second system is responsible for conjugating this critical protein to phosphatidylethanolamine (PE), allowing for its membrane association (Figure 1.3c) [60]. This requires the activity of the cysteine protease Atg4, which cleaves a C-terminal arginine from Atg8, exposing a C-terminal glycine residue [4]. Next, Atg8 is conjugated to the aforementioned Atg7 via a thioester bond. Following transfer to the E2 enzyme Atg3, Atg8 then forms an amide bond with a PE moiety [61]. Despite our understanding of the assembly of this complex, its mechanistic functions during autophagosome formation are still unclear [36]. While Atg8 protein associated with the outer membrane of the autophagosome is removed by the activity of Atg4, the Atg8 on the inner membrane is degraded along with the cargo. This has lead to the widespread use of Atg8 as an autophagosomal marker [62]. Furthermore, recent data indicate that Atg8 may stimulate the tethering and hemifusion of membranes in vitro, suggesting a role for the Atg8-conjugating system in regulating membrane fusion during autophagosome formation [63]. Interestingly, at least one other protein has been reported on the autophagosomal membrane, the plant-specific α-tonoplast intrinsic protein (alpha-TIP) [64].

Trafficking and degradation: By monitoring Atg8-GFP, we can follow the completed autophagosomes and cargo as they travel through the cytosol to the vacuole. Precisely how the autophagosomes travel has not been determined.

While it was initially thought that Atg8 was a microtubule binding protein, additional evidence for association of autophagosomes with microtubules has not been forthcoming [46]. Following transit, the final steps involve fusion of the outer membrane with the vacuole membrane, the tonoplast. It has been reported that common fusion machinery including the V-SNARE Vti1 [65] and the activity of associated Vam3 syntaxin and a Rab family GTPase [66] mediate fusion in yeast. Study of the two key *Arabidopsis* agravitropic mutants *sgr3* and *sgr4* identified plant homologs of these SNARES [67,68]. In addition, the proteins AtVAM3 and AtVTI1 localize to a prevacuolar compartment, supporting their function in vacuolar vesicle fusion [69]. Since plant cells can contain more than one vacuole type, additional research is needed to understand the mechanisms that specifically target autophagosomes to the lytic vacuole [70]. Upon fusion, a single membrane-bound autophagic body is released into the vacuolar lumen and the resident proteases then degrade the vesicle and cytosolic cargo. Treatment with PMSF or the cysteine protease inhibitor E-64 has been shown to inhibit this degradation. The resultant amino acid and macromolecule components are presumably exported and recycled to the cytosol to prolong cell survival [4].

Plant autophagy mutants

As mentioned above, homologs for many of the autophagy proteins characterized in yeast have been identified and studied in plants. A summary of the autophagy proteins with known *Arabidopsis* homologs is provided in Table 1.1. Both of the ubiquitin-like conjugation systems have been reconstituted [59-61], and subunits of the PI3K complex, TOR kinase signaling pathway, and several components of the Atg1 kinase complex have been identified [2,8]. However, it is the analysis of plant autophagy mutants that has been most revealing. While deletion of AtVPS34 leads to embryo lethality [71], the majority of ATG mutant plants are viable. For example, tobacco homologs of the PI3K VPS34 and ATG6 play important roles during programmed cell death (PCD) [20]. In plants, PCD occurs following the hypersensitive response in an effort to limit

the spread of pathogens [20]. In ATG6 mutants, PCD is not limited to the site of infection but spreads throughout the entire organ, indicating that the PI3K complex, and potentially the autophagy pathway, is required for regulation of PCD during the innate immune response [72]. In addition, the loss of *Arabidopsis* ATG6 leads to pollen germination defects, indicating a potential role for autophagy during gamete development [22-24].

Analysis of additional mutants indicates that deletion of key autophagy genes leads to perturbation of the autophagy pathway [61,73]. This was clearly demonstrated by a lack of autophagosome formation in the root tips of *atg2*, *atg5, atg4a/b,* and *atg18a* mutants [60,74,75]. The loss of ATG4 activity is particularly detrimental as it prevents the formation of ATG8-PE [60]. In addition, autophagy mutant plants exhibit similar phenotypic consequences that affect their ability to respond to stress, altering the normal developmental program, and shortening the life cycle.

Phenotypic analysis of the first autophagy mutants, *atg7* and *atg9,* provided evidence of a link between the autophagic recycling process and the process of senescence [76]. Following fifteen days of nitrogen limitation, wild-type plants appear healthy because the autophagy pathway presumably functions to prolong survival. In contrast, *atg9* mutants, which lack a functional autophagy pathway, suffer from signs of stress including chlorosis in both the cotyledons and mature rosette leaves [76]. They also exhibit decreased overall viability, leading to premature senescence and overall shortened life span. Similar phenotypes were later observed for *atg5, atg7, atg4a/b,* and *atg10* mutant plants which appeared smaller than their wild-type plant counterparts and also exhibited premature senescence in photosynthetic tissues [59-61,77]. In addition, these mutants produced fewer seeds than wild-type, possibly due to decreased branching in the inflorescence and a reduced number of flowers [60,61]. This early transition to senescence indicates that in the absence of autophagy nutrients quickly become limiting. Multiple groups have examined the expression patterns of known senescence-responsive genes in various *atg* mutants. Early induction of *SEN1, SAG12,* and *PED1* were observed, indicating that

perturbation of the autophagy pathway results in early activation of the natural process of senescence [74,78].

When Recycling Is Not Enough - Senescence

Senescence is a dynamic process that occurs naturally concurrent with age or is prematurely induced by a variety of biotic and abiotic factors [79]. The natural age-related senescent processes are regulated by internal genetic, hormonal, and metabolic cues and are keenly attenuated to external cues. In fact, the photoperiod, availability of water and macro/micro nutrients have a deep impact upon the initiation, rate of progression, and ultimate completion of senescence [80,81]. In contrast, induced senescence occurs independent of age and serves vital roles in plant defense against viral, bacterial, and fungal pathogens, controlling high levels of oxidative stress and in response to macro and micro nutrient limitation [82]. Like autophagy, senescence is responsible for the degradation and remobilization of macromolecules, including lipids, amino acids and nucleic acids [82]. Senescent degradation is achieved through the coordination of at least three intracellular degradation pathways: the ubiquitin/proteasome pathway, the vacuolar degradation pathway (particularly for chlorophyll breakdown), and the autophagy pathway. This allows for source-to-sink transport of vital nutrients from senescing mature leaves, roots, or floral organs to distal parts of the plant. These nutrients are used for maturation of developing tissues in young organs, for reproductive structures and seeds, or can be stored for periods of dormancy. However, in contrast to the autophagy pathway, senescence predominantly leads to death at the organismal, organ, tissue, or cellular level [83].

Definition of senescence

Senescence is easily seen in leaves, where the characteristic degradation of chlorophyll is readily observable. However, this visible morphological change has led to confusion regarding the definition of senescence as it pertains to programmed cell death. Senescence is often viewed as a plastic process that occurs in viable cells and involves functional and active transcription for initiation and regulation [83]. In contrast, programmed cell death typically occurs in damaged cells under extreme duress [84], or is associated with the

developmentally programmed death of individual cells or groups of cells during pollen incompatibility, synergid death, aleurone death in barley, pith autolysis, or formation of tracheary and sieve tube elements [85,86]. Consequently, one definition considers senescence and programmed cell death to be mutually exclusive processes, completion of the former leading to initiation of the latter [87]. This separation is based on several studies in tobacco and flax, which showed reversal of chlorophyll degradation and re-greening of tissues [88-90]. Since programmed cell death is a committed process [84], these studies indicated that two separate processes must be occurring, one that is reversible, considered senescence, and a second that is committed, considered programmed cell death [91]. An alternative definition refers to the deterioration of an entire organism/organ as senescence and the degradative-process at the cellular level as programmed cell death [79]. Another definition implies that only tissues that can undergo visible chlorophyll degradation, photosynthetic tissues, undergo senescence, while the rest undergo programmed cell death [79,87]. Consequently, many researchers consider senescence to be synonymous with programmed cell death (PCD), as one so often leads to the other [92]. Interestingly, some examples of programmed cell death involve senescence-related processes, such as degradation of organelles and the recycling of intracellular components [93]. However as we come to understand more about the molecular, physiological, and hormonal controls of senescence and programmed cell death, the differences between the two may become more prominent [91]. For the purpose of this discussion, I shall use the term programmed cell death to refer to irreversible changes during the final stages of senescence, rather than considering the terms to be synonymous.

Leaf senescence

The most well-studied form of senescence is the organ-specific degradation of leaves, termed leaf senescence. The most striking example occurs in deciduous trees in autumn [94], during which the high nitrogen composition in the chloroplasts is remobilized prior to leaf abscission, presumably for use in the

subsequent growing season [83]. In contrast, for many short-lived plant species leaf senescence is correlated with completion of the entire life cycle. This is especially true in monocarpic species that undergo a single reproductive event. In monocot cereal crops, including wheat, barley and corn, the onset of leaf senescence is tightly correlated with seed development [95]. Nutrients are continually mobilized from old to young leaves and ultimately to the flag leaf [96]. Up to 90% of the nitrogen in the vegetative portions of the plants is exported to allow for grain-filling and ripening of the kernels [96]. Following ripening, the plant undergoes organismal senescence.

In contrast, leaves can mature and senesce independently of the reproductive cycle [83]. This is readily observable in members of the Brassicaceae, which form a single tight rosette of leaves at the base of the plant. In the case of *Arabidopsis*, each leaf reaches maturity following a period of rapid expansion (peak photosynthetic activity) approximately twelve days after its emergence from the vegetative meristem as a leaf primordium [97]. After a period as a source organ, leaves begin to senesce about twenty-four days post emergence and enter the later stages of cell death between twenty-eight and thirty-two days post-emergence [82]. This is due, in part, to the addition of new rosette leaves, which self-shade the older leaves, and the accumulation of oxidative damage as a result of photosynthesis [97]. Upon flowering, the formation of leaves stops and nutrients are assimilated and relocated to the reproductive structures [98]. Following ovule fertilization and the onset of silique formation, floral organs, including petals and stamens, also undergo a controlled maturation and senescence program best evidenced by the wilting and subsequent abscission of petals from ornamental flowers like roses [99]. Ultimately, the loss of photosynthetic capacity due to leaf senescence leads to organismal death that is closely correlated with the production of mature seed.

Cellular changes during leaf senescence

While it is important to remember that senescence occurs in both photosynthetic and non-photosynthetic organs, I will focus on the well-studied process that

occurs in leaves. The major changes that occur at the cellular level are summarized in Figure 1.4. Leaf senescence is a gradual and organized process that begins in the cells at the leaf margin and continues inward toward the central veins, where nutrients are exported to the sink sites using the vascular system. On a cellular level, leaf senescence begins with a stark reduction in anabolic cellular processes, including protein synthesis, organelle biogenesis, and tRNA/rRNA synthesis. Photosynthetic activity decreases markedly, accompanied by corresponding changes in accessory pathways including photorespiration [83]. Total RNA in both the cytosol and chloroplast decreases rapidly due the activity of several RNases [82,96]. Next the chloroplast DNA (cpDNA) is degraded, the nucleus decreases in size, and the chromatin is condensed as transcription rates decrease [100].

The first morphologically observable changes occur in the chloroplasts [88]. Electron microscopy reveals progressive disruption and reduction of the thylakoid membrane system and the clustering of plastoglobules, small lipoprotein particles that contain tocopherol cyclase (VTE1) and mediate free-radical damage [101,102]. This is associated with the in situ and vesicle-mediated degradation of highly abundant nitrogen-rich chloroplastic proteins, including ribulose bisphosphate carboxylase (Rubisco) and chlorophyll a/b binding proteins (CAB) [79,96]. Following release, nitrogen may be remobilized prior to long distance transport, via conversion to glutamine or asparagine through one of the proposed GS/GOGAT or PPDK-GS/GLGOT pathways [83].

There has been extensive work aimed at identifying the proteases responsible for plastidic protein degradation. Early evidence revealed a low pH requirement for degradation of Rubisco, suggesting chloroplast proteins may be targeted to the vacuole [35]. In wheat leaves, small vesicles, called Rubisco containing bodies (RCBs), bud from chloroplasts and are then incorporated into autophagosome-like vesicles [103]. The evidence of autophagy's involvement in this degradation has been strengthened by reports of stromal proteins in ATG8-labeled vesicles during senescence [104]. In addition, multiple plastidic metallo-endoproteinases, aminopeptidases, and tobacco aspartic protease CND41 have

been suggested as hydrolytic candidates [96,105]. Surprisingly, many proteases are constitutively expressed, including the long-term degradation candidates, the Clp proteases. The catalytic subunits of the stroma-localized Clp Ser-type endopetidase protease complex are not up-regulated during senescence. However, two of the ATP-dependent HSP100-like regulators ClpD/ERD and ClpC1, which unfold proteins for the Clp proteases, are strongly induced during senescence, perhaps suggesting an altered specificity for the complex [106]. To date, this active area of research area has not yielded a definitive answer regarding the protease identity. Following the onset of photosystem complex degradation, the photosynthetic pigment chlorophyll is degraded. When the degradation is complete only the carotenoids, anthocyanins, tetrapyrollic catabolites, and phenolics remain in the leaves [82] (for a detailed review on chlorophyll degradation see ref [94]).

Despite this internal degradation, the majority of chloroplasts, like other intracellular organelles, remain intact until late senescence, though some perturbation of the outer membrane has been reported. In fact mitochondria and peroxisomes show many increased enzymatic activities [86]. The generation of hydrogen peroxide-derived activated-oxygen species, through the activity of lipooxygenese and the down-regulation of peroxisomal catalase [107], allows for rapid oxidative damage of biomolecules [108]. Normally the enzymatic and non-enzymatic antioxidant defense systems would eliminate these radicals, but this does not occur during senescence, resulting in high levels of cellular oxidative stress [109]. Lipases, such as phospholipase D and lytic acyl hydrolase [110], induced during senescence, break down membrane components, including the abundant galactolipids from thylakoid membranes [111]. The by-products of the lipase activity enter into the β-oxidation pathway and are used to produce α-ketoglutarate for gluconeogenesis [83]. For release of free amino acids, endo/exo-peptidases and hydrolases accumulate in the vacuole via transport in precursor protease vesicles (PPV) [112-114]. Cysteine proteases, including the maize See2 gene products and SAG12, a well known senescence-associated proteinase, are both strongly induced [115,116]. Throughout the process,

macroautophagy delivers cytoplasmic components into the vacuole. In addition, microautophagy has been observed, as cytoplasmic components directly enter the vacuole through tonoplast invaginations [82,88]. The cell then progresses toward total loss of viability and organ-wide programmed cell death. Ultimately, the leaf undergoes abscission from the plant.

Molecular regulation: Hints from genomics

Our understanding of the molecular and hormonal regulation of senescence has come from two main avenues of investigation - the identification of Senescence-Associated Genes (SAGS) using genomic techniques, and the analysis of mutant plants with altered senescence responses. These two approaches have hinted at the complexity of the process and its regulation at the molecular and hormonal level. Extensive work in multiple plant species, including maize, sweet potato, barley, and *Arabidopsis* has led to the identification of a large number of SAGs. Comparison of cDNA libraries from control and early-senescent field-grown aspen trees indicate that metallothionein and cysteine proteases are highly expressed in autumn leaves and identified 49 additional SAGs [117]. Similar work in the flag leaves of rice identified 533 senescence-associated genes [118]. Initial cDNA profiling experiments in *Arabidopsis* identified 12 genes that were induced or repressed during senescence [119]. In addition, analysis of 1,300 *Arabidopsis* enhancer trap lines led to the identification of 147 genes with senescence-specific activation of the GUS reporter gene [120].

However, microarray profiling performed on several plant species has yielded the largest subset of genes that show altered expression patterns during senescence [95,106,121]. Approximately sixteen percent of *Arabidopsis* genes have altered expression during senescence, and almost 800 genes have significant enough induction to be considered SAGS. These include families of transcription factors [122], components of signaling complexes including kinases and GTP binding proteins, ubiquitin-proteasome pathway proteins, autophagy proteins, degradative enzymes such as cysteine proteases and lipases, and proteins with established roles in hormone production, regulation, and signaling

[106,121]. One well-studied example is the ion transporter PPF1, which functions during senescence by controlling Ca^{2+} levels and regulating reproductive development [123]. The expression pattern of the vast majority of SAGs is similar during both induced and age-dependent senescence. However, at least one study has identified differences in the expression of several genes, depending upon the method of senescence induction [124]. In addition, SAGS induced in *Arabidopsis* rosette leaves have been profiled in an age-dependent and position-specific manner, further illustrating some differences [97].

Senescence-associated transcription factors

Approximately 300 transcription factors were up-regulated in the genomic analysis [125]. They represent many families including, but not limited to, bZIP, HSF, C2H2, NAC, and WRKY family members [95,106,126]. Several of these, including ATHSFB1/HSF4 and SAP12, which contain two AN1-like zinc finger domains, are involved in drought tolerance and maintenance of cell viability during senescence [127]. In addition, almost one-fifth of all NAC transcription factors are up-regulated during senescence and promote or repress the process. NTL9 is a NAC protein induced during oxidative stress. Like all NAC proteins, NTL9 is dormant in its native membrane-bound form and becomes active following condition-dependent proteolytic cleavage and nuclear localization [128]. Consistent with its designation as a senescence-associated transcription factor, NTL9 over-expression leads to premature activation of many SAGs [128]. However, only a subset of the activated genes is down-regulated in *ntl9* mutants hinting at possible functional redundancy in the signaling network [128]. Another NAC with an experimentally confirmed role during senescence is AtNAP [129]. As one would expect, AtNAP is a nuclear protein whose over-expression leads to precocious senescence. Conversely *atnap* mutant lines show delayed leaf senescence [129]. Little is known about the upstream activators of either NAC protein.

The most well-studied senescence-associated transcription factors are in the WRKY family. Seventy-four distinct proteins are members of the WRKY

family and together mediate plant responses to biotic factors, including pathogen defense by activation of the systemic acquired resistance pathway and through induction of senescence [130]. The abundance and activity of WRKY proteins is regulated by ethylene, jasmonic acid, or salicylic acid signaling, although no direct activation of a WRKY protein by a hormone-signaling cascade has been shown. Sequence analysis has revealed that the promoters of many SAGs contain potential WRKY factor binding sites, dubbed W-box motifs [95]. To date, three family members have received particular attention in regards to senescence: WRKY6, WRKY70 and WRKY53.

WRKY6 is induced by ethylene and jasmonic acid signaling [131] and functions in part by positively regulating the expression of SAGs, including *SEN1* (a protease), *NAC2* (a jasmonic acid regulatory protein), and the leaf senescence induced receptor kinase, *SIRK* [132]. Like other WRKY factors, WRKY6's activity is mediated by NPR1, a protein that controls the onset of systemic acquired resistance in response to pathogens [133]. WRKY6 also shows the characteristic auto-regulatory feedback seen with other WRKY proteins and regulates the activity of other *WRKY* genes [130]. However, *wrky6* plants, while dwarfed with curled leaves, do not have a senescence phenotype, indicating potential functional redundancy.

Like WRKY6, WRKY70 is also regulated by stress hormone signaling. This has been clearly demonstrated by the reduced levels or complete loss of *WRKY70* transcript in plants that lack functional salicylic acid signaling and synthesis pathways (*npr1, pad4* and *NahG*) [134]. In contrast to WRKY6, *wrky70* knock-out lines clearly show signs of premature senescence in mature rosette leaves, accompanied by elevated expression of SAGs and jasmonic acid/ethylene-related genes [134]. This indicates that unlike WRKY6, WRKY70 negatively regulates the expression of these senescence-promoting genes [134].

The final WRKY I shall highlight is WRKY53. A current model of the WRKY53 signaling pathway is shown in Figure 1.5. This transcription factor has been implicated in regulation of senescence, is involved in the systemic acquired resistance pathway and is induced by H_2O_2-mediated oxidative stress [135,136].

In contrast to WRKY70, RNAi and knockout lines for *WRKY53* show delayed senescence phenotypes, indicting that WRKY53 works to promote senescence. WRKY53 has been shown to directly bind to the promoters of many genes, including several catalase isoforms (CAT1, 2 and 3), multiple ethylene response proteins, a senescence-induced receptor-like serine/threonine kinase, SAG12 and eight other WRKY proteins (including *WRKY6)* [136]. In addition, WRKY53 may indirectly regulate *WRKY70* as indicated by analysis of WRKY53 over-expression plants [136]. In addition to identifying WRKY53 targets, upstream components in this pathway have been identified. At least two proteins have been shown to directly bind the *WRKY53* promoter including the mitogen-activated protein kinase kinase kinase (MEKK1), a component of the MAPK signaling pathway, and AD, a novel DNA-binding kinase [137,138]. Interestingly both kinases can also phosphorylate WRKY53 and directly interact with one another [138]. This phosphorylation increases WRKY53's ability to bind to its target gene [138]. This is the first instance where the upstream regulatory factors of a senescence-associated transcription factor have been described.

The complex WRKY regulatory web integrates pathogen defense and the process of senescence. Presumably, analysis of the remaining 290+ senescence associated transcription factors will determine how senescence is regulated in response to other biotic and abiotic cues. In addition, we may further understand how the developmental and environmental cues received through the hormonal signaling networks interact to regulate this complex process.

The role of sugar and plant hormones during senescence

Plant hormones attenuate plant growth and development with environmental conditions and also mediate defense responses. All of the biotic and abiotic factors that induce hormone production, including drought, pathogen attack, osmotic stresses, and oxidative stresses, can also induce senescence. Not surprisingly therefore, hormones implicated in the response to these stimuli have either positive or negative roles in the regulation of induced senescence. In addition, these same hormones have key roles in the regulation of natural

senescence, they attenuate development in response to environmental cues. Analysis of microarray data and enhancer trap lines reveals that many SAGs are induced by exogenous application of several key plant hormones, including abscisic acid (ABA), salicylic acid (SA), ethylene, and jasmonic acid (JA) [78,120]. Here I will summarize our current understanding of the roles that sugar and plant hormones play in the regulation of senescence. Figure 1.6 highlights the potential signaling components involved in each pathway.

Sugar signaling: The onset of senescence is mediated by the sugar signaling pathways [139]. A marked decrease in photosynthetic activity and the induction of senescence are correlated with high intracellular sugar concentrations. Microarray analysis indicates that the senescence-specific gene *SAG12* is induced more than 900-fold by glucose, and several enzymes involved in nitrogen assimilation, including the nitrate transporter AtNRT2 and glutamine synthetase GLN1, are also up-regulated [140]. It is unclear how sugars accumulate when photosynthetic activity decreases. There is evidence of up-regulation of peroxisomal enzymes involved in the glyoxylate cycle [141]. This pathway allows for production of cellular metabolites used for gluconeogensis from lipids, suggesting *de novo* sugar synthesis may occur during senescence [80,142] (see Figure 1.6b). In castor bean leaf blades, accumulation of callose deposition in the sieve plates prevents the flow of phloem. This leads to “back up” of excess sugars into the leaf tissues. Since this occurs just prior to the senescent breakdown of chlorophyll, it reinforces the connection between high sugar concentration and the onset of senescence [143]. Additional evidence of sugar’s role in the induction of senescence comes from the analysis of *Arabidopsis* “sugar” mutants. For example, the *Arabidopsis sweetie* mutant [144], which has increased sensitivity to glucose and sucrose, undergoes premature senescence, as do many other sugar hypersensitive mutants [139]. In addition, over-expression of the glucose sensor hexokinase (HXK) leads to premature senescence due to “over-active” sugar sensing [145]. As expected, the hexokinase mutants *gin2/hxk1* display retarded senescence phenotypes even

though the cellular sugar levels are comparable with wild type [146]. Microarray data indicate that many key sugar-associated enzymes and transporters [98] are induced during leaf senescence and programmed cell death, including hexokinase (HXK), the monosaccharide transporter homolog SFP1 [147], and the *Arabidopsis* high-affinity hexose transporter STP13 [148].

It is important to remember that the sugar-dependent regulation of senescence involves the coordination of many phytohormones. For example, two well-characterized glucose-insensitive mutants are actually defective in the regulation of key plant hormones: the abscisic acid deficient *gin1 (aba2)* and the constitutive ethylene mutant *gin4 (ctr1)* [139,149]. Additional evidence comes from the analysis of *cpr5/hys1/old1* mutants, which display a hyper-senescence phenotype [150-152]. CPR5/HYS1/OLD1 is associated with activation of pathogen response genes and its activity is modulated by sugars, and both salicylic acid and ethylene signaling [151,152]. *cpr5/hys1/old1* mutant plants show symptoms of high levels of oxidative stress, which may be responsible for the premature senescence phenotype. Data showing strong up-regulation of reactive oxygen species-related genes in the mutant support this hypothesis. In addition to salicylic acid, ethylene, and sugar, this up-regulation may also be mediated by abscisic acid signaling [150]. Taken together, analyses of the *cpr5/hys1/old1* and other sugar mutants provides evidence that complex interactions between sugar and hormone signaling are involved in regulating the onset of senescence [153]

Hormones: Cytokinin: Cytokinin, which functions during cell division, chloroplast maturation, and shoot/root morphogenesis, is also a potent inhibitor of senescence [80] (see Figure 1.6a). During the onset of senescence, IPT, the enzyme that catalyzes the first step in the cytokinin synthesis pathway, is down-regulated, while the degradation rate of cytokinin is increased through the activity of cytokine oxidase [124,125]. Conversely, the exogenous application of cytokinin, or increased endogenous production, for example via the SAG12-promoter-driven expression of a bacterial IPT gene [119] delays senescence in

tobacco plants [154]. Cytokinin functions by delaying chloroplast degradation and increasing the activities of photosynthesis-related enzymes, including Rubisco, NADH-dependent hydroxypyruvate reductase (HPR), NADP-dependent glyceraldehyde-3-phosphate dehydrogenase and fructose-1,6-bisphosphatase [154]. This activity is mediated by histidine kinase 3 (AHK3), a cytokinin receptor. An AHK3 gain-of-function mutant (*ore2*) displays increased leaf longevity through the phosphorylation of ARR2, which may directly regulate transcription suppressing senescence [155]. There is also evidence that the cytokinin mediated delay of senescence can be inhibited by high glucose levels, resulting in inhibition of photosynthesis and HPR activity [80].

Hormones: Abscisic acid (ABA), Auxin and Salicylic acid (SA): Abscisic acid (ABA), sometimes called the dormancy hormone, is a potent environmental stress hormone and mediates responses to drought (through stomata regulation) [156], high salt concentrations, and regulates hydrogen-peroxide metabolism [157,158], all factors that can contribute to induce senescence. In rice leaves, ABA stimulates the production of hydrogen-peroxide, resulting in increased oxidative stress and the promotion of senescence [158]. Several ABA-responsive proteins also promote senescence, including Tomato Stress Factor 1 (TSF1), an ethylene response factor that mediates the expression of senescence-associated genes when expressed in tobacco seedlings [159]. In addition, ABA levels are elevated in senescing leaves and stimulate leaf abscission, the final step of leaf senescence [78]. Auxin also regulates leaf abscission, but its role during senescence is not well understood [82,125]. Several key auxin biosynthesis enzymes are upregulated during senescence, and the exogenous auxin can suppress the transcription of some SAGs [82,125].

In contrast to ABA, microarray data suggest that salicylic acid (SA) functions predominantly during natural rather than induced senescence [124]. The levels of SA, which functions in the systemic acquired resistance pathway in response to pathogen infection, are increased almost four-fold in senescing *Arabidopsis* leaves. A recent transcriptome analysis of transgenic SA-deficient

NahG plants indicates SA is required for the up-regulation of many SAGs [124]. This includes the cysteine protease SAG12, which is undetectable in SA signaling, and biosynthesis mutants *pad4* and *npr1* [160]. SA has also been implicated in the regulation of the senescence-specific transcription factor WRKY53 [161].

Hormones: Ethylene and Jasmonic acid (JA)

It is ethylene and jasmonic acid that have the most clearly established roles in the induction and promotion of dark-induced senescence. Ethylene has long been associated with the ripening of fruit, maturation of reproductive organs and induction of senescence [162]. Analysis of the "Onset of Leaf Death" (OLD) mutants demonstrate ethylene's involvement in the regulation of senescence [163]. Three classes of mutants were described: those with ethylene-enhanced premature senescence phenotypes (*old1/cpr5/hys1, old5, old14*), those with ethylene-dependent senescence phenotypes (*old9, old11, old13*) and those with phenotypes so severe that ethylene treatment had no effect (*old3, old12*) [163]. In all cases, the effect of ethylene appears to be age-dependent since senescence could not be in cotyledons or young leaves. In addition, while increased duration of ethylene treatment causes leaf yellowing, variation is observed in the attenuation of the mutants to the ethylene signal. This suggests several of the genes may encode signaling components. In addition, ethylene-insensitive mutants such as *ein2* display a delayed-senescence phenotype [164] and three ethylene biosynthesis genes (including *ACC* synthases) are up-regulated during senescence [125]. EIN3, a known ethylene response factor, is also up-regulated during senescence [162], as are several of its targets, including AtERF1a whose transcriptional activation requires ethylene and jasmonic acid signaling pathways [165].

Jasmonic acid and several biosynthesis intermediates are biologically active hormones that regulate developmental processes, including root growth and reproductive development. In addition, they are involved in the response to wounding and defense against insects and pathogens [166]. A role for methyl

jasmonate in senescence was initially observed when wormwood (*Artemisia absinthium*) extract was applied to oat leaves, resulting in the rapid onset of senescence [167]. Exogenous application of JA, to either attached or detached *Arabidopsis* leaves, also results in premature senescence [168]. As expected, the JA-insensitive *coi1-1* mutant, which lacks a key protein component of the JA-responsive SCF complex, suffers from delayed leaf senescence [168,169]. At least one transcription factor has been identified as a mediator of JA signaling during senescence. OsDOS, a rice CCCH-type zinc finger protein is a negative regulator of JA signaling [170].

In addition, jasmonic acid concentrations increase in senescing leaves [168], as do transcripts for biosynthesis genes including *AtLOX2*, *AtAOS,* and *AtOPR3* [125]. The synthesis of jasmonic acid requires the peroxisomal β-oxidation machinery [171]. Chief among the enzymes required is 3-ketoacyl-CoA thiolase 2 (KAT2), which catalyzes the final step in the JA biosynthesis pathway [171]. KAT2 is activated during dark-induced and natural senescence and RNAi work has demonstrated that a reduction in KAT2 protein greatly slows the process of senescence [172]. There is also evidence that senescence-associated genes such as SAG101 may be involved in the release of α-linoleic acid for use in JA synthesis [168].

Summary of hormone receptors and cascades: The activity of all these hormones is mediated by a variety of cytosolic and membrane-localized receptors and/or ubiquitin-ligase-based receptors [173]. In most cases it is assumed that previously identified components of hormone signaling pathways function as upstream regulators during senescence [82], as many of them are up-regulated during senescence. This includes the multi-hormone mitogen-activated kinases (MAPK) [174], cytokinin receptors CK1/CRE1 [175], the ethylene response factors CTR1 and EIN3 [176], the jasmonic acid-associated COI1 SCF complex [177], and other components of the major signaling networks. In addition, microarray data have led to the identification of many novel kinases

and proteins of unknown function that may play a role in signal transduction [153].

During growth and development the different signaling pathways are integrated through shared molecular components and overlapping response profiles; the same appears to be true during senescence [178]. As with any signaling cascade, activation of receptors leads to signal amplification, and ultimately to altered transcription. In the case of senescence-inducing stimuli, including high sugar concentrations, this leads to induction of senescence-associated genes and initiation of cellular degradation processes. Additional transcription factors, which respond to senescence repressing stimuli, such as cytokinin, lead to increased transcription of photosynthetic enzymes or suppression of the senescence-associated genes. The integration of these repressive and inductive sugar and hormonal stimuli controls and regulates the initiation and progression of senescence. Additional research on novel SAGs will allow for a greater understanding of how the complex network of signaling pathways is regulated, during both natural and induced senescence.

The Role of Peroxisomes During Senescence

Due to the complex regulatory network and plethora of intracellular changes, the process of senescence is more easily considered in the context of a single signaling pathway, particular developmental stage, in response to specific stimulus, or through the examination of one subcellular compartment. Consequently, rather than focusing on the cellular level, recent studies have focused on understanding the molecular changes that occur in an individual organelle during a variety of developmental processes [179]. Proteomics approaches greatly aid this research by identifying changes in the protein complement that occur during a particular development stage or in response to specific inductive stimuli. One example is our proteomic analysis of peroxisomes isolated from senescing *Arabidopsis* leaves (see Chapter 4). Peroxisomes are

responsible for a wide array of biochemical processes, many of which are essential during senescence. Through examination of the proteins present in peroxisomes, we hope to add to our understanding of senescence as a whole. Throughout this review, I have tried to highlight the senescence-related peroxisomal functions, and here I will integrate the information to paint a clearer picture of this organelle's involvement in senescence. This information is also presented in Figure 1.7.

There are a number of significant changes in peroxisome metabolism during senescence. As photosynthesis is down-regulated, the peroxisomal enzymes responsible for the carbon salvage pathway photorespiration, glycolate oxidase and hydroxypyruvate reductase, are degraded. This is accompanied by up-regulation of enzymes involved in fatty acid metabolism [106]. As previously mentioned, many of the membrane lipids from chloroplast degradation enter the peroxisomal β-oxidation cycle for energy production [180]. In addition to the active β-oxidation cycle, the enzymes involved in the peroxisomal glyoxylate cycle, which are absent from mature leaf peroxisomes, are re-induced during senescence. In developing seedlings this pathway breaks down lipids providing intermediates for gluconeogenesis and it presumably performs a similar function in senescing tissues [142]. The high levels of intracellular sugars, which lead to repression of the cytokinin-mediated inhibition of senescence, may come in part from the *de novo* synthesis of glucose from succinate generated in the peroxisome.

The increased concentration of JA present in senescing tissues comes from increased synthesis. As previously mentioned, the synthesis of jasmonic acid from α-linolenic acid relies upon peroxisomally-localized enzymes [181]. After transport into peroxisomes, OPDA (12-oxo-phytoenoic acid) is converted into the oxylipin jasmonic acid through the activities of multiple enzymes, including thiolase (KAT2) and OPR3. Jasmonic acid actively promotes the onset of senescence and the beginning of chlorophyll degradation. Peroxisomes may also be involved in this vital process. Like mammalian peroxisomes, plant peroxisomes contain the enzymes required for the α-oxidation of fatty acids

[182]. While the degradation of chlorophyll may occur via RCBs/autophagy, direct vacuolar uptake, or cytosolic enzymes, it is hypothesized that phytanic acid, a chlorophyll degradation by product, may be metabolized via peroxisomal α-oxidation [183]. Alternatively, two cucumber peroxidases, which are induced during ethylene treatment, might be involved in chlorophyll degradation [184], though no direct link between chlorophyll degradation and peroxisome α-oxidation has been shown. Whether or not peroxisomes function in chlorophyll degradation is an intriguing, but still unanswered, question.

Finally, the high levels of oxidative stress, which are key factors in the induction of senescence, are derived from increased peroxisomal metabolism in conjunction with ABA signaling [111]. Peroxisomes are named for their role in the production and metabolism of hydrogen peroxide and are characterized by their dense crystalline core composed of catalase [142,185]. Normally hydrogen peroxide is metabolized by catalase activity. CAT2, the isoform present in photosynthetic tissues, is not expressed during senescence at a time when MnSOD (a superoxide dismutase) activity is highest [107,186]. This leads to the accumulation of reactive oxygen species. In addition, xanthine and urate oxidase are induced during senescence. These enzymes are involved in the catabolism of purines, presumably from the degradation of RNA, and their increased activity accelerates the production of ROS. The release of these free radicals and reactive oxygen species allows for the breakdown of macromolecules. In addition, many SAGs including *LSC54*, which encodes a metallothionenin protein, are strongly induced in response to oxidative stress [111,187].

To summarize, due to their roles in many essential senescence-related processes, including fatty acid metabolism, jasmonic acid biosynthesis, oxidative stress regulation, and purine catabolism, the study of senescent peroxisomes affords us a greater understanding of the complex biochemical changes that occur during senescence.

When You Reach the Point of No Return - Cell Death

Senescence is a complicated process, which requires the coordination of complex molecular machinery, including protein degradation and nutrient mobilization pathways, hormone and sugar signaling pathways, and the regulation of oxidative stress and the ROS network. Ultimately, all this activity has one main goal, to prepare the cell, tissue, organ or organism for death. Programmed cell death occurs at the end of the committed senescence process and is regulated by reactive oxygen species (ROS), nitric oxide levels and several hormones [188]. Whether it is age-related or the result of biotic or abiotic factors, cell death is characterized by a series of specific cellular events which ultimately lead to the loss of cell viability through a predominantly non-apoptotic mechanism [82,86]. During PCD there is localized accumulation of reactive oxygen species (ROS), which leads to repression of jasmonic acid signaling and activation of the salicylic acid signaling pathway. In addition ethylene produced in one cell, spreads to surrounding cells and induces PCD [189].

Unlike mammalian cells, plants lack caspase homologs indicating that PCD is regulated by a novel mechanism [190]. The role of the mitochondria has also not been demonstrated beyond reports of specific vesicles containing mitochondria and an apparent increase in intracellular Ca^{2+} [191,192]. In addition, due to the plant cell wall, there is no heterophagic removal of cell “corpses” as typically seen during mammalian apoptotic death [91]. In plant cells, the final stages begin with complete internucleosomal fragmentation of DNA and histone degradation due to rupture of the nuclear membrane [100,192]. Oxidative damage leads to disruption of the endomembrane system and the membranes of metabolic organelles, including peroxisomes and mitochondria. Shortly thereafter, their enzymatic functions cease. Finally, loss of tonoplast integrity leads to degradation of any remaining cytoplasmic components, loss of turgor, and cell death [79,82].

Foreshadowing the Thesis

The first chapter of this thesis has introduced the reader to two different pathways that have overlapping functions during plant stress responses. Both autophagy and senescence occur in response to abiotic and biotic cues and can result in programmed cell death. In addition, each process is partially reversible and each results in the targeted degradation of internal cellular components, nutrient recycling, and retooling of the cell's metabolic and catabolic functions. In this thesis, I explore both of these processes by investigating the function of three very different proteins. In Chapter Two I present my work on Autophagy-related Protein 6 (ATG6), which highlights a novel role for the autophagy pathway during pollen development [22]. In Chapter Three, I present my identification and characterization of FDC, a novel ATG6-binding partner, which contains a FYVE domain. In Chapter Four, I focus on the role of peroxisomes during senescence utilizing the collaborative proteomic analysis of senescent peroxisomes. I present data on the identification and characterization of a novel senescence-associated peroxisomal protein, whose function hints at an exciting link between peroxisomes, and senescence-related chlorophyll degradation. Finally, my conclusions and future directions are presented in Chapter Five.

Table 1.1: Yeast autophagy proteins: While sequence-based homologs are present for many autophagy proteins in the *Arabidopsis* genome, many key proteins lack homologues. Relevant publications are indicated for those proteins whose function has been experimentally determined in Arabidopsis.

Yeast protin	Homologue	Function
TOR	Single gene	*Protein kinase, negative autophagy regulator*
Atg1 Kinase complex		
Atg1	Three	*Serine/threonine kinase*
Atg13	Two genes	*Hypophosphorylation leads to autophagy*
Atg17	None	*Interacts with Atg1*
AtgG11	None	*Peripheral membrane protein*
Atg20	Gene family	*Interacts with Atg24 and Atg17*
Atg24	None	*Interacts with Atg20 and Atg17*
Cargo recognition		
Atg11	None	*Interacts with Atg1 and Atg19*
Atg19	None	*Involved in cargo recognition for cvt pathway*
Nucleation - Phosphatidylinositol-3-Kinase complex		
Atg6	Single gene	*Subunit of PI3K complex* [21-24]
Atg14	None	*Subunit of PI3K complex*
Vps15	Single gene	*Vps34 activating kinase*
Vps34	Single gene	*PI3K catalytic subunit [20,50,71]*
Atg5:Atg12:Atg16 complex [77]		
Atg5	Single gene	*Forms complex with Atg12 [74]*
Atg7	Single gene	*E1-like enzyme for Atg8 and Atg12 activation*
Atg10	Single gene	*E2 protein [59]*
Atg12	Two genes	*Interacts with Atg5 [59]*
Atg16	Single gene	*Forms complex with Atg5 and Atg12*
Atg8 conjugation pathway [77]		
Atg3	Single gene	*E2 protein [20]*
Atg4	Two genes	*Cysteine protease [58,60]*
Atg7	Single gene	*E1-like enzyme for Atg8 and Atg12 activation*
Atg8	Gene family	*Conjugated to PE, autophagosome formation*
Membrane cycling		
Atg2	Single gene	*Involved in ATG9 recycling [74]*
Atg9	Single gene	*Membrane protein [32,74,76]*
Atg11	None	*Needed for Atg9 recycling*
Atg18	Gene family	*Needed for Atg9 recycling [75,193]*
Atg23	None	*Involved in Atg9 recycling*
Atg27	None	*PI3P binding protein*
Additional proteins		
Atg15	None	*Lipase*
Atg21	ND	*Atg8 recruitment*
Atg22	Single gene	*Integral membrane permease*

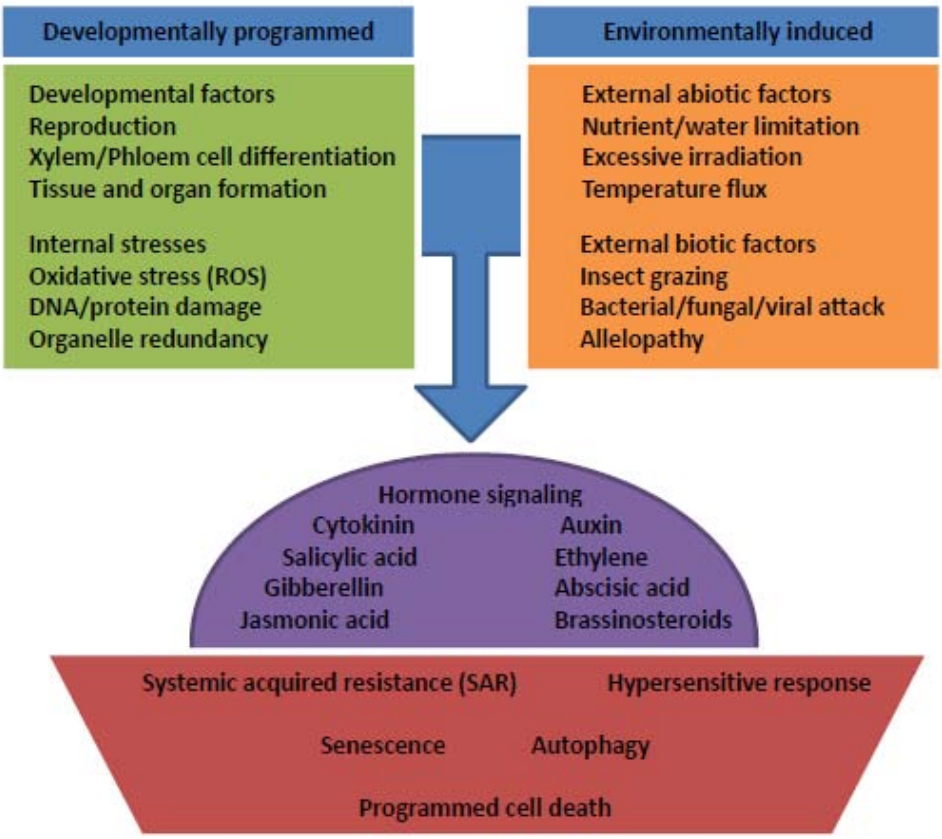

Figure 1.1. Plant stress stimuli and response pathways.

Plant responds to a wide variety of developmentally programmed and environmentally-induced stimuli. These initial stimuli result in alterations of the hormone-signaling network and corresponding changes in transcription and translation. In the case of nutrient limitation, or in response to damaged organelles, the autophagy pathway is induced to prolong cell survival. Because of continued nutrient deprivation, or in response to additional abiotic factors, plants can begin the process of induced or premature senescence. Alternatively developmentally programmed senescence can occur during advanced age, typically correlated with the reproductive cycle and oxidative stress levels. In response to pathogen attack, the hypersensitive response and the systemic acquired resistance pathway function to limit the spread of infection. The affected tissues or organs undergo senescence and programmed cell death.

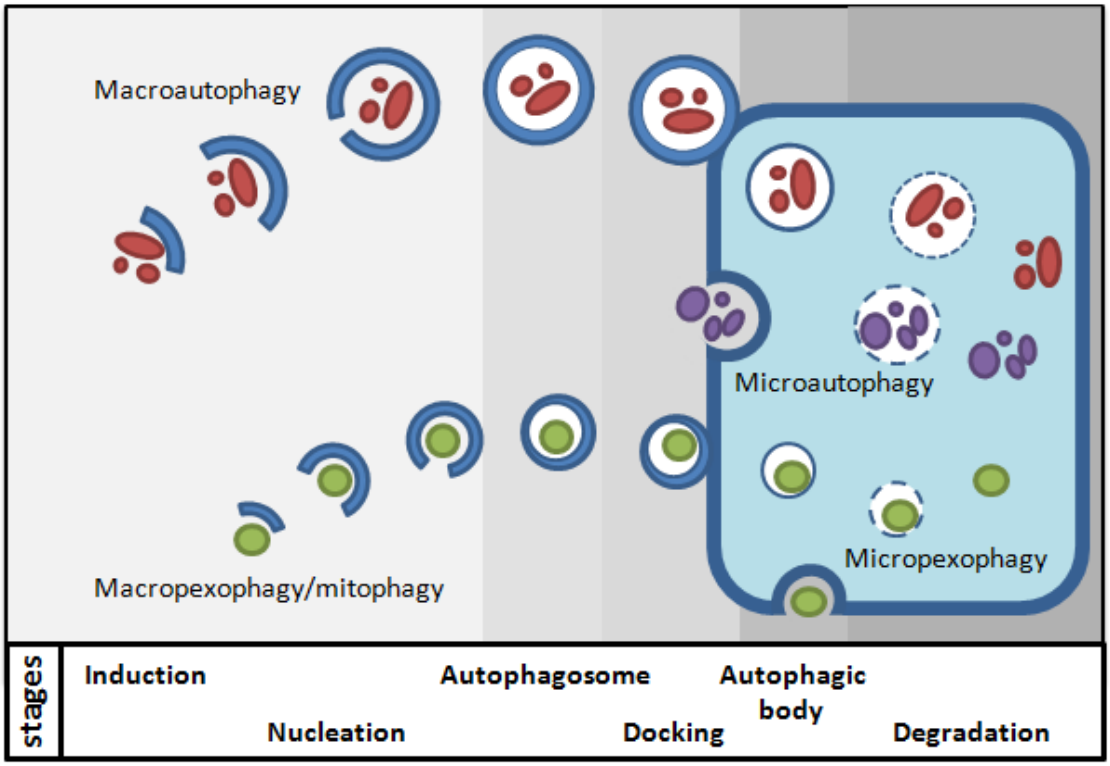

Figure 1.2. Macro- and microautophagy.

Following perception of a starvation signal, nonselective bulk macroautophagy proceeds with the uptake of cytoplasmic components into double-membrane vesicles called autophagosomes. Once completely formed, autophagosomes traffic through the cytosol and dock at the vacuolar membrane. The outer membrane fuses with the tonoplast, releasing a single membrane-bound autophagic body into the vacuole for degradation. Nutrients are then recycled back to the cytosol. Microautophagy involves the direct uptake of cytoplasmic components adjacent to the vacuole through invagination of the tonoplast. Selective autophagy can also occur, including macro- and micropexophagy and mitophagy.

Figure 1.3. Autophagic molecular machinery.

A) In the absence of an inductive signal, TOR kinase maintains Atg1 and Atg13 and their hyperphosphorylated and unassociated forms. Following induction of autophagy, TOR activity is repressed, allowing for formation of the Atg1 kinase complex. Proteins with dashed outlines do not have identified homologues in *Arabidopsis*. B) The phosphatidylinositol-3-kinase complex (type III) is composed of Atg6, Atg14, Vps15, and Vps34, and allows for enrichment of the sequestration membrane with PI3P. This recruits additional ATG proteins, including the Atg18-Atg2 complex (not pictured), which functions in the cycling of Atg9. C) Following proteolytic cleavage by Atg4, Atg8 is conjugated to phosphatidylethanolamine (PE) by the E1 and E2 like proteins, Atg7 and Atg3, respectively. Atg8-PE then associates with the forming autophagosome. This conjugation is reversible by the activity of Atg4. D) Atg12 is conjugated to Atg5 via Atg7 and the E2-conjugating enzyme Atg10. Subsequently a large hetero-tetrameric complex with Atg16 is formed (one of the four subunits is indicated), which may aid in the expansion and curvature of the autophagosome membrane. Adapted, in part, from [4,5,36,46].

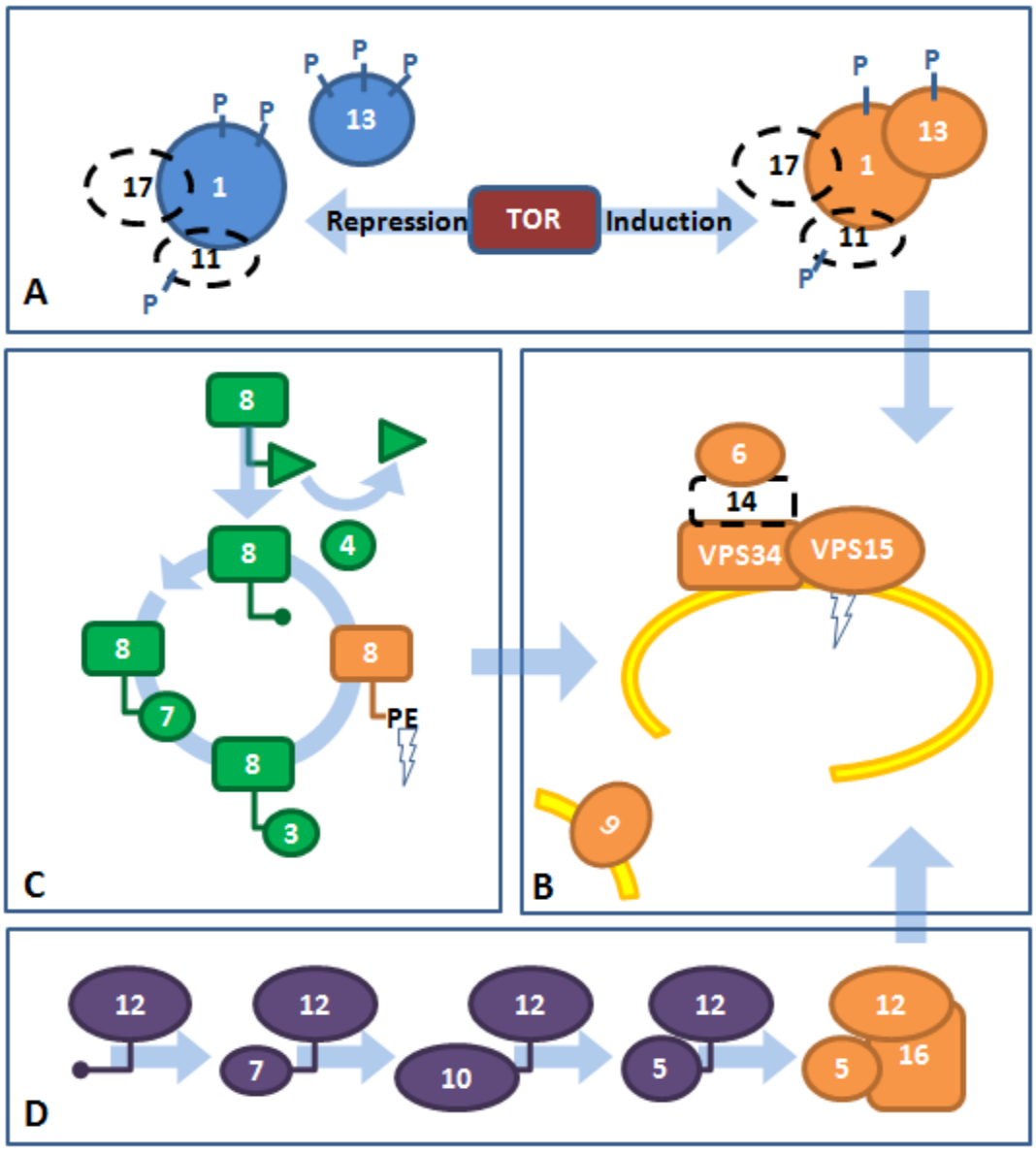
A
P
13
17
1
11
Repression
TOR
Induction
B
6
14
VPS34
VPS15
9
C
8
4
7
3
PE
D
12
7
10
5
16

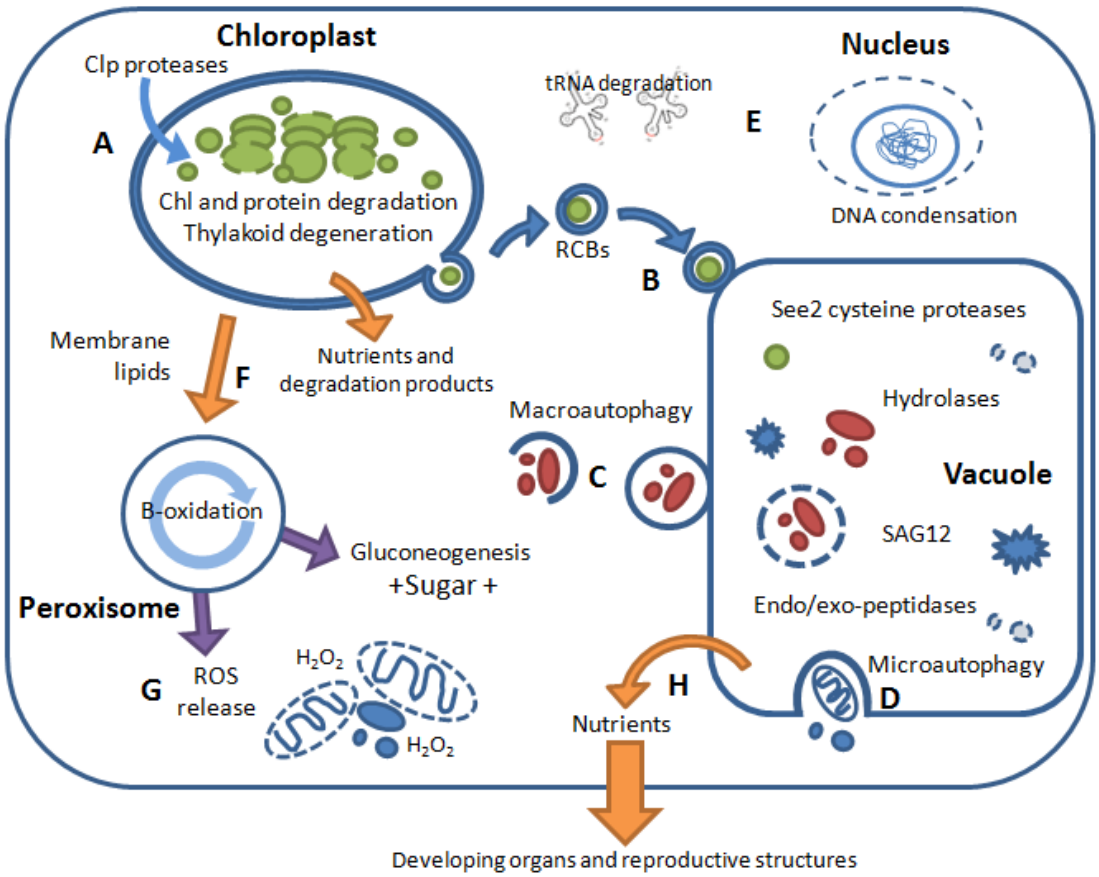

Figure 1.4. Cellular changes during *Arabidopsis* leaf senescence.

A) Senescence in photosynthetic tissues begins with degradation of chloroplast DNA (cpDNA) and degeneration of thylakoid membranes. Chlorophyll is rapidly degraded, as are the photosystems and other chloroplast proteins, perhaps by Clp proteases. B) Rubisco-containing bodies also deliver proteins to the vacuole for degradation by the senescence-enriched proteases, hydrolases, and peptidases. Macro- (C) and microautophagy (D) allow for bulk degradation of cytosolic components. E) Following brief production of senescence-associated proteins, the nucleus shrinks, nuclear DNA is condensed, and tRNAs are degraded as transcription slows. F) Lipids are assimilated in peroxisomes, via the β-oxidation pathway, a process that may allow for sugar accumulation through gluconeogenesis. G) Peroxisomes release reactive-oxygen species into the cytosol, which then oxidize biomolecules, aiding the degradative process. H) The resulting nutrients are exported to developing organs and reproductive structures.

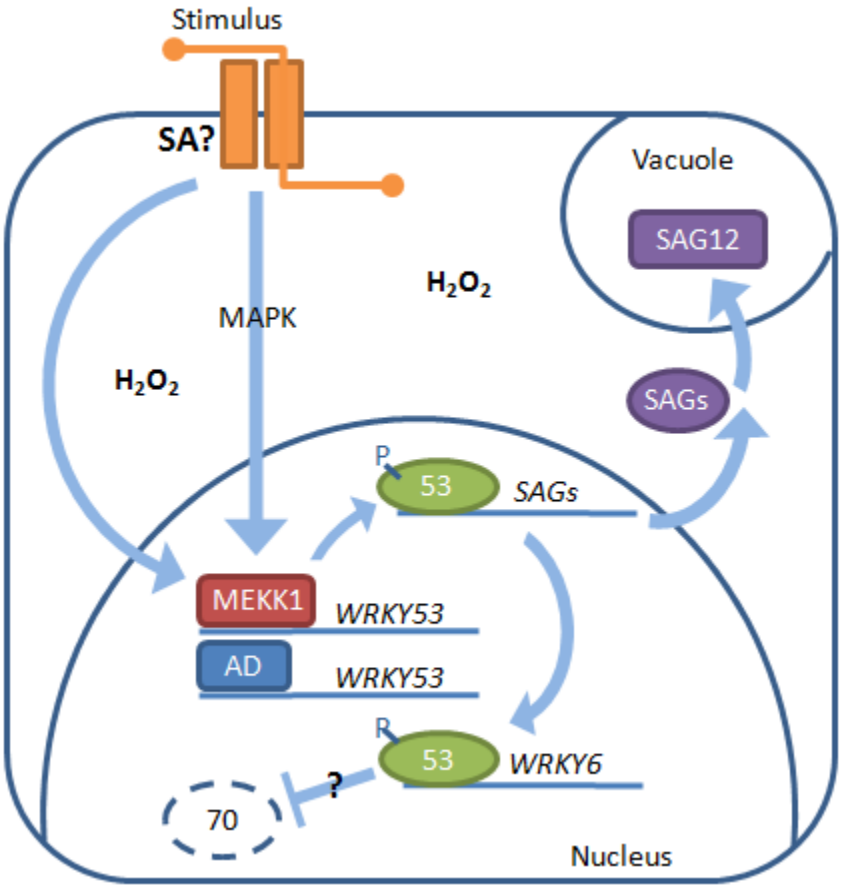

Figure 1.5. Transcriptional regulation of senescence: WRKY53 example

It is predicted that several hundred transcription factors are involved in the regulation of senescence, including members of the WRKY family. Many members of the family are active during oxidative stress and in response to pathogen attack. *WRKY53* is directly regulated by MEKK1 activity that not only binds to the *WRKY53* promoter, but also directly phosphorylates WRKY53. In addition, AD, a novel DNA-binding kinase also binds directly to the *WRKY53* promoter. WRKY53 is responsible for the induction of many SAGs, including the vacuolar protease SAG12. Since the transcription of *SAG12* is salicylic acid-dependent, WRKY53 may be regulated by SA signaling. WRKY53 also directly promotes transcription of *WRKY6*, a senescence-promoting transcription factor, and indirectly represses *WRKY70*, a senescence repressor.

Figure 1.6. The role of hormone and sugar signaling during senescence.

Hormones regulate the induction of senescence by responding to internal biosensors, which monitor nutrients and oxidative stress, and by signaling to neighboring cells. A) Cytokinin, a potent repressor of senescence, functions via many receptors, including histidine kinase 3 (AHK3), and is actively degraded by cytokinin oxidase. B) This repression is modulated by sugar sensors including hexokinase 1 (HXK). C) At least four major hormones promote senescence by activating transcription of SAGS through predominantly unknown mechanisms. These hormones respond to internal stimuli, including sugar levels, nutrient sensors, and oxidative stress, or to external stimuli. i) Jasmonic acid may function via the well-studied Coi1-SCF complex. ii) Salicylic acid functions via NPR1-mediated SAR-pathway components to activate transcription of defense/PCD, and senescence-associated genes (SAGs). iii) ABA signaling, perhaps via the G-coupled receptor GCR2, and ABI1/ABI2, promotes reactive oxygen species. iv) Mutant analysis suggests that ethylene functions via the OLD genes and EIN3 receptor. As previously reported during pathogen defense, the ethylene and jasmonic acid signaling pathways may converge at ethylene response factors such as ERF1. In addition, proteins are targeted for degradation via the hormone-mediated ubiquitin proteasome degradation pathway.

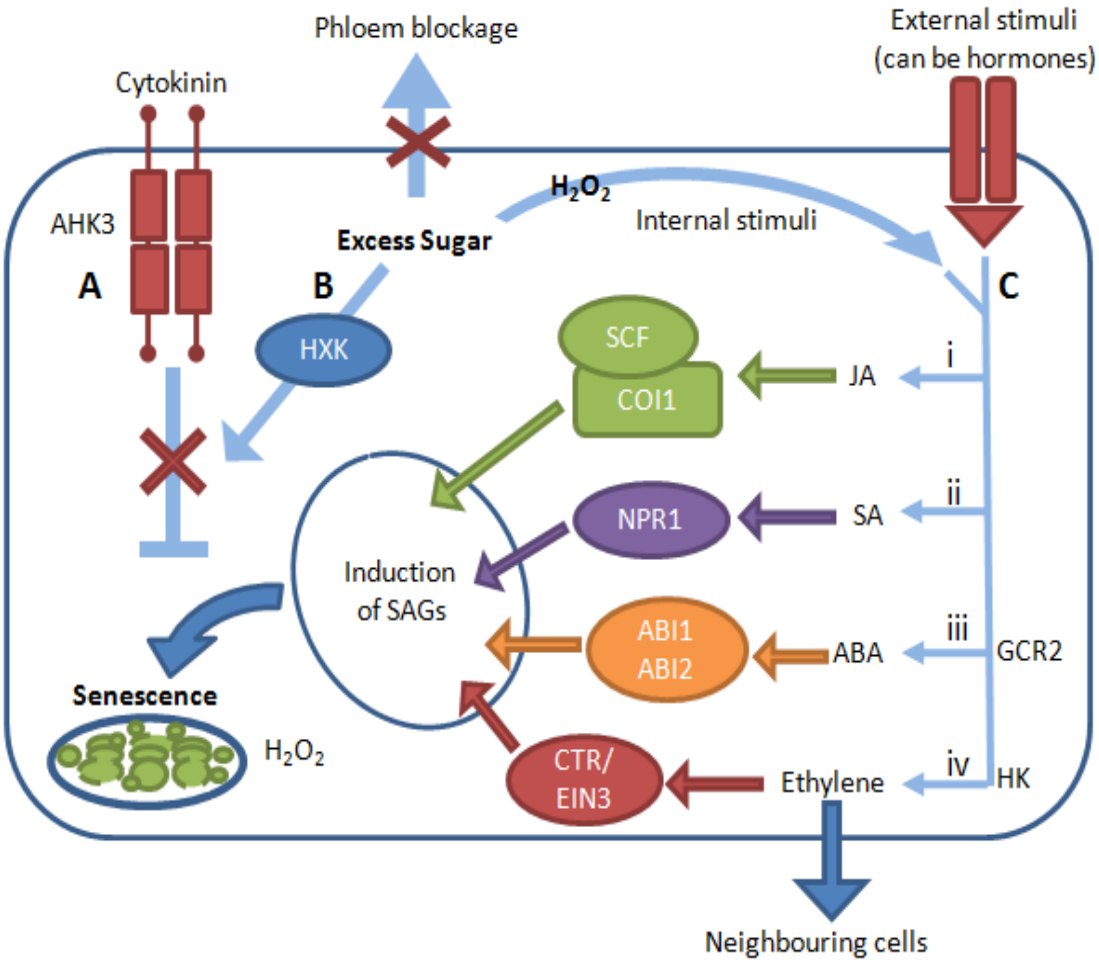
Phloem blockage
External stimuli
(can be hormones)
Cytokinin
AHK3
A
B
Excess Sugar
H_2O_2
Internal stimuli
C
HXK
SCF
COI1
JA
i
NPR1
SA
ii
Induction
of SAGs
ABI1
ABI2
ABA
iii
GCR2
Senescence
H_2O_2
CTR/
EIN3
Ethylene
iv
HK
Neighbouring cells

Figure 1.7. Alterations in peroxisomal biochemistry are integral to senescence.

A) The jasmonate precursor 12-oxo-phytodienoic acid (OPDA), produced in the chloroplast and cytosol, is imported into the peroxisome where it is converted to jasmonic acid via OPR3 and β-oxidation enzymes, including thiolase (KAT2). B) During senescence, membrane lipids from degradation of the chloroplast and thylakoid membranes, enter the β-oxidation cycle producing acetyl-CoA. C) Following up-regulation of the glyoxysomal enzymes, malate synthase (MS) and isocitrate lyase (IL), acetyl-CoA can enter the glyoxylate cycle, producing metabolites for gluconeogensis. D) Phytanic acid, a toxic by-product of chlorophyll degradation, may be converted to pristanic acid via α-oxidation in the peroxisome, after which it can enter the β-oxidation cycle. E) The enzymes involved in photorespiration (GLO and HPR) are down-regulated as chloroplast function ceases. F) Urate oxidase and xanthine oxidase, which function in purine degradation, generate hydrogen peroxide (H_2O_2), as do peroxisomal superoxidise dismutases, MnSOD and CuSOD. G) Catalase, which would normally degrade the excess H_2O_2, is down-regulated, leading to an increase in reactive-oxygen species that leach into the cytosol and degrade biomolecules.

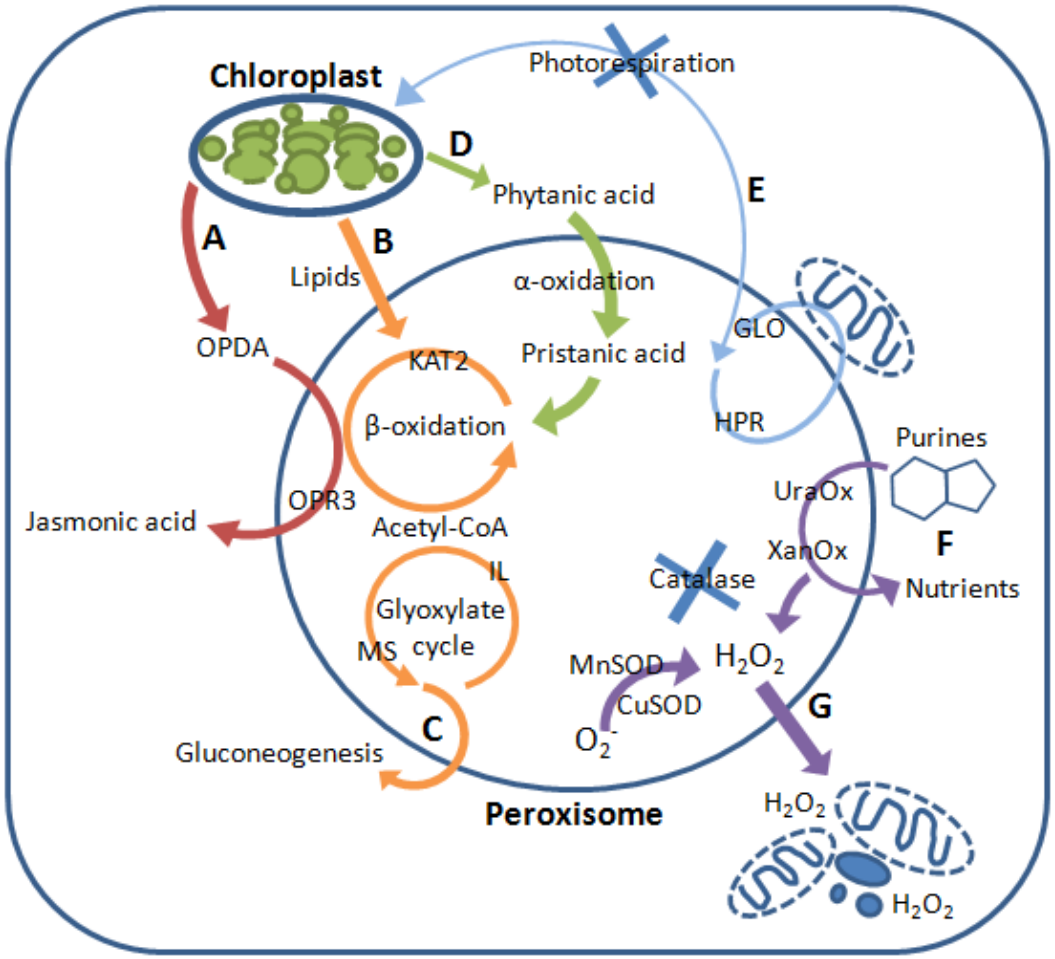
Chloroplast
Photorespiration
D
Phytanic acid
E
A
B
Lipids
α-oxidation
OPDA
KAT2
Pristanic acid
GLO
β-oxidation
HPR
Purines
UraOx
OPR3
Jasmonic acid
Acetyl-CoA
XanOx
F
IL
Catalase
Nutrients
Glyoxylate
MS cycle
MnSOD
H_2O_2
CuSOD
O_2^-
G
C
Gluconeogenesis
Peroxisome
H_2O_2
H_2O_2

Literature cited

1. Clark, S.L., 1957, Cellular differentiation in the kidneys of newborn mice studied with the electron microscope. J Biophys Biochem Cyto. **3**: 349-&.
2. Bassham, D.C., M. Laporte, F. Marty, Y. Moriyasu, Y. Ohsumi, L.J. Olsen, and K. Yoshimoto, 2006, Autophagy in development and stress responses of plants. Autophagy. **2**: 2-11.
3. Scott, R.C., O. Schuldiner, and T.P. Neufeld, 2004, Role and regulation of starvation-induced autophagy in the *Drosophila* fat body. Dev Cell. **7**: 167-178.
4. Abeliovich, A. and D.J. Klionsky, 2001, Autophagy in yeast: Mechanistic insights and physiological function. Microbiol Mol Biol Rev. **65**: 463-479.
5. Yorimitsu, T. and D.J. Klionsky, 2005, Autophagy: molecular machinery for self-eating. Cell Death Differ. **12**: 1542-1552.
6. Smalle, J. and R.D. Vierstra, 2004, The ubiquitin 26S proteasome proteolytic pathway. Annu Rev Plant Biol. **55**: 555-590.
7. Sakai, Y., M. Oku, I.J. van der Klei, and J. Kiel, 2006, Pexophagy: Autophagic degradation of peroxisomes. Biochim Biophys Acta-Mol Cell Res. **1763**: 1767-1775.
8. Diaz-Troya, S., M.E. Perez-Perez, F.J. Florencio, and J.L. Crespo, 2008, The role of TOR in autophagy regulation from yeast to plants and mammals. Autophagy. **4**: 851-865.
9. Klionsky, D.J., 2007, Autophagy: from phenomenology to molecular understanding in less than a decade. Nat Rev Mol Cell Biol. **8**: 931-937.
10. Samara, C. and N. Tavernarakis, 2008, Autophagy and cell death in *Caenorhabditis elegans*. Curr Pharm Design. **14**: 97-115.
11. Melendez, A., Z. Tallóczy, M. Seaman, E.-L. Eskelinen, D.H. Hall, and B. Levine, 2003, Autophagy genes are essential for dauer development and life-span extension in *C.elegans*. Science. **301**: 1387-1391.
12. Melendez, A. and T.P. Neufeld, 2008, The cell biology of autophagy in metazoans: a developing story. Development. **135**: 2347-2360.
13. Larsen, K.E. and D. Sulzer, 2002, Autophagy in neurons: a review. Histol Histopath. **17**: 897-908.
14. Kuma, A., M. Hatano, M. Matsui, A. Yamamoto, H. Nakaya, T. Yoshimori, Y. Ohsumi, T. Tokuhisa, and N. Mizushima, 2004, The role of autophagy during the early neonatal starvation period. Nature. **432**: 1032-1036.
15. Otto, G.P., M.Y. Wu, N. Kazgan, O.R. Anderson, and R.H. Kessin, 2003, Macroautophagy is required for multicellular development of the social amoeba *Dictyostelium discoideum*. J Biol Chem. **278**: 17636-17645.
16. Mizushima, N., B. Levine, A.M. Cuervo, and D.J. Klionsky, 2008, Autophagy fights disease through cellular self-digestion. Nature. **451**: 1069-1075.
17. Botti, J., M. Djavaheri-Mergny, Y. Pilatte, and P. Codogno, 2006, Autophagy signaling and the cogwheels of cancer. Autophagy. **2**: 67-73.
18. Levine, B., 2005, Eating oneself and uninvited guests: Autophagy-related pathways in cellular defense. Cell. **120**: 159-162.

19. Nixon, R.A., 2007, Autophagy, amyloidogenesis and Alzheimer disease. J Cell Sci. **120**: 4081-4091.
20. Liu, Y., M. Schiff, K. Czymmek, Z. Talloczy, B. Levine, and S.P. Dinesh-Kumar, 2005, Autophagy regulates programmed cell death during the plant innate immune response. Cell. **121**: 567-577.
21. Patel, S. and S.P. Dinesh-Kumar, 2008, Arabidopsis ATG6 is required to limit the pathogen-associated cell death response. Autophagy. **4**: 20-27.
22. Harrison-Lowe, N.J. and L.J. Olsen, 2008, Autophagy Protein 6 (ATG6) is required for pollen germination in *Arabidopsis thaliana*. Autophagy. **4**: 339 - 348
23. Qin, G., et al., 2007, Arabidopsis AtBECLIN 1/AtAtg6/AtVps30 is essential for pollen germination and plant development. Cell Res. **17**: 249-263.
24. Fujiki, Y., K. Yoshimoto, and Y. Ohsumi, 2007, An Arabidopsis homolog of yeast ATG6/VPS30 is essential for pollen germination. Plant Physiol. **143**: 1132-1139.
25. Vanderwilden, W., E.M. Herman, and M.J. Chrispeels, 1980, Protein bodies of mung bean cotyledons as autophagic organelles. Proc Natl Acad Sci U S A. **77**: 428-432.
26. Aubert, S., E. Gout, R. Bligny, D. MartyMazars, F. Barrieu, J. Alabouvette, F. Marty, and R. Douce, 1996, Ultrastructural and biochemical characterization of autophagy in higher plant cells subjected to carbon deprivation: Control by the supply of mitochondria with respiratory substrates. J Biol Chem. **133**: 1251-1263.
27. Matsushima, R., Y. Hayashi, K. Yamada, T. Shimada, M. Nishimura, and I. Hara-Nishimura, 2003, The ER body, a novel endoplasmic reticulum-derived structure in Arabidopsis. Plant Cell Physiol. **44**: 661-666.
28. Toyooka, K., T. Okamoto, and T. Minamikawa, 2001, Cotyledon cells of *Vigna mungo* seedlings use at least two distinct autophagic machineries for degradation of starch granules and cellular components. J Biol Chem. **154**: 973-982.
29. Chen, M.H., L.F. Liu, Y.R. Chen, H.K. Wu, and S.M. Yu, 1994, Expression of alpha-amylases, carbohydrate-metabolism, and autophagy in cultured rice cells is coordinately regulated by sugar nutrient. Plant J. **6**: 625-636.
30. Abeliovich, H., W.A. Dunn, J. Kim, and D.J. Klionsky, 2000, Dissection of autophagosome biogenesis into distinct nucleation and expansion steps. J Biol Chem. **151**: 1025-1033.
31. Moriyasu, Y. and Y. Ohsumi, 1996, Autophagy in tobacco suspension-cultured cells in response to sucrose starvation. Plant Physiol. **111**: 1233-1241.
32. Suzuki, K., T. Kirisako, Y. Kamada, N. Mizushima, T. Noda, and Y. Ohsumi, 2001, The pre-autophagosomal structure organized by concerted functions of APG genes is essential for autophagosome formation. Embo Journal. **20**: 5971-5981.
33. Kim, J., W.-P. Huang, P.E. Stromhaug, and D.J. Klionsky, 2002, Convergence of multiple autophagy and cytoplasm to vacuole targeting

components to a perivacuolar membrane compartment prior to de novo vesicle formation. J Biol Chem. **277**: 763-773.
34. Marty, F., 1978, Cytochemical studies on gerl, provacuoles, and vacuoles in root meristematic cells of Euphorbia. Proc Natl Acad Sci U S A. **75**: 852-856.
35. Marty, F., 1999, Plant vacuoles. Plant Cell. **11**: 587-599.
36. Thompson, A.R. and R.D. Vierstra, 2005, Autophagic recycling: lessons from yeast help define the process in plants. Curr Opin Plant Biol. **8**: 165-173.
37. Axe, E.L., S.A. Walker, M. Manifava, P. Chandra, H.L. Roderick, A. Habermann, G. Griffiths, and N.T. Ktistakis, 2008, Autophagosome formation from membrane compartments enriched in phosphatidylinositol 3-phosphate and dynamically connected to the endoplasmic reticulum. J Biol Chem. **182**: 685-701.
38. Yano, K., S. Matsui, T. Tsuchiya, M. Maeshima, N. Kutsuna, S. Hasezawa, and Y. Moriyasu, 2004, Contribution of the plasma membrane and central vacuole in the formation of autolysosomes in cultured tobacco cells. Plant Cell Physiol. **45**: 951-957.
39. Bassham, D.C., 2007, Plant autophagy-more than a starvation response. Curr Opin Plant Biol. **10**: 587-593.
40. Niwa, Y., T. Kato, S. Tabata, M. Seki, M. Kobayashi, K. Shinozaki, and Y. Moriyasu, 2004, Disposal of chloroplasts with abnormal function into the vacuole in *Arabidopsis thaliana* cotyledon cells. Protoplasma. **223**: 229-232.
41. Dice, J.F., 2007, Chaperone-mediated autophagy. Autophagy. **3**: 295-299.
42. Scott, S.V., A. HefnerGravink, K.A. Morano, T. Noda, Y. Ohsumi, and D.J. Klionsky, 1996, Cytoplasm-to-vacuole targeting and autophagy employ the same machinery to deliver proteins to the yeast vacuole. Proc Natl Acad Sci U S A. **93**: 12304-12308.
43. Deprost, D., L. Yao, R. Sormani, M. Moreau, G. Leterreux, M. Nicolai, M. Bedu, C. Robaglia, and C. Meyer, 2007, The Arabidopsis TOR kinase links plant growth, yield, stress resistance and mRNA translation. EMBO Rep. **8**: 864-870.
44. Kamada, Y., T. Funakoshi, T. Shintani, K. Nagano, M. Ohsumi, and Y. Ohsumi, 2000, Tor-mediated induction of autophagy via an Apg1 protein kinase complex. J Biol Chem. **150**: 1507-1513.
45. Carrera, A.C., 2004, TOR signaling in mammals. J Cell Sci. **117**: 4615-4616.
46. Xie, Z.P. and D.J. Klionsky, 2007, Autophagosome formation: Core machinery and adaptations. Nat Cell Biol. **9**: 1102-1109.
47. Backer, J.M., 2008, The regulation and function of Class III PI3Ks: novel roles for Vps34. Biochem J. **410**: 1-17.
48. Juhasz, G., J.H. Hill, Y. Yan, M. Sass, E.H. Baehrecke, J.M. Backer, and T.P. Neufeld, 2008, The class III PI(3)K Vps34 promotes autophagy and endocytosis but not TOR signaling in *Drosophila*. J Biol Chem. **181**: 655-666.

49. Matsuoka, K., D.C. Bassham, N.V. Raikhel, and K. Nakamura, 1995, Different sensitivity to wortmannin of two vacuolar sorting signals indicates the presence of distinct sorting machineries in tobacco cells. J Biol Chem. **130**: 1307-1318.
50. Takatsuka, C., Y. Inoue, K. Matsuoka, and Y. Moriyasu, 2004, 3-methyladenine inhibits autophagy in tobacco culture cells under sucrose starvation conditions. Plant Cell Physiol. **45**: 265-274.
51. Kihara, A., T. Noda, N. Ishihara, and Y. Ohsumi, 2001, Two distinct Vps34 phosphatidylinositol 3-kinase complexes function in autophagy and carboxypeptidase Y sorting in *Saccharomyces cerevisiae*. J Biol Chem. **152**: 519-530.
52. Obara, K., T. Noda, K. Niimi, and Y. Ohsumi, 2008, Transport of phosphatidylinositol 3-phosphate into the vacuole via autophagic membranes in *Saccharomyces cerevisiae*. Genes Cells. **13**: 537-547.
53. Kim, D.H., Y.J. Eu, C.M. Yoo, Y.W. Kim, K.T. Pih, J.B. Jin, S.J. Kim, H. Stenmark, and I. Hwang, 2001, Trafficking of phosphatidylinositol 3-phosphate from the trans-Golgi network to the lumen of the central vacuole in plant cells. Plant Cell. **13**: 287-301.
54. Meijer, H.J. and T. Munnik, 2003, Phospholipid-based signaling in plants. Annu Rev Plant Biol. **54**: 265-306.
55. Obara, K., T. Sekito, K. Niimi, and Y. Ohsumi, 2008, The Atg18-Atg2 complex is recruited to autophagic membranes via phosphatidylinositol 3-phosphate and exerts an essential function. J Biol Chem. **283**: 23972-23980.
56. He, C.C., H. Song, T. Yorimitsu, I. Monastyrska, W.-L. Yen, J.E. Legakis, and D.J. Klionsky, 2006, Recruitment of Atg9 to the preautophagosomal structure by Atg11 is essential for selective autophagy in budding yeast. J Biol Chem. **175**: 925-935.
57. Monastyrska, I., C. He, J.F. Geng, A.D. Hoppe, Z.J. Li, and D.J. Klionsky, 2008, Arp2 links autophagic machinery with the actin cytoskeleton. Mol Biol Cell. **19**: 1962-1975.
58. Su, W., H.J. Ma, C. Liu, J.X. Wu, and J.S. Yang, 2006, Identification and characterization of two rice autophagy associated genes, OsAtg8 and OsAtg4. Mol Biol Rep. **33**: 273-278.
59. Phillips, A.R., A. Suttangkakul, and R.D. Vierstra, 2008, The ATG12-conjugating enzyme ATG10 is essential for autophagic vesicle formation in *Arabidopsis thaliana*. Genetics. **178**: 1339-1353.
60. Yoshimoto, K., H. Hanaoka, S. Sato, T. Kato, S. Tabata, T. Noda, and Y. Ohsumi, 2004, Processing of ATG8s, ubiquitin-like proteins, and their deconjugation by ATG4s are essential for plant autophagy. Plant Cell. **16**: 2967-2983.
61. Doelling, J.H., J.M. Walker, E.M. Friedman, A.R. Thompson, and R.D. Vierstra, 2002, The APG8/12-activating enzyme APG7 is required for proper nutrient recycling and senescence in *Arabidopsis thaliana*. J Biol Chem. **277**: 33105-33114.

62. Contento, A.L., Y. Xiong, and D.C. Bassham, 2005, Visualization of autophagy in Arabidopsis using the fluorescent dye monodansylcadaverine and a GFP-AtATG8e fusion protein. Plant J. **42**: 598-608.
63. Nakatogawa, H., Y. Ichimura, and Y. Ohsumi, 2007, Atg8, a ubiquitin-like protein required for autophagosome formation, mediates membrane tethering and hemifusion. Cell. **130**: 165-178.
64. Moriyasu, Y., M. Hattori, G.Y. Jauh, and J.C. Rogers, 2003, Alpha tonoplast intrinsic protein is specifically associated with vacuole membrane involved in an autophagic process. Plant Cell Physiol. **44**: 795-802.
65. Ishihara, N., M. Hamasaki, S. Yokota, K. Suzuki, Y. Kamada, A. Kihara, T. Yoshimori, T. Noda, and Y. Ohsumi, 2001, Autophagosome requires specific early Sec proteins for its formation and NSF/SNARE for vacuolar fusion. Mol Biol Cell. **12**: 3690-3702.
66. Darsow, T., S.E. Rieder, and S.D. Emr, 1997, A multispecificity syntaxin homologue, Vam3p, essential for autophagic and biosynthetic protein transport to the vacuole. J Biol Chem. **138**: 517-529.
67. Lipka, V., C. Kwon, and R. Panstruga, 2007, SNARE-Ware: The role of SNARE-Domain proteins in plant biology. Annu Rev Cell Dev Biol. **23**: 147-174.
68. Kato, T., M.T. Morita, H. Fukaki, Y. Yamauchi, M. Uehara, M. Niihama, and M. Tasaka, 2002, SGR2, a phospholipase-like protein, and ZIG/SGR4, a SNARE, are involved in the shoot gravitropism of Arabidopsis. Plant Cell. **14**: 33-46.
69. Yano, D., M. Sato, C. Saito, M.H. Sato, M.T. Morita, and M. Tasaka, 2003, A SNARE complex containing SGR3/AtVAM3 and ZIG/VTI11 in gravity-sensing cells is important for Arabidopsis shoot gravitropism. Proc Natl Acad Sci U S A. **100**: 8589-8594.
70. Bassham, D.C. and N.V. Raikhel, 2000, Unique features of the plant vacuolar sorting machinery. Curr Opin Cell Biol. **12**: 491-495.
71. Welters, P., K. Takegawa, S.D. Emr, and M.J. Chrispeels, 1994, AtVPS34, a phosphatidylinositol 3-kinase of *Arabidopsis thaliana*, is an essential protein with homology to a calcium-dependent lipid binding domain. Proc Natl Acad Sci U S A. **91**: 11398-11402.
72. Seay, M.D. and S.P. Dinesh-Kumar, 2005, Life after death - Are autophagy genes involved in cell death and survival during plant innate immune responses? Autophagy. **1**: 185-186.
73. Slavikova, S., G. Shy, Y.L. Yao, R. Giozman, H. Levanony, S. Pietrokovski, Z. Elazar, and G. Galili, 2005, The autophagy-associated Atg8 gene family operates both under favourable growth conditions and under starvation stresses in Arabidopsis plants. J Exp Bot. **56**: 2839-2849.
74. Inoue, Y., T. Suzuki, M. Hattori, K. Yoshimoto, Y. Ohsumi, and Y. Moriyasu, 2006, AtATG genes, homologs of yeast autophagy genes, are involved in constitutive autophagy in Arabidopsis root tip cells. Plant Cell Physiol. **47**: 1641-1652.

75. Xiong, Y., A.L. Contento, and D.C. Bassham, 2005, AtATG18a is required for the formation of autophagosomes during nutrient stress and senescence in *Arabidopsis thaliana*. Plant J. **42**: 535-546.
76. Hanaoka, H., T. Noda, Y. Shirano, T. Kato, H. Hayashi, D. Shibata, S. Tabata, and Y. Ohsumi, 2002, Leaf senescence and starvation-induced chlorosis are accelerated by the disruption of an Arabidopsis autophagy gene. Plant Physiol. **129**: 1181-1193.
77. Thompson, A.R., J.H. Doelling, A. Suttangkakul, and R.D. Vierstra, 2005, Autophagic nutrient recycling in Arabidopsis directed by the ATG8 and ATG12 conjugation pathways. Plant Physiol. **138**: 2097-2110.
78. Weaver, L.M., S.S. Gan, B. Quirino, and R.M. Amasino, 1998, A comparison of the expression patterns of several senescence-associated genes in response to stress and hormone treatment. Plant Mol Biol. **37**: 455-469.
79. Nooden, L.D., J.J. Guiamet, and I. John, 1997, Senescence mechanisms. Physiol Plant. **101**: 746-753.
80. Wingler, A., A. von Schaewen, R.C. Leegood, P.J. Lea, and W.P. Quick, 1998, Regulation of leaf senescence by cytokinin, sugars, and light - Effects on NADH-dependent hydroxypyruvate reductase. Plant Physiol. **116**: 329-335.
81. Hensel, L.L., V. Grbic, D.A. Baumgarten, and A.B. Bleecker, 1993, Developmental and age-related processes that influence the longevity and senescence of photosynthetic tissues in Arabidoposis. Plant Cell. **5**: 553-564.
82. Lim, P.O., H.J. Kim, and H.G. Nam, 2007, Leaf senescence. Annu Rev Plant Biol. **58**: 115-136.
83. Liu, J., Y.H. Wu, J.J. Yan, Y.D. Liu, and F.F. Shen, 2008, Protein degradation and nitrogen remobilization during leaf senescence. J Plant Biol. **51**: 11-19.
84. Reape, T.J., E.M. Molony, and P.F. McCabe, 2008, Programmed cell death in plants: distinguishing between different modes. J Exp Bot. **59**: 435-444.
85. Bleecker, A.B. and S.E. Patterson, 1997, Last exit: Senescence, abscission, and meristem arrest in Arabidopsis. Plant Cell. **9**: 1169-1179.
86. Beers, E.P., 1997, Programmed cell death during plant growth and development. Cell Death Differ. **4**: 649-661.
87. van Doorn, W.G. and E.J. Woltering, 2005, Many ways to exit? Cell death categories in plants. Trends Plant Sci. **10**: 117-122.
88. Greening, M.T., F.J. Butterfield, and N. Harris, 1982, Chloroplast ultrastructure during denescence and regreening of flax cotyledons. New Phytol. **92**: 279-&.
89. Zavaleta-Mancera, H.A., B.J. Thomas, H. Thomas, and I.M. Scott, 1999, Regreening of senescent Nicotiana leaves II. Redifferentiation of plastids. J Exp Bot. **50**: 1683-1689.
90. Zavaleta-Mancera, H.A., K.A. Franklin, H.J. Ougham, H. Thomas, and I.M. Scott, 1999, Regreening of senescent Nicotiana leaves I. Reappearance

of NADPH-protochlorophyllide oxidoreductase and light-harvesting chlorophyll a/b-binding protein. J Exp Bot. **50**: 1677-1682.
91. Thomas, H., H.J. Ougham, C. Wagstaff, and A.D. Stead, 2003, Defining senescence and death. J Exp Bot. **54**: 1127-1132.
92. van Doorn, W.G. and E.J. Woltering, 2004, Senescence and programmed cell death: substance or semantics? J Exp Bot. **55**: 2147-2153.
93. Coupe, S.A., L.M. Watson, D.J. Ryan, T.T. Pinkney, and J.R. Eason, 2004, Molecular analysis of programmed cell death during senescence in *Arabidopsis thaliana* and *Brassica oleracea*: cloning broccoli LSD1, Bax inhibitor and serine palmitoyltransferase homologues. J Exp Bot. **55**: 59-68.
94. Hoertensteiner, S., 2006, Chlorophyll degradation during senescence. Annu Rev Plant Biol. **57**: 55-77.
95. Gregersen, P.L. and P.B. Holm, 2007, Transcriptome analysis of senescence in the flag leaf of wheat (*Triticum aestivum* L.). Plant Biotechnol J. **5**: 192-206.
96. Gregersen, P.L., P.B. Holm, and K. Krupinska, 2008, Leaf senescence and nutrient remobilisation in barley and wheat. Plant Biol. **10**: 37-49.
97. Zentgraf, U., J. Jobst, D. Kolb, and D. Rentsch, 2004, Senescence-related gene expression profiles of rosette leaves of *Arabidopsis thaliana*: Leaf age versus plant age. Plant Biol. **6**: 178-183.
98. Guo, Y., Z. Cai, and S. Gan, 2004, Transcriptome of Arabidopsis leaf senescence. Plant Cell Environ. **27**: 521-549.
99. Kumar, N., G.C. Srivastava, and K. Dixit, 2008, Hormonal regulation of flower senescence in roses (*Rosa hybrida* L.). Plant Growth Regul. **55**: 65-71.
100. Simeonova, E., A. Sikora, M. Charzynska, and A. Mostowska, 2000, Aspects of programmed cell death during leaf senescence of mono- and dicotyledonous plants. Protoplasma. **214**: 93-101.
101. Austin, J.R., E. Frost, P.A. Vidi, F. Kessler, and L.A. Staehelin, 2006, Plastoglobules are lipoprotein subcompartments of the chloroplast that are permanently coupled to thylakoid membranes and contain biosynthetic enzymes. Plant Cell. **18**: 1693-1703.
102. Inada, N., A. Sakai, H. Kuroiwa, and T. Kuroiwa, 1998, Three-dimensional analysis of the senescence program in rice (*Oryza sativa* L.) coleoptiles - Investigations by fluorescence microscopy and electron microscopy. Planta. **206**: 585-597.
103. Chiba, A., H. Ishida, N.K. Nishizawa, A. Makino, and T. Mae, 2003, Exclusion of ribulose-1,5-bisphosphate carboxylase/oxygenase from chloroplasts by specific bodies in naturally senescing leaves of wheat. Plant Cell Physiol. **44**: 914-921.
104. Ishida, H., K. Yoshimoto, M. Izumi, D. Reisen, Y. Yano, A. Makino, Y. Ohsumi, M.R. Hanson, and T. Mae, 2008, Mobilization of rubisco and stroma-localized fluorescent proteins of chloroplasts to the vacuole by an ATG gene-dependent autophagic process. Plant Physiol. **148**: 142-155.

105. Kato, Y., S. Murakami, Y. Yamamoto, H. Chatani, Y. Kondo, T. Nakano, A. Yokota, and F. Sato, 2004, The DNA-binding protease, CND41, and the degradation of ribulose-1,5-bisphosphate carboxylase/oxygenase in senescent leaves of tobacco. Planta. **220**: 97-104.
106. Lin, J.F. and S.H. Wu, 2004, Molecular events in senescing Arabidopsis leaves. Plant J. **39**: 612-628.
107. Zimmermann, P., C. Heinlein, G. Orendi, and U. Zentgraf, 2006, Senescence-specific regulation of catalases in *Arabidopsis thaliana* (L.) Heynh. Plant Cell Environ. **29**: 1049-1060.
108. Thompson, J.E., R.L. Legge, and R.F. Barber, 1987, The role of free-radicals in senescence and wounding. New Phytol. **105**: 317-344.
109. Prochazkova, D. and N. Wilhelmova, 2007, Leaf senescence and activities of the antioxidant enzymes. Biol Plant. **51**: 401-406.
110. Thompson, J., C. Taylor, and T.W. Wang, 2000, Altered membrane lipase expression delays leaf senescence. Biochem Soc Trans. **28**: 775-777.
111. del Rio, L.A., G.M. Pastori, J.M. Palma, L.M. Sandalio, F. Sevilla, F.J. Corpas, A. Jimenez, E. Lopez-Huertas, and J.A. Hernandez, 1998, The activated oxygen role of peroxisomes in senescence. Plant Physiol. **116**: 1195-1200.
112. Rojo, E., J. Zouhar, C. Carter, V. Kovaleva, and N.V. Raikhel, 2003, A unique mechanism for protein processing and degradation in *Arabidopsis thaliana*. Proc Natl Acad Sci U S A. **100**: 7389-7394.
113. Wittenbach, V.A., W. Lin, and R.R. Hebert, 1982, Vacuolar localization of proteases and degradation of chloroplasts in mesophyll protoplasts from senescing primary wheat leaves. Plant Physiol. **69**: 98-102.
114. Roberts, I.N., S. Passeron, and A.J. Barneix, 2006, The two main endoproteases present in dark-induced senescent wheat leaves are distinct subtilisin-like proteases. Planta. **224**: 1437-1447.
115. Donnison, I.S., A.P. Gay, H. Thomas, K.J. Edwards, D. Edwards, C.L. James, A.M. Thomas, and H.J. Ougham, 2007, Modification of nitrogen remobilization, grain fill and leaf senescence in maize (*Zea mays*) by transposon insertional mutagenesis in a protease gene. New Phytol. **173**: 481-494.
116. Muntz, K., 2007, Protein dynamics and proteolysis in plant vacuoles. J Exp Bot. **58**: 2391-2407.
117. Bhalerao, R., et al., 2003, Gene expression in autumn leaves. Plant Physiol. **131**: 430-442.
118. Liu, L., Y. Zhou, G. Zhou, R.J. Ye, L. Zhao, X.H. Li, and Y.J. Lin, 2008, Identification of early senescence-associated genes in rice flag leaves. Plant Mol Biol. **67**: 37-55.
119. Lohman, K.N., S.S. Gan, M.C. John, and R.M. Amasino, 1994, Molecular analysis of natural leaf senescence in *Arabidopsis thaliana*. Physiol Plant. **92**: 322-328.
120. He, Y.H., W.N. Tang, J.D. Swain, A.L. Green, T.P. Jack, and S.S. Gan, 2001, Networking senescence-regulating pathways by using Arabidopsis enhancer trap lines. Plant Physiol. **126**: 707-716.

121. Buchanan-Wollaston, V., S. Earl, E. Harrison, E. Mathas, S. Navabpour, T. Page, and D. Pink, 2003, The molecular analysis of leaf senescence - a genomics approach. Plant Biotechnol J. **1**: 3-22.
122. Chen, W.Q., et al., 2002, Expression profile matrix of Arabidopsis transcription factor genes suggests their putative functions in response to environmental stresses. Plant Cell. **14**: 559-574.
123. Wang, D.Y., Q. Li, K.M. Cui, and Y.X. Zhu, 2008, PPF1 may suppress plant senescence via activating TFL1 in transgenic Arabidopsis plants. J Integr Plant Biol. **50**: 475-483.
124. Buchanan-Wollaston, V., et al., 2005, Comparative transcriptome analysis reveals significant differences in gene expression and signalling pathways between developmental and dark/starvation-induced senescence in Arabidopsis. Plant J. **42**: 567-585.
125. Van der Graaff, E., R. Schwacke, A. Schneider, M. Desimone, U.I. Flugge, and R. Kunze, 2006, Transcription analysis of arabidopsis membrane transporters and hormone pathways during developmental and induced leaf senescence. Plant Physiol. **141**: 776-792.
126. Yang, S.H., T. Berberich, H. Sano, and T. Kusano, 2001, Specific association of transcripts of tbzF and tbz17, tobacco genes encoding basic region leucine zipper-type transcriptional activators, with guard cells of senescing leaves and/or flowers. Plant Physiol. **127**: 23-32.
127. Breeze, E., E. Harrison, T. Page, N. Warner, C. Shen, C. Zhang, and V. Buchanan-Wollaston, 2008, Transcriptional regulation of plant senescence: from functional genomics to systems biology. Plant Biol. **10**: 99-109.
128. Yoon, H.K., S.G. Kim, S.Y. Kim, and C.M. Park, 2008, Regulation of leaf senescence by NTL9-mediated osmotic stress signaling in Arabidopsis. Mol Cells. **25**: 438-445.
129. Guo, Y.F. and S.S. Gan, 2006, AtNAP, a NAC family transcription factor, has an important role in leaf senescence. Plant J. **46**: 601-612.
130. Eulgem, T. and I.E. Somssich, 2007, Networks of WRKY transcription factors in defense signaling. Curr Opin Plant Biol. **10**: 366-371.
131. Robatzek, S. and I.E. Somssich, 2001, A new member of the Arabidopsis WRKY transcription factor family, AtWRKY6, is associated with both senescence- and defence-related processes. Plant J. **28**: 123-133.
132. Robatzek, S. and I.E. Somssich, 2002, Targets of AtWRKY6 regulation during plant senescence and pathogen defense. Genes Dev. **16**: 1139-1149.
133. Cao, H., J. Glazebrook, J.D. Clarke, S. Volko, and X.N. Dong, 1997, The Arabidopsis NPR1 gene that controls systemic acquired resistance encodes a novel protein containing ankyrin repeats. Cell. **88**: 57-63.
134. Ulker, B., M.S. Mukhtar, and I.E. Somssich, 2007, The WRKY70 transcription factor of Arabidopsis influences both the plant senescence and defense signaling pathways. Planta. **226**: 125-137.

135. Hinderhofer, K. and U. Zentgraf, 2001, Identification of a transcription factor specifically expressed at the onset of leaf senescence. Planta. **213**: 469-473.
136. Miao, Y., T. Laun, P. Zimmermann, and U. Zentgraf, 2004, Targets of the WRKY53 transcription factor and its role during leaf senescence in Arabidopsis. Plant Mol Biol. **55**: 853-867.
137. Miao, Y., T.M. Laun, A. Smykowski, and U. Zentgraf, 2007, Arabidopsis MEKK1 can take a short cut: it can directly interact with senescence-related WRKY53 transcription factor on the protein level and can bind to its promoter. Plant Mol Biol. **65**: 63-76.
138. Miao, Y., A. Smykowski, and U. Zentgraf, 2008, A novel upstream regulator of WRKY53 transcription during leaf senescence in *Arabidopsis thaliana*. Plant Biol. **10**: 110-120.
139. Leon, P. and J. Sheen, 2003, Sugar and hormone connections. Trends Plant Sci. **8**: 110-116.
140. Pourtau, N., R. Jennings, E. Pelzer, J. Pallas, and A. Wingler, 2006, Effect of sugar-induced senescence on gene expression and implications for the regulation of senescence in Arabidopsis. Planta. **224**: 556-568.
141. Chen, H.J., W.C. Hou, W.N. Jane, and Y.H. Lin, 2000, Isolation and characterization of an isocitrate lyase gene from senescent leaves of sweet potato (*Ipomoea batatas* cv. Tainong 57). J Plant Physiol. **157**: 669-676.
142. Michels, P.A., J. Moyersoen, H. Krazy, N. Galland, M. Herman, and V. Hannaert, 2005, Peroxisomes, glyoxysomes and glycosomes (review). Mol Mem Biol. **22**: 133-145.
143. Jongebloed, U., J. Szederkenyi, K. Hartig, C. Schobert, and E. Komor, 2004, Sequence of morphological and physiological events during natural ageing and senescence of a castor bean leaf: sieve tube occlusion and carbohydrate back-up precede chlorophyll degradation. Physiol Plant. **120**: 338-346.
144. Veyres, N., et al., 2008, The Arabidopsis sweetie mutant is affected in carbohydrate metabolism and defective in the control of growth, development and senescence. Plant J. **55**: 665-686.
145. Jang, J.C., P. Leon, L. Zhou, and J. Sheen, 1997, Hexokinase as a sugar sensor in higher plants. Plant Cell. **9**: 5-19.
146. Xiao, W.Y., J. Sheen, and J.C. Jang, 2000, The role of hexokinase in plant sugar signal transduction and growth and development. Plant Mol Biol. **44**: 451-461.
147. Quirino, B.F., W.D. Reiter, and R.D. Amasino, 2001, One of two tandem Arabidopsis genes homologous to monosaccharide transporters is senescence-associated. Plant Mol Biol. **46**: 447-457.
148. Norholm, M.H.H., H.H. Nour-Eldin, P. Brodersen, J. Mundy, and B.A. Halkier, 2006, Expression of the Arabidopsis high-affinity hexose transporter STP13 correlates with programmed cell death. FEBS Lett. **580**: 2381-2387.

149. Rolland, F., B. Moore, and J. Sheen, 2002, Sugar sensing and signaling in plants. Plant Cell. **14**: S185-S205.
150. Jing, H.C., et al., 2008, Early leaf senescence is associated with an altered cellular redox balance in Arabidopsis cpr5/old1 mutants. Plant Biol. **10**: 85-98.
151. Jing, H.C., L. Anderson, M.J.G. Sturre, J. Hille, and P.P. Dijkwel, 2007, Arabidopsis CPR5 is a senescence-regulatory gene with pleiotropic functions as predicted by the evolutionary theory of senescence. J Exp Bot. **58**: 3885-3894.
152. Yoshida, S., M. Ito, I. Nishida, and A. Watanabe, 2002, Identification of a novel gene HYS1/CPR5 that has a repressive role in the induction of leaf senescence and pathogen-defence responses in Arabidopsis thaliana. Plant J. **29**: 427-437.
153. Wingler, A. and T. Roitsch, 2008, Metabolic regulation of leaf senescence: interactions of sugar signalling with biotic and abiotic stress responses. Plant Biol. **10**: 50-62.
154. Gan, S.S. and R.M. Amasino, 1995, Inhibition of leaf senescence by autoregulated production of cytokinin. Science. **270**: 1986-1988.
155. Kim, H.J., H. Ryu, S.H. Hong, H.R. Woo, P.O. Lim, I.C. Lee, J. Sheen, H.G. Nam, and I. Hwang, 2006, Cytokinin-mediated control of leaf longevity by AHK3 through phosphorylation of ARR2 in Arabidopsis. Proc Natl Acad Sci U S A. **103**: 814-819.
156. Lopez, M.A., G. Bannenberg, and C. Castresana, 2008, Controlling hormone signaling is a plant and pathogen challenge for growth and survival. Curr Opin Plant Biol. **11**: 420-427.
157. Hirayama, T. and K. Shinozaki, 2007, Perception and transduction of abscisic acid signals: keys to the function of the versatile plant hormone ABA. Trends Plant Sci. **12**: 343-351.
158. Hung, K.T. and C.H. Kao, 2004, Hydrogen peroxide is necessary for abscisic acid-induced senescence of rice leaves. J Plant Physiol. **161**: 1347-1357.
159. Zhang, H.B., Y.H. Yang, Z.J. Zhang, J. Chen, X.C. Wang, and R.F. Huang, 2008, Expression of the ethylene response factor gene TSRF1 enhances abscisic acid responses during seedling development in tobacco. Planta. **228**: 777-787.
160. Morris, K., S.A.H. Mackerness, T. Page, C.F. John, A.M. Murphy, J.P. Carr, and V. Buchanan-Wollaston, 2000, Salicylic acid has a role in regulating gene expression during leaf senescence. Plant J. **23**: 677-685.
161. Miao, Y. and U. Zentgraf, 2007, The antagonist function of Arabidopsis WRKY53 and ESR/ESP in leaf senescence is modulated by the jasmonic and salicylic acid equilibrium. Plant Cell. **19**: 819-830.
162. Grbic, V. and A.B. Bleecker, 1995, Ethylene regulates the timing of leaf senescence in Arabidopsis. Plant J. **8**: 595-602.
163. Jing, H.C., J.H.M. Schippers, J. Hille, and P.P. Dijkwei, 2005, Ethylene-induced leaf senescence depends on age-related changes and OLD genes in Arabidopsis. J Exp Bot. **56**: 2915-2923.

164. Oh, S.A., J.H. Park, G.I. Lee, K.H. Paek, S.K. Park, and H.G. Nam, 1997, Identification of three genetic loci controlling leaf senescence in *Arabidopsis thaliana*. Plant J. **12**: 527-535.
165. Lorenzo, O., R. Piqueras, J.J. Sanchez-Serrano, and R. Solano, 2003, ETHYLENE RESPONSE FACTOR1 integrates signals from ethylene and jasmonate pathways in plant defense. Plant Cell. **15**: 165-178.
166. Devoto, A. and J.G. Turner, 2003, Regulation of jasmonate-mediated plant responses in Arabidopsis. Ann Bot. **92**: 329-337.
167. Ueda, J. and J. Kato, 1980, Isolation and identification of a senescence-promoting substance from Wormwood (*Artemisia-Absinthium* L). Plant Physiol. **66**: 246-249.
168. He, Y.H., H. Fukushige, D.F. Hildebrand, and S.S. Gan, 2002, Evidence supporting a role of jasmonic acid in Arabidopsis leaf senescence. Plant Physiol. **128**: 876-884.
169. Katsir, L., H.S. Chung, A.J.K. Koo, and G.A. Howe, 2008, Jasmonate signaling: a conserved mechanism of hormone sensing. Curr Opin Plant Biol. **11**: 428-435.
170. Kong, Z.S., M.N. Li, W.Q. Yang, W.Y. Xu, and Y.B. Xue, 2006, A novel nuclear-localized CCCH-type zinc finger protein, OsDOS, is involved in delaying leaf senescence in rice. Plant Physiol. **141**: 1376-1388.
171. Delker, C., B.K. Zolman, O. Miersch, and C. Wasternack, 2007, Jasmonate biosynthesis in *Arabidopsis thaliana* requires peroxisomal beta-oxidation enzymes - Additional proof by properties of pex6 and aim1. Phytochem. **68**: 1642-1650.
172. Castillo, M.C. and J. Leon, 2008, Expression of the beta-oxidation gene 3-ketoacyl-CoA thiolase 2(KAT2) is required for the timely onset of natural and dark-induced leaf senescence in Arabidopsis. J Exp Bot. **59**: 2171-2179.
173. Spartz, A.K. and W.M. Gray, 2008, Plant hormone receptors: new perceptions. Genes Dev. **22**: 2139-2148.
174. Zhang, T., Y. Liu, T. Yang, L. Zhang, S. Xu, L. Xue, and L. An, 2006, Diverse signals converge at MAPK cascades in plant. Plant Physiol Biochem. **44**: 274-283.
175. To, J.P.C. and J.J. Kieber, 2008, Cytokinin signaling: two-components and more. Trends Plant Sci. **13**: 85-92.
176. Zhu, Z.Q. and H.W. Guo, 2008, Genetic basis of ethylene perception and signal transduction in Arabidopsis. J Integr Plant Biol. **50**: 808-815.
177. Kazan, K. and J.M. Manners, 2008, Jasmonate signaling: Toward an integrated view. Plant Physiol. **146**: 1459-1468.
178. Gazzarrini, S. and P. McCourt, 2003, Cross-talk in plant hormone signalling: What arabidopsis mutants are telling us. Ann Bot. **91**: 605-612.
179. Reumann, S., et al., 2007, Proteome analysis of Arabidopsis leaf peroxisomes reveals novel targeting peptides, metabolic pathways, and defense mechanisms. Plant Cell. **19**: 3170-3193.

180. Poirier, Y., V.D. Antonenkov, T. Glumoff, and J.K. Hiltunen, 2006, Peroxisomal beta-oxidation--a metabolic pathway with multiple functions. Biochim Biophys Acta. **1763**: 1413-1426.
181. Turner, J.G., C. Ellis, and A. Devoto, 2002, The jasmonate signal pathway. Plant Cell. **14**: S153-S164.
182. Hamberg, M., A. Sanz, and C. Castresana, 1999, alpha-oxidation of fatty acids in higher plants - Identification of a pathogen-inducible oxygenase (PIOX) as an alpha-dioxygenase and biosynthesis of 2-hydroperoxylinolenic acid. J Biol Chem. **274**: 24503-24513.
183. Wierzbicki, A.S., 2007, Peroxisomal disorders affecting phytanic acid alpha-oxidation: a review. Biochem Soc Trans. **35**: 881-886.
184. Abeles, F.B., L.J. Dunn, P. Morgens, A. Callahan, R.E. Dinterman, and J. Schmidt, 1988, Induction of 33-Kd and 60-Kd peroxidases during ethylene-induced senescence of cucumber cotyledons. Plant Physiol. **87**: 609-615.
185. Olsen, L.J. and J.J. Harada, 1995, Peroxisomes and their assembly in higher-plants. Annu Rev Plant Physiol Plant Molec Biol. **46**: 123-146.
186. Pastori, G.M. and L.A. delRio, 1997, Natural senescence of pea leaves - An activated oxygen-mediated function for peroxisomes. Plant Physiol. **113**: 411-418.
187. Navabpour, S., K. Morris, R. Allen, E. Harrison, S. A-H-Mackerness, and V. Buchanan-Wollaston, 2003, Expression of senescence-enhanced genes in response to oxidative stress. J Exp Bot. **54**: 2285-2292.
188. Brodersen, P., M. Petersen, H.M. Pike, B. Olszak, S. Skov, N. Odum, L.B. Jorgensen, R.E. Brown, and J. Mundy, 2002, Knockout of Arabidopsis ACCELERATED-CELL-DEATH11 encoding a sphingosine transfer protein causes activation of programmed cell death and defense. Genes Dev. **16**: 490-502.
189. Overmyer, K., M. Brosche, and J. Kangasjarvi, 2003, Reactive oxygen species and hormonal control of cell death. Trends Plant Sci. **8**: 335-342.
190. Trobacher, C.P., A. Senatore, and J.S. Greenwood, 2006, Masterminds or minions? Cysteine proteinases in plant programmed cell death. Can J Bot-Rev Can Bot. **84**: 651-667.
191. Aleksandrushkina, N.I., V.A. Zamyatnina, L.E. Bakeeva, A.V. Seredina, E.G. Smirnova, L.S. Yaguzhinsky, and B.F. Vanyushin, 2004, Apoptosis in wheat seedlings grown under normal daylight. Biochem-Moscow. **69**: 285-294.
192. Collazo, C., O. Chacon, and O. Borras, 2006, Programmed cell death in plants resembles apoptosis in animals. Biotec Aplic. **23**: 1-10.
193. Xiang, Y., A.L. Contento, and D. Bassham, 2007, Disruption of autophagy results in constitutive oxidative stress in Arabidopsis. Autophagy. **3**: 257-258.

Chapter 2

Autophagy Protein 6 (ATG6) is Required for Pollen Germination in *Arabidopsis thaliana*

Abstract

Autophagy is an intracellular recycling pathway that extends the life of an organism in hostile growth conditions. Yeast autophagy protein 6 (Atg6/Vps30) is required for formation of autophagosomes during starvation. Here we show that the Arabidopsis *ATG6* homolog is an essential gene required for pollen germination and plant development. Analysis of multiple *atg6* lines of Arabidopsis containing T-DNA inserts indicated that the homozygous *atg6* plants were never recovered and heterozygous plants displayed variable growth phenotypes. *atg6* heterozygous pollen test crosses confirmed that a male gametophyte defect was responsible for the loss of homozygous segregants. PCR performed on the pollen samples showed that the T-DNA was present, suggesting the defect occurs after microsporogenesis. Furthermore, plants homozygous for *qrt1(-/-)* and heterozygous for *atg6* produced tetrads that were trinucleate and stained uniformly with Alexander stain. *qrt1(-/-)/atg6(+/-)* pollen grains exhibited greatly decreased germination efficiencies *in vitro*. In addition, defective pollen grains were positive for GUS activity (encoded by the insertional T-DNA) indicating that they were the *atg6*(-) segregants. Finally, a series of *in vivo* pollen tube guidance experiments suggested no additional pollen defects during pollen tube growth or guidance. Whether ATG6 acts in an autophagy-dependent or independent manner during pollen development, these data suggest novel connections between plant stress responses and reproductive biology.

Introduction

When eukaryotic cells encounter growth-limiting nutrient conditions, such as carbon or nitrogen deprivation, they begin the process of autophagy. This inducible pathway allows for extensive intracellular recycling in an effort to extend the life of the cell [1]. Autophagy occurs through the sequestration of cytoplasmic components into vesicles, which are subsequently degraded in the vacuole/lysosome [2,3]. The autophagy pathway has been implicated in a variety of cellular processes including sporulation in yeast [4], moderation of disease states such as neurodegenerative disorders, cancer, and viral infection in mice and humans [5-7], fruiting body formation in *Dictyostelium* [8], and regulation of programmed cell death following the hypersensitive response in tobacco [9]. While extensively studied in yeasts, until recently little was known about molecular or genetic aspects of autophagy in plants.

Ultrastructural analysis provides evidence that macroautophagy, where autophagosomes form in the cytosol, and microautophagy, where the tonoplast invaginates to cause direct uptake of cytoplasmic contents into the vacuole, occur in plant cells [10-12]. The two processes take place during different developmental stages; macroautophagy is observed in vegetative plant tissues, while microautophagy is observed during seedling germination and senescence [10,11]. Further evidence of plant autophagy comes from carbohydrate-starved tobacco cell cultures, which accumulate acidic vesicles. These vesicles have the characteristics of autophagosomes, indicating that the autophagy pathway is indeed conserved in plants [13,14]. Utilizing data from the extensive molecular and genetic work completed with *Saccharomyces cerevisiae*, bioinformatics has allowed the identification of over 30 Arabidopsis homologs of autophagy proteins [2]. The first genetic evidence for conservation of the autophagy pathway came from examination of *atg9* [15] and *atg7* [16] mutants in Arabidopsis. Plants with mutations in either gene suffer reduced viability under stress conditions, early senescence, and chlorosis, consistent with a role for these proteins in stress and nutrient metabolism [15]. Additional proteins have been characterized in plants

including ATG8, a known autophagosomal marker, and components of the ubiquitin-like conjugation pathways [2,17-19].

AtATG6, is the Arabidopsis homolog of yeast Atg6/Vps30, and mammalian and tobacco Beclin1 proteins. Like other ATG6 homologs, AtATG6 contains the evolutionarily conserved coiled-coil protein-interaction domain and a putative amino-terminal nuclear export signal. Though untested in plants, this export signal is required for the function of human Beclin1 in the autophagy pathway [20]. The mouse homolog of ATG6 was identified as a haplo-insufficient tumor suppressor. Mice that are heterozygous for the Beclin1 gene suffer from deregulation of the autophagy pathway and an increase in spontaneous tumor growth [21]. In yeast, Atg6/Vps30 is an essential part of the phosphoinositol-3-kinase (PI3K) complex that regulates autophagosome initiation. Yeast mutants lacking Atg6/Vps30 fail to form autophagosomes under starvation conditions, causing disruption of the autophagy pathway [22]. Recent work indicates that the tobacco homolog (Beclin1) plays a role in regulating programmed cell death following the hypersensitive response [9,22,23].

We investigated the role of AtATG6 and found it is essential for male gametophyte development. In angiosperms, male gametes (pollen) develop in the anthers of the parent plant. The process, known as microsporogenesis, begins with two rounds of meiosis to generate four microspores (tetrads). Each of these microspores then undergoes mitosis and a cell fusion event to produce a single pollen grain with two nuclei, the vegetative nucleus and generative (sperm) nucleus. A separate mitotic event then produces the two sperm nuclei from the generative nucleus. Following dehiscence, the mature tri-nucleate pollen grains are released from the anthers of the parent plant and, after landing on a stigma, germinate. While multiple factors have been identified that affect pollen germination rates, the exact mechanisms that regulate the process remain unclear [24,25]. The observable process begins with grain hydration and leads to polar pollen tube growth through the pistilate tissues [24]. We examined microsporogenesis, and pollen grain germination and guidance in *atg6* heterozygous pollen populations and found that disruption of the *ATG6* gene led

to pollen germination defects, consistent with others' recent results [26,27]. Microarray experiments conducted on pollen samples show that mRNA transcript levels for many autophagy components, including *AtATG6* mRNA, are enriched [28,29]. In addition, autophagosome-like structures have been observed in pollen grains [30]. We cannot yet determine, however, whether AtATG6 is acting in an autophagy-dependent or independent manner during pollen germination or whether its role requires conserved PI3K-mediated signaling [29].

Materials and Methods

Cloning. Using Pfu Turbo (Stratagene, Cedar Creek, TX), Arabidopsis *ATG6* was amplified with and without the native stop codon from the full-length cDNA clone U12843, which was obtained from ABRC, and ligated into the Gateway® pENTR/SD/TOPO vector (Invitrogen, Carlsbad, CA). Resultant clones were fully sequenced. The primers used were ATG6 LP: 5'-CACCATGAGGAAAGAGGAGATTCCA-3', RPstop: 5'CTAAGTTTTTTTACAGTAAGG3' and RPnostop: 5'AGTTTTTTTACAGTAAGGCTT3'. For the yeast (*S. cerevisiae*) studies, the yeast vector pYL435 was obtained from ABRC (deposited by S. Dinesh-Kumar, Yale University) and Quick-Change® site-directed mutagenesis (Stratagene, Cedar creek, TX) was used to introduce a stop codon following the his tag (primers used were LP: 5'CATCACCATCACCTGTAAGTTCTGTTCCAGGGG3', RP: 5'CCCCTGGAACAGAACTTACAGGTGATGGTGATG3'). LR clonase™ recombination reactions (Invitrogen, Carlsbad, CA) were performed to transfer the *ATG6* cDNA without a stop codon from pENTR/SD/TOPO into this modified pYL435 vector (the TAP tag was modified with a truncation that removed 144 amino acids after the His tag epitope). Both Fujiki's group [27] and Gu's group [26] also used carboxyl terminal, GFP-tagged versions of AtATG6, and saw no significant effect on function. For overexpression of ATG6 in plants, LR clonase™ recombination reactions were performed to transfer the *ATG6* cDNA with a stop codon from pENTR/SD/TOPO into pCHF3-GW, a 35S:His-tagged

plant overexpression vector (gift from Jianming Li, University of Michigan; pCHF3-GW is pCHF3 modified with a Gateway® cassette).

Yeast complementation. SEY6210 wild-type yeast (*S. cerevisiae*) were transformed with *pYL435:ATG6* and grown on SC–ura media supplemented with galactose (6.7 g/L yeast nitrogen base (YNB) without amino acids, 10 g/L ammonium sulfate, 0.67 g/L amino acids–ura/–trp, 24 mg/L trp, 2% galactose, pH 5.6) to test for protein production. Protein was detected by western blot using an anti-PentaHis antibody (Qiagen, Valencia, CA) raised against the his tag on the protein. For yeast complementation experiments, SEY6210, BY4742*Δvac8*, SEY6210*Δvps30*, SEY6210*Δvps30::pr414-atg6* and SEY6210*Δvps30::pYL435AtATG6* strains were grown to mid-log phase in SC–ura+galactose media. Cells were pelleted, washed, and resuspended at 0.2 OD_{660} in SC–ura–nitrogen+galactose media (0.67 g/L amino acids–ura/–trp, 24 mg/L trp, 2% galactose, pH 5.6) and grown for four hours. Cells (1 OD_{660}) were harvested, TCA precipitated and subjected to SDS-PAGE [31]. Proteins were transferred to Immobilon™ membrane (Millipore) and probed with antibodies against aminopeptidase 1 (α-Ape1, 1:30,000; generously provided by D. Klionsky, University of Michigan) or against the his tag on the protein (anti-PentaHis, 1:10,000) in TBS-Tween with 3% BSA. Proteins were visualized using HRP-conjugated secondary antibodies and Millipore chemiluminescent substrate, according to manufacturer's instructions. D. Klionsky, University of Michigan, generously provided all yeast strains.

Multiplex RT-PCR. Total RNA was extracted from the indicated plant tissues using the RNeasy Plant Mini kit (Qiagen, Valencia, CA) with on-column DNase digestion, according to manufacturer's directions. RNA was quantified using a spectrophotometer. RT-PCR was performed using the Access Quick (Promega, Madison, WI) RT-PCR kit (PCR portion = 55^{o}C annealing, 23 cycles, 3 minute extension) with 50-100 ng RNA template and 100 ng *ATG6* gene-specific primers or 10 ng β-tubulin gene-specific primers. (The primers used were; *ATG6* primer 1: 5'TGATATATTAGAAGGCAGAGAGAC3', *ATG6* primer 2: 5'TAGAAGAAACAGAGAAACAAAATG3', β-tubulin primer 1:

5’ATACAGAACAAGAACTCGTCTTAC3’, β-tubulin primer 2: 5’CTCTTCTTCTTCAACATCATACTC3’).

Mutant plant lines. Seeds with potential mutations in *AtATG6* were obtained from the ABRC seed stock center [32]. The lines and their corresponding allele designations are: SALK_051168 is *atg6-1*, SALK_109281 is *atg6-2*, SAIL_656-FO8 is *atg6-3*, SAIL_543-G11 is *atg6-4*, SAIL_80_B10 is *atg6-5* (Figure 2.3). Seedlings were grown under 16L/8D at 22^{o}C. DNA was extracted from young rosette leaves. Leaf tissue was homogenized in 200 µL extraction buffer (200 mM Tris-HCl, pH 7.5, 250 mM NaCl, 25 mM EDTA, 0.5% SDS), vortexed, and centrifuged 2 min. at full speed in a standard microfuge at room temperature. Then 150 µL supernatant was transferred to a new tube containing 150 µL isopropanol. The DNA was pelleted by centrifugation for 5 min. at full speed in a standard microfuge at room temperature. The DNA pellet was washed with 70% ethanol, allowed to air dry, and then was resuspended in 50 µL water. The presence of the T-DNA insert was tested by PCR using the gene-specific primers suggested for each line at http://signal.salk.edu/cgi-bin/T-DNAexpress. The LBc1 primer was used to detect the T-DNA inserts in the SALK lines (LBc1: 5’GCCGATTTCGGAAGGAGGATC3’); the LBb1 primer was used to detect the T-DNA insert in the SAIL lines (LBb1: 5’ GCCTTTTCAGAAATGGATAAATAGCCTT GCTTCC3’). PCR conditions used were 50-55^{o}C annealing, 25 cycles, 2 min. extension.

Construction of plant over-expression lines. Three-week-old Col-0 Arabidopsis plants were transformed with *pCHF3-GW-ATG6* using the simplified Agrobacterium-mediated transformation protocol developed by Bent [33]. T1 plants were grown on MS media with kanamycin (50 µg/mL). DNA was extracted and integration of the transgene was determined by PCR, as described above. Leaf tissue was ground directly into standard SDS-PAGE sample buffer. Expression of the ATG6 protein was measured by western blots using the anti-PentaHis antibody (1:10,000, Qiagen, Valencia, CA). After confirming the presence of the transgene and overexpression of the protein, multiple

independent lines were selected for further analysis. Homozygous progeny in the T2 were identified by kanamycin segregation tests.

Crosses. Pollen from *atg6-2* (Salk_109281) heterozygotes was crossed into *gl2* plants (which lack trichomes) and the resulting progeny with trichomes were analyzed by PCR for the *atg6* T-DNA insertion. For the reciprocal cross, Arabidopsis pollen from the Landsberg *erecta* (L*er*) ecotype was crossed into *atg6-2* (Salk_109281) heterozygotes and the progeny screened by PCR for the T-DNA insertion. Plants were then allowed to self-fertilize. Homozygotes with the *erecta* mutant phenotype (short stature) were seen in the F2, indicating that the outcross was successful. Finally, pollen from four independent *35S:ATG6:HIS* overexpression lines was crossed into *atg6-2* (Salk_109281) heterozygotes. The resulting F1 plants were screened by PCR for the *atg6* T-DNA insert and for the presence of the *35S:ATG6:HIS* transgene, and by western blot for the presence of the transgenic protein using an anti-PentaHis antibody (1:10,000 dilution; Qiagen, Valencia, CA). F1 plants were then allowed to self-fertilize. Screening for the transgene and the engineered protein was repeated on the F2 and the F3 progeny to identify homozygous segregants. The S. Clark lab (University of Michigan) provided the first generations of *gl2* and L*er* Arabidopsis plants.

Seed counts. Mature green siliques were collected from multiple positions on the inflorescence, bleached for 4 hours in an ethanol:acetic acid solution (3:1 ratio) to remove the chlorophyll, and incubated in 1 N NaOH overnight. The cleared siliques were placed on slides and observed under a light microscope. The total number of seeds and locations/frequency of gaps in each silique was recorded.

Pollen analysis. For examination of microsporogenesis, small (central), medium (green) and large (white tipped) Arabidopsis flower buds were collected from wild-type and *atg6-2* heterozygous plants and vacuum infiltrated for 2 hours in fixative (4% formaldehyde, 3.125% glutaraldehyde in 50 mM sodium cacodylate buffer, pH 7). Tissues were washed with buffer (50 mM sodium cacodylate, pH 7), stained with 2% OsO_4 in buffer, taken through an ethanol

dehydration series (30%, 50%, 70%, 90%, 95%, 100%, 100%, 100% new bottle), embedded in medium Spurr's resin using 25%, 75%, and 100% resin changes, and finally cured until firm (8-10 hours at 80°C). Resin blocks were sectioned for light microscopy and stained with toluidine blue [34]. The developmental stage represented by each section was determined and the sections were examined for any observable phenotypic differences.

Using *ATG6* heterozygous plants, pollen from 10 individual open flowers was collected by suction onto filter paper using a device similar to that described previously [35]. To determine whether the T-DNA insert was present, DNA was extracted from the pollen. First, the pollen was released from the filter by washing in extraction buffer (200 mM Tris-HCl, pH 7.5, 250 mM NaCl, 25 mM EDTA, 0.5% SDS). The pollen grains were then ground by mortar and pestle for 1 min. and frozen in liquid nitrogen; this sequence was repeated four times. Isopropanol (0.4 vol) was added and the DNA was precipitated by centrifugation at 4^{o}C for 20 min at full speed in a microcentrifuge. The DNA pellet was washed with 70% ethanol, air dried on the bench top, and then resuspended in 5-10 µl water. PCR was performed using the T-DNA screening primers described above (using *Taq* polymerase (Promega, Madison, WI), 55^{o}C annealing, 30 cycles, 2 min. extension).

To assess pollen viability, total pollen from one wild-type or heterozygous flower was transferred to a slide and examined under a light microscope. Samples were stained with Alexander stain for 10 min. and examined using light microscopy [36]. For germination assays, total pollen from one flower was transferred to solid germination media (protocol from Zhenbiao Yang lab University of California, Riverside: 18% sucrose, 0.01% boric acid, 1 mM $CaCl_2$,1 mM $Ca(NO_3)_2$, 1 mM $MgSO_4$, 0.5% agar, pH 7.0) and incubated at 22^{o}C overnight. The number of germinated pollen grains was counted. For the lines homozygous for *qrt1*, each tetrad was scored for the number of pollen grains that germinated. For GUS staining, 20 µl GUS staining solution (50 mM $NaHPO_4$, pH 7.2, 5% Triton X-100, 0.4 mM X-Gluc (5-bromo-4-chloro-3-indolyl-beta-D-glucuronic acid in dimethyl-formamide)) was applied to each collection of pollen

grains. After incubation at 37°C for 2 hours, grains were observed under a light microscope and the scoring process was repeated for each tetrad. To observe pollen nuclei, pollen was transferred onto glass slides, 4',6-diamidino-2-phenylindole (1 µg/ml, DAPI) solution was applied and the slides were incubated either at 4^{o}C overnight or at room temperature for 20 min [37]. Nuclei were visualized using fluorescence microscopy (DAPI channel) and the number per cell recorded.

To examine pollen tube guidance, Col-0 virgin pistils (from closed immature buds) were demasculated using fine tweezers, hand pollinated, and incubated on pollen germination media at 22^{o}C for 24 hours. Pistils were fixed for 30 min. in an ethanol:acetic acid mixture (3:1 ratio) and softened overnight in 1 N NaOH. Pollen tubes were stained using decolorized aniline blue (0.1% w/v) and visualized using fluorescence microscopy (GFP channel). A 10X stock (1% w/v) of decolorized aniline blue was made by mixing 0.2 g aniline blue with 20 ml 1 M K_3PO_4. The stock was stored in the dark overnight and diluted 1:10 with water before using.

Results

Yeast complementation. Yeast Atg6/Vps30 functions in both the CVT (cytoplasm-to-vacuole targeting) pathway and the autophagy pathway [1,23]. To determine whether AtATG6 function is conserved between yeast and plants, AtATG6 was expressed in yeast *atg6/vps30* mutants. First, the processing of Ape1 under normal growth conditions was observed. Yeast lacking Atg6/Vps30 were unable to correctly traffic Ape1 to the vacuole, where it is normally processed to its mature form (Fig. 2.1A, compare WT vs. vector lanes). Ape1 was not processed in AtATG6-expressing cells, indicating that AtATG6 did not complement the *Δatg6/vps30* CVT pathway defect (Fig. 2.1A, compare WT vs. AtATG6 lanes). Second, to test whether AtATG6 can complement the *Δatg6/vps30* autophagy pathway defect, Ape1 processing was analyzed following induction of autophagy under nitrogen starvation conditions. Again no processing of Ape1 was seen (Fig. 2.1B, compare WT vs. AtATG6 lanes),

indicating that AtATG6 did not complement the *Δatg6/vps30* autophagy pathway defect. Ape1 is processed only under autophagy-inducing conditions in the yeast *Δvac8* strain [38]. Therefore, the yeast *Δvac8* strain was included as a control to show that autophagy was induced by nitrogen starvation in Fig. 2.1B (compare the *Δvac8* lanes in Fig. 2.1A vs. Fig. 2.1B).

***AtATG6* expression.** To determine whether *ATG6* expression is spatially regulated, RNA was extracted from multiple tissue types and multiplex RT-PCR was performed. Similar levels of *ATG6* mRNA were detected in all tissues, indicating that there was no spatial regulation of *ATG6* expression (Fig. 2.2A). In addition, *ATG6* expression was analyzed in leaves from wild- type plants grown under several stress conditions. No significant difference in *ATG6* expression was detected in wild-type plants grown at 22^{o}C in the light or in the dark (at 4^{o}C or 22^{o}C; Fig. 2.2B). Plants grown under relatively low light conditions at 4^{o}C also showed no differences, within the time period tested (data not shown). Minor to moderate effects were seen when *ATG6* expression was tested in wild-type plants that were challenged with 100 mM NaCl (data not shown).

***atatg6* mutant analysis.** To assess the physiological role of AtATG6, multiple T-DNA insertional mutant lines were obtained from the ABRC stock center: SALK_051168 (*atg6-1*) SALK_109281 (*atg6-2*), SAIL_656-F08 (*atg6-3*), SAIL_543-G11 (*atg6-4*), and SAIL_80-B10 (*atg6-5*) - a line generated in the quartet (*qrt1*) background [39] (Fig 2.3). *atg6-1* (SALK_051168), *atg6-2* (SALK_109281), *atg6-4* (SAIL_543-G11) and *atg6-5* (SAIL_80-B10) have T-DNA inserts in the indicated exons, while *atg6-3* (SAIL_656-F08) has a T-DNA insert in the fifth intron (Fig. 2.3). Heterozygous plants were identified for all lines except SALK_051168 (*atg6-1*). Multiple attempts, by several people and from several seed stock re-orders, to isolate *atg6-1* heterozygotes were all unsuccessful. Thus, this putative mutant allele was not further studied.

Phenotypic analysis was performed primarily on the *atg6-2* line. *atg6-2* heterozygotes displayed a variety of growth phenotypes when compared to wild-type plants. Some differences that were noted included retarded growth, increased anthocyanin production, and decreased silique production (Fig. 2.4).

Heterozygotes grown on complete MS media supplemented with 5% sucrose did not exhibit this growth phenotype (not shown). In addition, *atg6-2* heterozygotes had lower levels of *ATG6* transcript compared to wild-type plants, measured by RT-PCR using *ATG6* gene-specific primers (Fig 2.4B).

No homozygous segregants were recovered in any *atg6* mutant line. This suggests that AtATG6 may be essential for plant development. Segregation ratios were obtained for all confirmed mutant alleles and revealed a 50:50, wild type to heterozygote ratio for each mutant line (Table 1A). To determine whether the loss of ATG6 was embryo lethal, siliques on heterozygous plants were examined. No aborted seeds were seen in any of the mutant lines (Fig. 2.5), consistent with a germ-cell defect. In addition, no abnormal gapping due to re-absorption of mutant seeds was observed, suggesting that all ovules were fertilized. Because all ovules on heterozygotes developed into viable seeds, the defect was most likely in the paternal rather than maternal germ line. The defect did not appear to be post-fertilization. To determine whether the germ-cell defect was paternal or maternal, a series of crosses was performed. First, pollen from *atg6-2* heterozygotes was crossed into homozygote *gl2* plants. Homozygous *gl2* plants lack trichomes, therefore any progeny bearing trichomes must be the result of a successful outcross. The plants produced by this cross were screened for transmission of the T-DNA at the *ATG6* locus. All progeny were found to be wild type, strongly suggesting that a pollen defect prevents transmission of the allele (Table 1B). This suggested that fertilization in *atg6* heterozygous plants occurred between wild-type pollen and either a wild type or an *atg6* mutant egg. Next, the reciprocal cross was performed using pollen from Landsberg *erecta* (L*er*) mutant plants crossed into female *atg6* heterozygotes. These progeny segregated with the previously observed 50:50 ratio (Table 1B). The F1 plants were allowed to self fertilize. The success of the initial outcross was confirmed when homozygotes with the *erecta* mutation were recovered in the F2 generation. This indicates that the *atg6* mutant allele was only inherited maternally, due to a pollen defect that does not allow normal transmission of the allele (Table 1).

Complementation of the *atg6-2* heterozygote phenotype. Transgenic plants were engineered to express *ATG6* under the control of the constitutive 35S promoter. Pollen from multiple transgenic lines overexpressing *ATG6* was used to manually fertilize *atg6-2*(+/-) plants. Overexpression of the ATG6 protein (with a 6XHis tag) in each paternal transgenic line was confirmed by western blot (Fig 2.6A), following PCR detection of the transgene. The progeny of the cross were allowed to self-fertilize. Plants from the F1 and F2 generations were screened for T-DNA inserts. While phenotypically complemented *atg6-2* (+/-)/*ATG6*:*HIS*(+/-) plants were observed in the F1 generation (Fig. 2.6B-D), no homozygous segregants were found in their progeny (F2 and F3 generations). This indicated that overexpression of *ATG6,* under the control of the constitutive 35S promoter, could only rescue the growth phenotype (anthocyanin production, number of siliques, and internodal length were also normal). The lack of complementation of the pollen germination phenotype suggests that the primary pollen defect may occur prior to activation of the 35S promoter.

Effect of *atg6* on pollen development. The mature pollen population was examined to determine when, during pollen development, the defect responsible for loss of transmission occurred. First, DNA was extracted from pollen from *atg6* heterozygous plants. PCR was performed to test whether the T-DNA was present in the mature pollen. The T-DNA insert was detected, suggesting that the effect of the mutation began after microsporogenesis (data not shown). Next, buds from *atg6-2* heterozygotes at a variety of development ages were harvested and embedded in Spurr's resin for examination under light microscopy. No morphologically observable defects were seen in the microsporocytes, tetrads, or mature pollen from *atg6-2* heterozygous plants (Fig. 2.7).

Since no defect was seen during microsporogenesis, the next step was to test whether the mature pollen had any gross structural or viability defects. Pollen from all heterozygous mutant lines was collected and examined by light microscopy. All of the pollen grains appeared uniform and indistinguishable from wild-type (and *qrt1*) controls (Fig. 2.8). In addition, staining with Alexander stain

[36] (a vital stain), produced uniformly purple pollen grains (Fig. 2.8, panels B, E, H, J), indicating that the pollen was viable. Note that freshly collected pollen grains (Fig. 2.8, panels A, D, G, I) become more rounded after hydration during staining (Fig. 2.8, panels B, C, E, F, H, J). Next, to examine post-microsporogenesis pollen development, *atg6-5* plants (SAIL_80-B10), which were homozygous for *qrt1(-/-)* and heterozygous for *atg6,* were grown. These plants produce the expected fused tetrad clusters characteristic of the *qrt1* mutation,[39] further indicating that microsporogenesis was unaffected. In addition, *atg6-2* and *atg6-5* pollen was trinucleate, as revealed by DAPI staining (Fig. 2.8C, F). Together, these experiments indicated that pollen produced by *atg6* heterozygotes was viable, had normal morphology, and was trinucleate.

The next step was to assess the effect of *atg6* mutations on pollen germination using *in vitro* pollen germination assays. *atg6-2* pollen germinated less than wild type, with an overall germination efficiency under 50% (data not shown). This raised the possibility that only the wild-type pollen grains in the *atg6-2* sample germinated. All of these pollen grains looked alike. To distinguish between mutant and wild-type pollen grains, the *atg6-5* line was chosen for further analysis. Because *atg6-5* was generated in the *qrt1* mutant background, two pollen grains in each of the fused tetrads would be wild type and two would be mutant. Thus, if *atg6-5* mutant grains could not germinate, then only the wild-type pollen grains in each tetrad would be predicted to germinate. As expected, pollen grains in tetrads from *atg6-5(+/-)* plants germinated with lower efficiency, *in vitro,* than pollen grains in tetrads from *qrt1(-/-)* plants (Fig. 2.9A). In more than 95% of all *atg6-5* tetrads, at least two pollen grains failed to germinate. GUS staining was used to determine which pollen grains displayed the germination defect. Only the mutant grains, which contain a T-DNA with LAT52, a post-meiotic pollen-specific promoter driving the expression of □-glucuronidase (GUS), should stain positive [40]. GUS staining on *in vitro* germinated *atg6-5* tetrads revealed that the two non-germinating pollen grains were positive for GUS activity (Fig. 2.9C). Thus, they were the *atg6-5* mutant pollen grains. In rare instances, however, pollen grains positive for GUS activity were seen at

intermediate stages of pollen tube growth (Fig. 2.9D). The growth of these pollen tubes was slower and led to shorter pollen tubes than those observed for wild-type pollen in the same tetrad.

To be sure that there were no subsequent defects caused by the mutation, a series of *in vivo* pollen tube guidance experiments were performed. Pollen from *atg6-2, atg6-3, atg6-4,* and *atg6-5* plants was applied to demasculated pistils and aniline blue staining performed. As expected no defects in pollen tube growth or guidance were observed (Fig. 2.10; *atg6-5* not shown because each grain in *qrt1* tetrads does not contact the stigma surface equally). Therefore, the primary defect in pollen development caused by the *atg6* mutation was the inability of *atg6* mutant pollen to germinate.

Discussion

ATG6 is essential for pollen germination in Arabidopsis. The greatly reduced efficiency of pollen germination seen in *atg6-2* and *atg6-5* mutant grains, compared to wild type, was responsible for loss of homozygote segregants (Fig. 2.9). Other stages of pollen development were not affected: 1) microsporogenesis was unaffected in *atg6* heterozygotes (Fig. 2.7) plants homozygous for *qrt1* and heterozygous for *atg6-5* produced viable trinucleate tetrads (Fig. 2.8) mature *atg6-2, atg6-3, atg6-4,* and *atg6-5* pollen grains appeared normal (Fig. 2.8). These observations are consistent with those previously reported [26,27]. This study, however, examined multiple mutant alleles. Surprisingly, rare instances of *atg6-5* pollen germination were observed (Fig. 2.9D), suggesting that the defect caused by loss of ATG6 was variable. It is interesting that, even in these cases, no homozygotes were recovered, suggesting that those *atg6-5* grains that germinated were also defective in later stages of pollen tube growth. No differences between *atg6-2, atg6-3*, *atg6-4, atg6-5,* and wild-type pollen were detected by *in vivo* pollen tube guidance experiments (Fig. 2.10, and data not shown), suggesting that any mutant pollen tube growth must terminate prior to significant penetration into pistilate tissues. The ability of some pollen grains with LAT52-driven GUS activity to germinate

(Fig. 2.9D), however, implies that there are cellular or environmental variants that can periodically allow progression into later stages of pollen development.

It is possible that loss of ATG6 has additional effects during both pollen germination and vegetative growth. When the 35S promoter was used to drive ATG6:HIS6 expression in *atg6-2* heterozygotes, the mutant growth phenotype was rescued (Fig. 2.6). No homozygotes were recovered in the next generation (data not shown), however, suggesting that the pollen germination phenotype was not rescued. This is interesting because the 35S promoter is activated [41] before the observable pollen defect occurs. This suggests that an additional, as yet unidentified, *atg6* defect occurs prior to activation of the 35S promoter, shortly after microsporogenesis. The *atg6* heterozygote phenotype also suggests that ATG6 is required during vegetative growth. This is consistent with *ATG6* expression analyses, which show that *ATG6* is ubiquitously expressed in most plant tissues [27] (Fig. 2.2), though several groups have reported higher *ATG6* expression in pollen [26,28]. Although the mRNA levels did not change, the severity of the heterozygote growth phenotype was generally increased under stress conditions, such as high salt treatment (data not shown). Thus, the vegetative defect is probably a response to autophagy or stress-induced metabolism [12]. It remains unknown, however, whether AtATG6 functions in the same manner during pollen germination and vegetative growth or whether AtATG6 has two distinct functions - one during pollen development and one during vegetative tissue growth and maintenance.

In yeast and mammalian systems, Atg6 is part of the highly conserved class III phosphoinositol-3-kinase (PI3K) complex, which includes Vps34 as the catalytic subunit [42]. This complex is responsible for phosphorylating the inositol ring at the 3' position, generating phosphoinositol-3-phosphate (PI3P), an important lipid in intracellular signaling [43]. PI3P and other phosphoinositide lipids are involved in vesicular trafficking and membrane transport [44]. In plant cells, trafficking of PI3P from the *trans*-Golgi network to the lumen of the vacuole has been reported [45,46], consistent with other systems [47]. Despite this apparent conservation of function, overexpression of AtATG6 was unable to

complement the yeast Δ*atg6/vps30* mutant phenotype, independent of nutrient limitations (Fig. 2.1). The lack of complementation seen in this study is not entirely surprising, however. Other PI3K complex components, such as AtVPS34, are also unable to complement the corresponding Δ*vps34* yeast mutant phenotype [48]. This suggests that the protein components in the yeast and Arabidopsis PI3K complexes have sufficiently different protein-protein interactions or general functions that they are not fully interchangeable in heterologous systems.

Others have reported partial[9] or complete[27] complementation of the yeast mutant by overexpression of AtATG6. These groups, however, were evaluating complementation of different pathways and used different assays. First, visual examination of autophagosome accumulation [10,27] can be difficult and subjective, though it may represent a qualitative response to complementation. It is important to include appropriate controls (such as co-localizing proteins) for proper identification of autophagic bodies. In addition, Fujiki's group measured the amount of CPY (now called Prc1) that was delivered to vacuoles in mutant yeast that were complemented with *AtATG6* [27]. Prc1 is delivered to vacuoles by the vps (vacuolar protein sorting) pathway; it is secreted in *atg6* mutants. These results can also be somewhat difficult to interpret. It seems that AtATG6 only partially restores targeting of Prcp1 to vacuoles in yeast *atg6* mutants (see Fig. 2.1 in ref. 26), though the authors claim full complementation. The current study, however, used maturation of the protein Ape1 as a marker for cvt vs. autophagy pathway complementation (Fig. 2.1). This is a different, and more direct assay for these pathways. AtATG6 very clearly does not restore Ape1 processing under normal or autophagy-inducing conditions in yeast *atg6* mutants. The effects of AtATG6 on the cvt pathway and on autophagosome accumulation were not determined in this study.

There is evidence for a conserved role for AtATG6 in a PI3K complex, making it entirely possible that AtATG6 functions primarily in a phosphoinositol signaling event during pollen germination. While a direct interaction between AtATG6 and AtVPS34 has not been shown, like *AtATG6*, *AtVPS34* homozygotes

are not viable (data not shown). Dinesh-Kumar's group also found that the programmed cell death phenotype, seen with loss of tobacco *beclin1/atg6*, was phenocopied by expression of NbVPS34 RNAi [9]. This suggests a possible conserved interaction between AtATG6 and AtVPS34 in plants, similar to that in yeast [23]. It was also previously shown that *AtVPS34* heterozygotes have reduced PI3P signaling [48]. Taken together, these observations provide indirect evidence that AtATG6 may associate with a conserved PI3K complex. While other phosphoinositol lipids have been implicated in pollen tube growth, there is currently no direct evidence for the involvement of PI3P [49]. Pollen tube growth and germination both require membrane trafficking and cytoskeletal remodeling [49]. Thus, it is possible that components of vesicular trafficking pathways and PI3P signaling, such as AtATG6 and AtVPS34, could be involved in pollen germination.

Because of the complexity of the process, it is difficult to determine whether AtATG6 is acting in the autophagy pathway during pollen germination. The yeast PI3K complex can act in an autophagy or non-autophagy capacity, depending on the nutrient conditions [23]. The energy requirements of pollen germination may mimic severe nutrient stress, leading to activation of the autophagy pathway [24]. Phosphoinositol lipids are also essential, however, for placement of the actin cytoskeleton and for the process of endocytosis - both of which occur continually[50] and through non-autophagic processes. Furthermore, additional Arabidopsis homologs of yeast proteins required for vacuolar protein sorting, which is a non-autophagic trafficking pathway, are essential for pollen development [51,52]. Thus, during pollen germination, ATG6 may be involved in non-autophagic vesicular trafficking or in an autophagic process.

A final possibility is that AtATG6 has a novel function in plants during pollen germination. Human Beclin1:GFP is localized to both the cytosol and Golgi membranes [53]. AtATG6:GFP had a similar dual localization to cytosol and to punctate structures, when expressed in tobacco BY2 cells (Harrison-Lowe, unpublished results) or in Arabidopsis protoplasts [27]. This may be caused by two separate pools of AtATG6 in plants cells, which could represent two distinct

functions for the protein. AtATG6 could function in a membrane-bound PI3K complex during autophagic or non-autophagic processes [23,42]. Presumably, this would be nutrient dependent, as in yeast and mammalian systems [1,3,10,13]. In addition, ATG6 could have a second, as yet unknown, function that requires a cytosolic localization. This may or may not be nutrient regulated, or it may instead be limited to a specific developmental stage, such as pollen development, or to a specific tissue type. For now, it is unknown which of these potential functions is required for pollen germination in Arabidopsis. Regardless, it appears that AtATG6 may have multiple roles in plants, including an essential role in pollen germination.

Acknowledgements

We thank Dr. Marianne Laporte (Eastern Michigan University), Dr. Jennifer Gagne, and Antionette Williams for their helpful comments throughout this project. Dr. Ju Huang provided invaluable assistance with the yeast experiments, and Dr. Joanne Dannenhoffer (Central Michigan University) was instrumental in the microsporogenesis analysis. Dr. Ravishankar Palanivelu (University of Arizona) was very helpful with the pollen germination experiments. Thanks to the Arabidopsis Biological Resource Center for the T-DNA seed stocks.[32] NHL was partially supported by the NIH-funded Cellular Biotechnology Training Program at the University of Michigan. This chapter was published as Harrison-Lowe, N.J. and L.J. Olsen, Autophagy Protein 6 (ATG6) is required for pollen germination in Arabidopsis Thaliana. Autophagy, 2008. **4**(3): p. 339-348.

A

Genotype	*atg6* +/+	*atg6* -/+	*atg6* -/-	% w/ T-DNA	Confidence
atg6-2	92	96	0	51.1	99.99
atg6-3	11	13	0	54.2	99.89
atg6-4	15	13	0	46.4	99.97
atg6-5	16	14	0	46.7	99.98

B

	atg6 +/+	*atg6* - /+	% w/ T-DNA
atg6-2 male w/*gl2*	21	0	0
atg6-2 female w/*er-1*	9	10	52.63

Table 2.1. *atg6-2, atg6-3, atg-4,* and *atg6-5* mutant alleles did not segregate with the expected ratio.

A) No homozygous segregants were found by screening all mutant plant lines containing a T-DNA in the *ATG6* coding region. The progeny segregated with a 1:1 ratio of wild type to heterozygous plants. The probability that the mutant allele was not segregating in the expected ratio (1 wild type: 2 heterozygotes: 1 homozygote) is shown in the confidence column. B) Crosses performed to test for gametophytic defects showed that the mutant allele, containing the T-DNA insert, was not transmitted through the pollen.

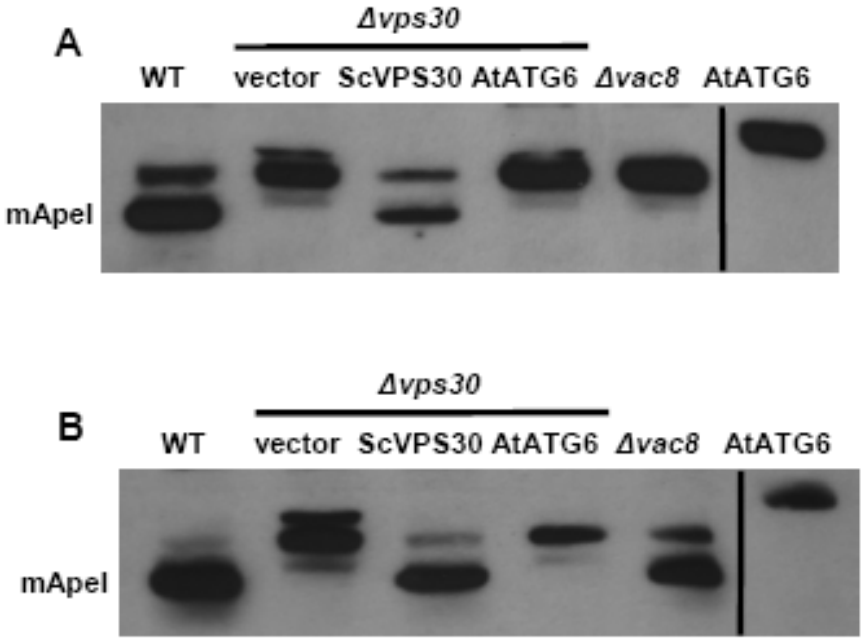

Figure 2.1. *AtATG6* did not complement yeast Δ*atg6/vps30* mutants.

Ape1 was processed to its mature form in WT yeast via the CVT pathway (A, normal growth conditions) and during autophagy (B, nitrogen starvation), detected by western blots using antibodies raised against yeast Ape1. This processing did not occur in *Δvps30/atg6* yeast (vector lane, *Δvps30* strain), but was restored by overexpression of *ScVPS30/ATG6* under both growth conditions (ScVPS30 lane, *Δvps30* strain). Processing was not restored by overexpression of AtATG6 under normal (A) or autophagy-inducing (B) conditions (AtATG6 lane, *Δvps30* strain), indicating that AtATG6 did not complement the yeast CVT or autophagy pathway defects in *Δvps30/atg6* yeast. *Δvac8* yeast were included as a control to show that the nitrogen starvation conditions induced autophagy (B); APE1 is processed to its mature form in *Δvac8* yeast only under autophagy-inducing conditions [38]. *Δvps30* yeast transformed with *AtATG6* expressed detectable levels of AtATG6 (last lane of panels A and B).

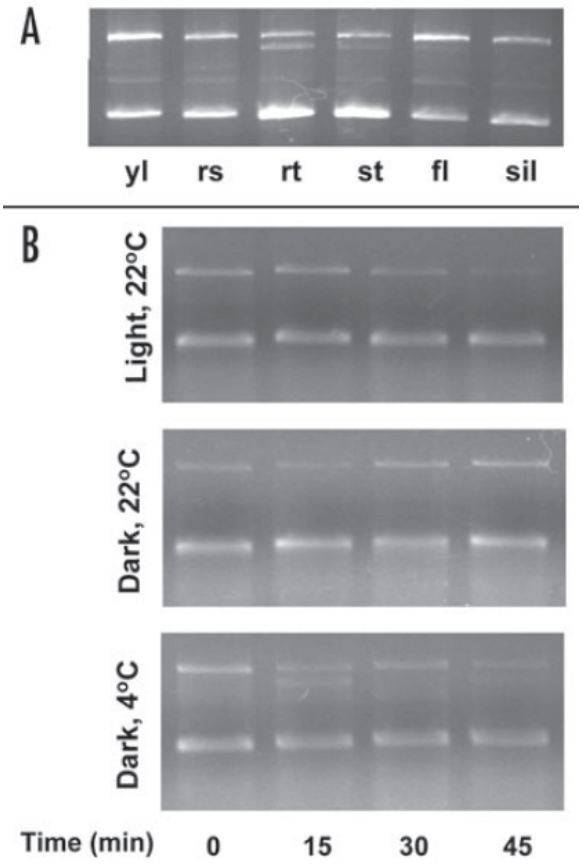

Figure 2.2. *AtATG6* was expressed ubiquitously.

A) Multiplex RT-PCR was performed with *ATG6*-specific primers (upper band) using mRNA extracted from young leaves (yl), rosette leaves (rs), roots (rt), stems (st), flowers (fl), and siliques (sil). Comparable levels of *ATG6* transcript were present in all tissues tested. β-tubulin was used as a control (lower band). B) Three-week-old Arabidopsis plants were transferred from normal growth conditions (light, 22^{o}C) at time 0 min into the dark or into the dark at 4^{o}C. mRNA was extracted from leaves samples collected at three different time points after transfer (15, 30 and 45 min) and multiplex RT-PCR was performed with *ATG6*-specific primers (upper band). β-tubulin was used as a control (lower band). No significant differences were observed in the *ATG6* transcript levels at any time point or under any condition. This experiment was repeated many times, with comparable results.

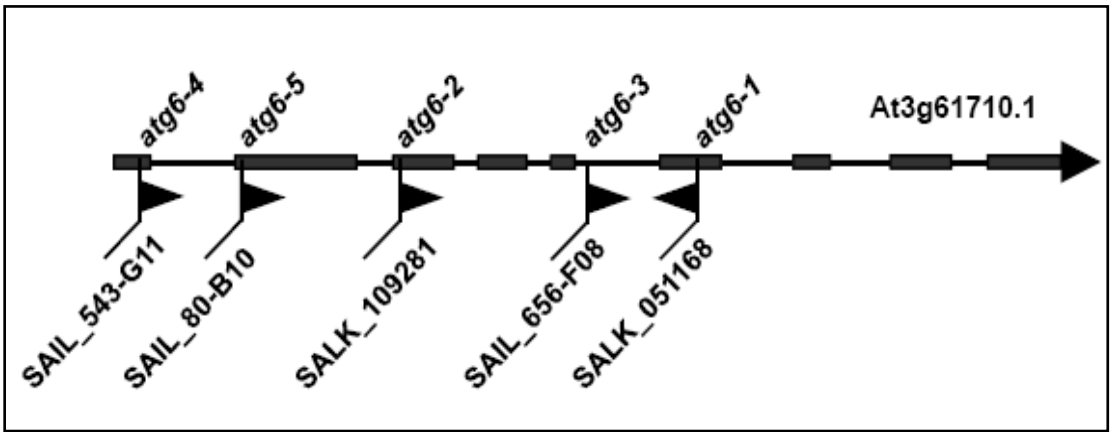

Figure 2.3. Summary of *ATG6* alleles.

Five mutant lines were obtained from ABRC that contained a T-DNA insertion within the *ATG6* coding region (At3g61710.1). Although additional splice variants are annotated, only At3g61710.1 was confirmed by RT-PCR and sequence analysis (data not shown). The *atg6-5* (SAIL_80-B10) line was generated in the *qrt1* mutant background. The T-DNA insert present in the *atg6-5* line also contains a LAT52:GUS, pollen specific promoter. T-DNA insertion sites and orientation are indicated by arrowheads. Exons are depicted by boxes on the gene.

Figure 2.4. *atg6-2* heterozygous plants had variable growth phenotypes.

No homozygous mutants were identified. Heterozygotes exhibited variable growth phenotypes, including increased internodal length and decreased production of siliques (A). In addition, many *atg6-2* heterozygotes exhibited retarded growth and overall dwarfed stature (B, red flag) compared to wild-type plants (B, blue flags). The *ATG6* transcript level was reduced in *atg6-2* heterozygotes (lower panel in B).

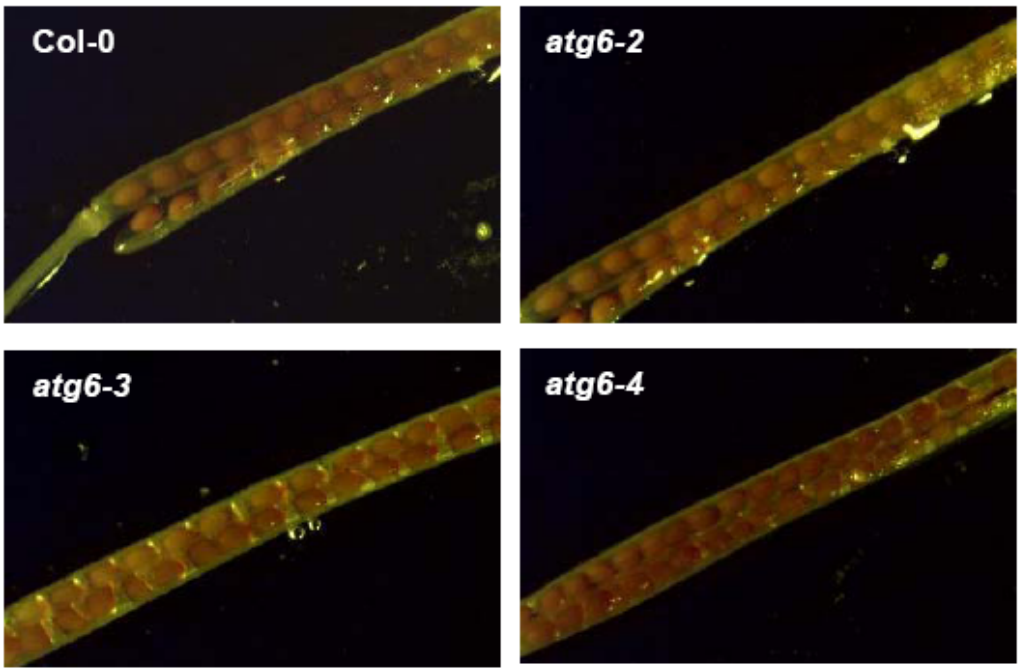

Allele	Seeds per silique	% filled
wt (Col-0)	45 ± 7.7	96 ± 3.1
atg6-2	38 ± 2.8	97 ± 2.0
atg6-3	37 ± 3.5	98 ± 2.6
atg6-4	42 ± 4.0	95 ± 4.4

Figure 2.5. Siliques from *atg6-2*, *atg6-3,* and *atg6-4* heterozygotes did not contain aborted seeds and were filled.

The total of number seeds and gaps (spaces due to early seed abortion) in siliques for *atg6-2*, *atg6-3,* and *atg6-4* heterozygous plants was determined. No statistically significant difference between any allele and wild-type plants was observed (table). All siliques were filled. Developing seeds in mutant and wild-type siliques were visually indistinguishable.

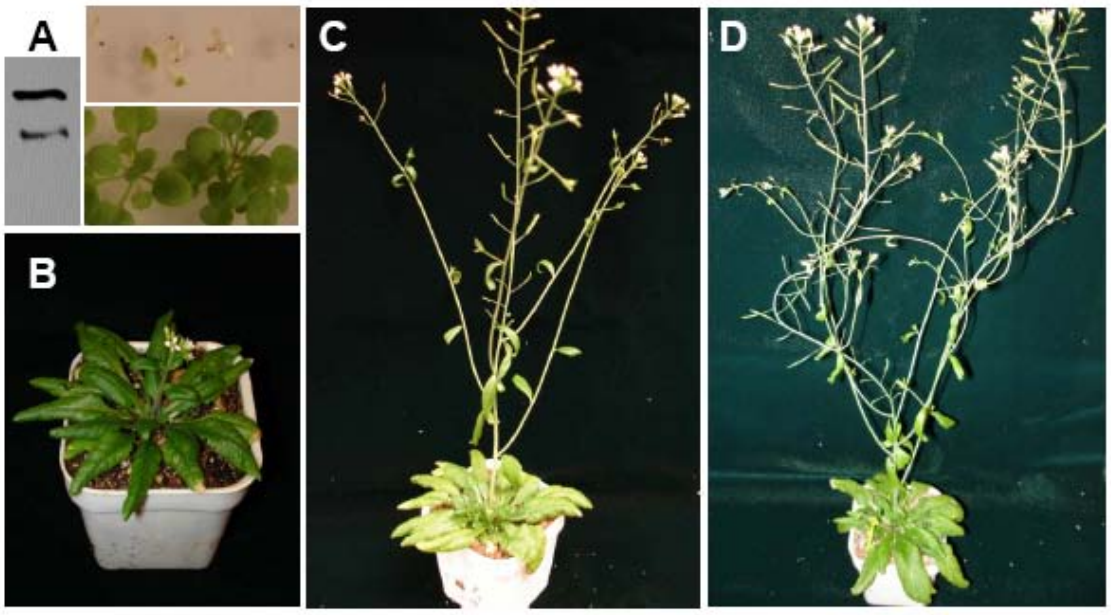

Figure 2.6. Overexpression of *ATG6* complemented the *atg6-2* heterozygous phenotype.

One of the four homozygous *35S:ATG6* transgenic plant lines (A, bottom) was grown on kanamycin selection media for comparison to wild-type plants, which are not kanamycin resistant (A, top). Expression of the his-tagged protein was confirmed by western blot (A, left panel, top band). Pollen from *35S:ATG6* plants was crossed into *atg6-2* heterozygote plants (B). The resultant F1 *atg6-2* heterozygotes overexpressing ATG6 (D) appeared equal to or larger than wild-type plants (C). No *atg6-2* homozygous segregants, however, were recovered in the F2 or F3 generations. This indicated that the overexpression of *ATG6* complemented only the *atg6-2* heterozygote phenotype.

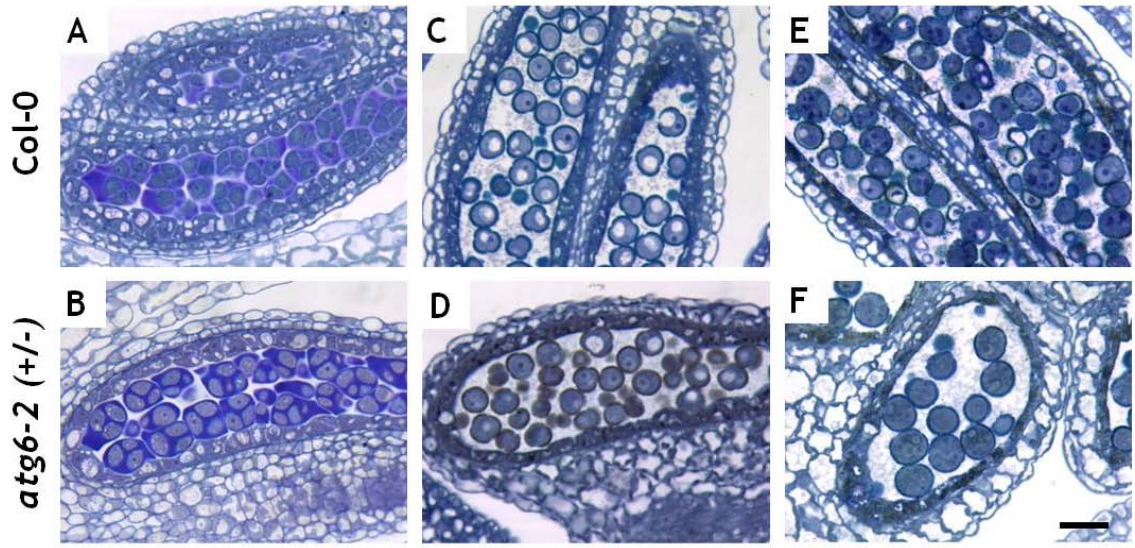

Figure 2.7. Microsporogenesis was unaffected by *atg6-2*.

Small (center), medium (green), and large (white tipped) Arabidopsis buds were collected from wild-type and *atg6-2* heterozygous plants, embedded in Spurr's resin, sectioned for light microscopy and stained with toluidine blue. No differences were observed between wild-type (Col-0, top) and *atg6-2* heterozygotes (bottom) during any stage of microsporogenesis. Tetrads (A, B), microspores (C, D), and mature pollen (E, F) appeared normal in *atg6-2* heterozygotes. Bar = 100 µm

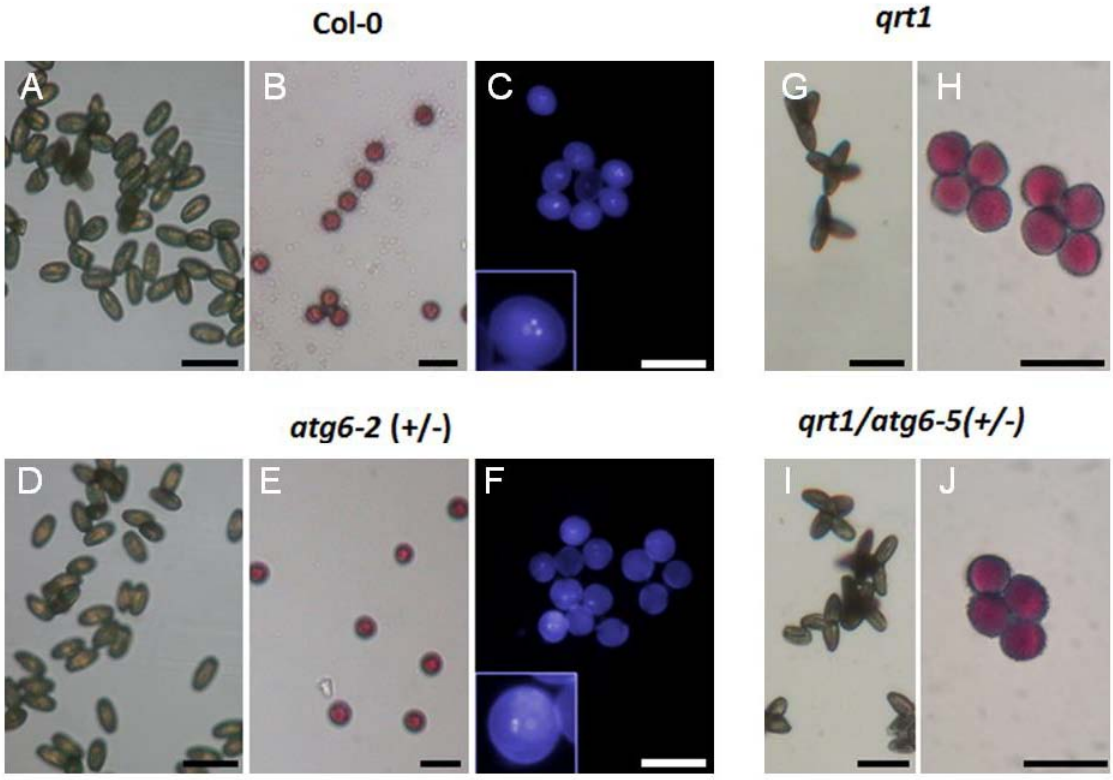

Figure 2.8. *atg6* plants produced viable, trinucleate pollen with normal morphology.

Mature pollen was collected from wild-type plants (Col-0) and from heterozygous mutants (*atg6-2* and *atg6-5*) and observed under a light microscope before (A, D, G, I) and after (B, E, H, J) staining with Alexander stain. Mature pollen from was also DAPI-stained and observed by fluorescence microscopy (C, F). No apparent differences were observed in gross morphology, staining intensity, or nuclei number when compared to wild-type pollen. *atg6-5* plants (which are in the *qrt1* background) produced the characteristic fused tetrad of pollen grains (G, I). All grains in each *qrt1* and *atg6-5* tetrad cluster stained uniformly with Alexander stain (H, J), consistent with the results from the *atg6-2* line (B, E). Freshly collected pollen grains (A, D, G, I) become more rounded after hydration during staining (B, C, E, F, H, J). Bars = 50 µm.

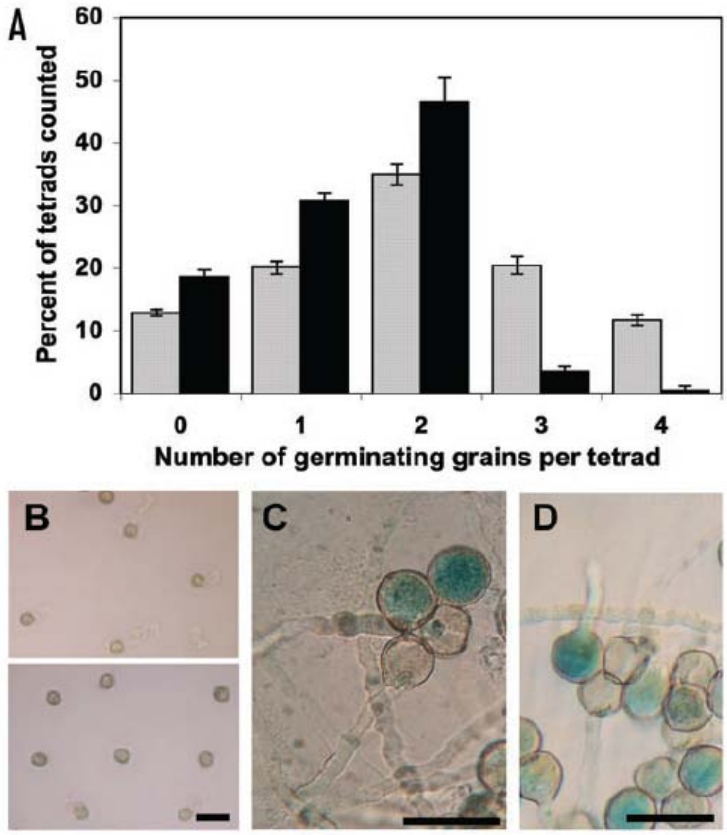

Figure 2.9. Pollen germination efficiency was decreased in *atg6-2* and *atg6-5* heterozygote plants.

In vitro germination assays were conducted with mature pollen from *atg6* heterozygotes. Pollen was incubated on germination media for 24 hours at 22^{o}C. *atg6-2* pollen was directly observed by light microscopy (B, wild-type top, *atg6-2*-lower), while *atg6-5* was first GUS stained to allow for identification of the mutant grains. The number of pollen grains per tetrad that formed a pollen tube was counted for *qrt1* (open gray bars) and *atg6-5* lines (solid black bars) (A). Of those *atg6-5* grains that germinated, more than 90% were negative for GUS activity, indicating they were the wild-type grains in the tetrad (C). A rare example of an *atg6-5* tetrad in which three grains germinated is shown in D. Bars = 50 µm.

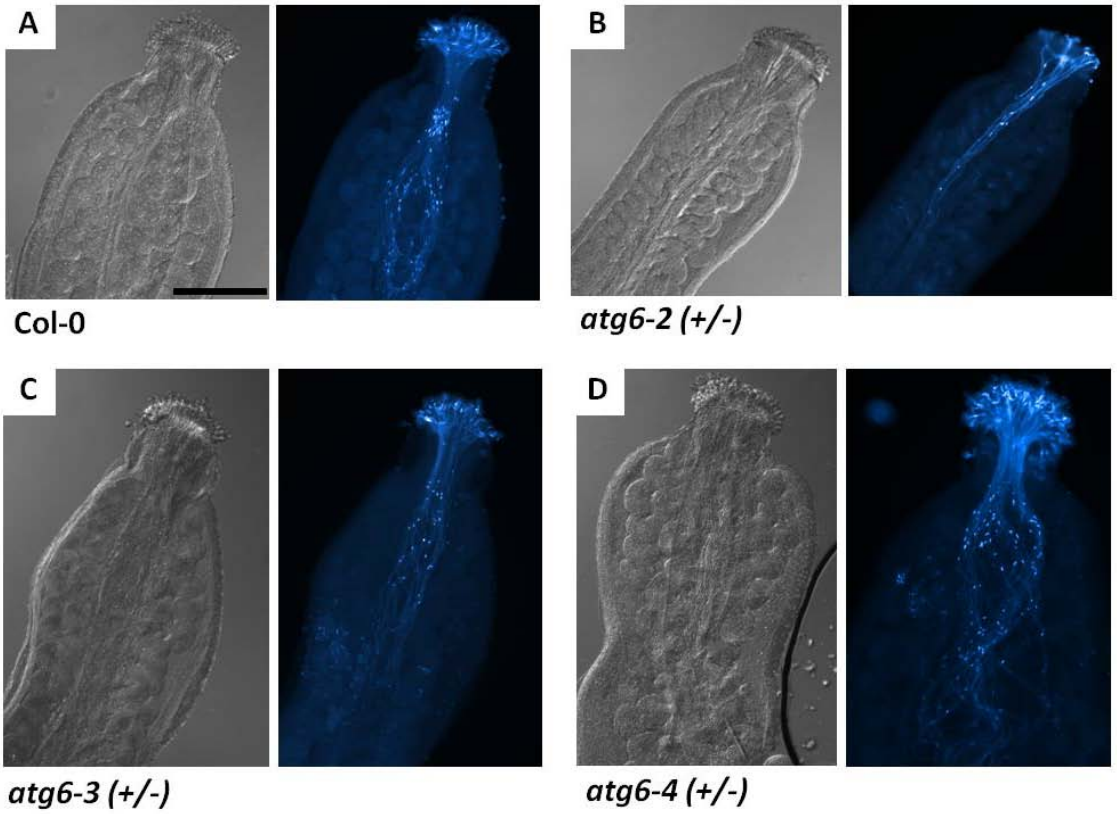

Figure 2.10. *In vivo* pollen tube guidance was unaffected in *atg6-2, atg6-3,* and *atg6-4* heterozygous plants.

Col-0 flowers were demasculated and hand-pollinated with wild-type (A), *atg6-2* (B), *atg6-3* (C*),* or *atg6-4* (D) pollen and incubated at 22^{o}C for 18 hours. Pistils were fixed, stained with decolorized aniline blue, and the pollen tubes observed by both DIC (left) and fluorescence microscopy (right). No differences were seen in pollen tube growth rates or guidance through the pistil tissues in any of the lines. As seen with the *atg6-2* line, less than 50% of the pollen grains, from all mutant lines, germinated. Bar = 300 µm.

Literature cited

1. Abeliovich, H. and D. Klionsky, 2001, Autophagy in yeast: mechanistic insights and physiological function. Microbiol Mol Biol Rev. **65**: 463-479.
2. Bassham, D., M. Laporte, F. Marty, Y. Moriyasu, Y. Ohsumi, L. Olsen, and K. Yoshimoto, 2006, Autophagy in development and stress responses of plants. Autophagy. **2**: 2-11.
3. Seglen, P. and P. Bohley, 1992, Autophagy and other vacuolar protein degradation mechanisms. Experimentia. **48**: 158-172.
4. Tsukada, M. and Y. Ohsumi, 1993, Isolation and characterization of autophagy-defective mutants of *Saccharomyces cerevisiae*. FEBS Letts. **333**: 169-174.
5. Espert, L., P. Codogno, and M. Biard-Piechaczyk, 2007, Involvement of autophagy in viral infections: antiviral function and subversion by viruses. J Exp Mol Med. **85**: 811-823.
6. Levine, B., 2005, Eating oneself and uninvited guests; autophagy-related pathways in cellular defense. Cell. **120**: 159-162.
7. He, C. and K. DJ., 2006, Autophagy and neurodegeneration. ACS Chem Biol. **1**: 211-213.
8. Otto, G., M. Wu, N. Kazgani, O. Anderson, and R. Kessin, 2004, *Dictyostelium* macroautophagy mutants vary in the severity of their developmental defects. J Biol Chem.
9. Liu, Y., M. Schiff, K. Czymmek, Z. Talloczy, B. Levine, and S. Dinesh-Kumar, 2005, Autophagy regulates programmed cell death during the plant innate immune response. Cell. **121**: 567-577.
10. Aubert, S., E. Gout, R. Bligny, D. Marty-Mazars, F. Barrieu, J. Alabouvette, F. Marty, and R. Douce, 1996, Ultrastructural and biochemical chracterization of autophagy in higher plant cells subjected to carbon deprivation: control by the supply of mitochondria with respiratory substrates. J Cell Biol. **133**: 1251-1263.
11. Chem, M., L. Liu, Y. Chen, H. Wu, and S. Yu, 1994, Expression of alpha amylases, carbohydrate metabolism and autophagy in cultured rice cells is coordinately regulated by sugar nutrient. Plant J. **6**: 625-636.
12. Marty, F., 1999, Plant vacuoles. Plant Cell. **11**: 587-599.
13. Moriyasu, Y. and Y. Ohsumi, 1996, Autophagy in tobacco suspension-cultured cells in response to sucrose starvation. Plant Physiol. **111**: 1233-1241.
14. Takatsuka, C., Y. Inoue, K. Matsuoka, and Y. Moriyasa, 2004, 3-Methyladenine inhibits autophagy in tobacco culture cells under sucrose starvation conditions. Plant Cell Physiol. **45**: 265-274.
15. Hanaoka, H., T. Noda, U. Shirano, T. Kato, H. Hayashi, D. Shibata, S. Tabata, and Y. Ohsumi, 2002, Leaf senescence and starvation induced chlorosis are accelerated by the disruption of an Arabidopsis autophagy gene. Plant Physiol. **129**: 1181-1193.
16. Doelling, J.H., J.M. Walker, E.M. Friedman, A.R. Thompson, and R.D. Vierstra, 2002, The APG8/12-activating enzyme APG7 is required for

proper nutrient recycling and senescence in Arabidopsis thaliana. J Biol Chem. **277**: 33105-33114.
17. Thompson, A. and R. Vierstra, 2005, Autophagic recycling: lessons from yeast help define the process in plants. Curr Opin Plant Biol. **8**: 165-173.
18. Slávikovám, S., G. Shy, Y. Yao, R. Glozman, H. Levanony, P. S., Z. Elazar, and G. Galili, 2005, The autophagy-associated Atg8 gene family operates both under favourable growth conditions and under starvation stresses in Arabidopsis plants. J Expt Bot. **56**: 2839-2849.
19. Yoshimoto, K., H. Hanaoka, T.K. Sato, S. Tabata, T. Noda, and Y. Ohsumi, 2004, Processing of ATG8s, ubiquitin-like proteins, and their deconjugation by ATG4s are essential for plant autophagy. Plant Cell. **16**: 2967-2983.
20. Liang, X., J. Yu, K. Brown, and B. Levine, 2001, Beclin 1 contains a leucine-rich nuclear export signal that is required for its autophagy and tumor suppressor function. Cancer Res. **61**: 3443-3449.
21. Yue, Z., S. Jin, C. Yang, A. Levine, and N. Heintz, 2003, Beclin 1, an autophagy gene essential for early embryonic development, is a haploinsufficient tumor suppressor. Proc Natl Acad Sci, USA. **100**: 15077-15082.
22. Kamataka, S., T. Okano, M. Ohsumi, and Y. Ohsumi, 1998, Apg14 and Apg6/Vps30 form a protein complex essential for autophagy in the yeast, *Saccharomyces cerevisiae*. J Biol Chem. **273**: 22284-22291.
23. Kihara, A., T. Noda, N. Ishihara, and Y. Ohsumi, 2001, Two distinct Vps34 phosphotidylinositol 3-kinase complexes function in autophagy and the carboxypeptidase Y sorting in *Saccharomyces cerevisiae*. J Cell Biol. **152**: 519-530.
24. Taylor, L., 1997, Pollen germination and tube growth. Annu Rev Plant Physiol Plant Mol Biol. **48**: 461-491.
25. Zonia, L. and J. Tupy, 1995, Lithium-sensitive calcium activity in the germination of apple (*Malus domestica* Borkh.), tobacco (*Nicotiana tabacum* L.), and potato (*Solanum tuberosum* L.) pollen. J Expt Bot. **46**: 973-979.
26. Qin, G., et al., 2007, Arabidopsis AtBECLIN 1/AtAtg6/AtVps30 is essential for pollen germination and plant development. Cell Res. **17**: 249-263.
27. Fujiki, Y., K. Yoshimoto, and Y. Ohsumi, 2007, An Arabidopsis homolog of yeast ATG6/VPS30 is essential for pollen germination. Plant Physiol. **143**: 1132-1139.
28. Honys, D. and D. Twell, 2003, Comparative analysis of the Arabidopsis pollen transcriptome. Plant Physiol. **132**: 640-652.
29. Becker, J., L. Boavida, J. Carneiro, M. Haury, and J. Feijó, 2003, Transcriptional profiling of Arabidopsis tissues reveals the unique characteristics of the pollen transcriptome. Plant Physiol. **133**: 713-725.
30. Sangwan, R., V. Mathivet, and G. Vasseur, 1989, Ultrastructural localization of acid phosphatase during male meiosis and sporogenesis in Datura: Evidence for digestion of cytoplasmic structures in the vacuoles. Protoplasma. **149**: 38-46.

31. Oda, M.N., S.V. Scott, A. Hefner-Gravink, A.D. Caffarelli, and D.J. Klionsky, 1996, Identification of a cytoplasm to vacuole targeting determinant in aminopeptidase I. J Cell Biol. **132**: 999-1010.
32. Alonso, J.M., et al., 2003, Genome-wide insertional mutagenesis of *Arabidopsis thaliana*. Science. **301**: 653-657.
33. Clough, S. and A. Bent, 1998, Floral dip: a simplified method for *Agrobacterium*-mediated transformation of *Arabidopsis thaliana*. Plant J. **16**: 735.
34. Schu, P., K. Tahegawa, M. Fry, J. Stack, M. Waterfield, and S.D. Emr, 1993, Phosphotidylinositol 3-kinase encoded by yeast VPS34 gene essential for protein sorting. Science. **260**: 88-91.
35. Johnson-Brousseau, S. and S. McCormick, 2004, A compendium of methods useful for characterizing Arabidopsis pollen mutants and gametophytically expressed genes. Plant J. **39**: 761-775.
36. Alexander, M., 1969, Differential staining of aborted and non-aborted pollen. Stain Technol. **47**: 117-122.
37. Regan, S. and B. Moffatt, 1990, Cytochemical analysis of pollen development in wild-type Arabidopsis and a male-sterile mutant. Plant Cell. **2**: 877-889.
38. Cheong, H., T. Yorimitsu, F. Reggiori, J.E. Legakis, C.-W. Wang, and D. Klionsky, 2005, Atg17 regulates the magnitude of the autophagic response. Mol Biol Cell. **16**: 3438-3453.
39. Preuss, D., S. Rhee, and R. Davis, 1994, Tetrad analysis possible in Arabidopsis with mutation of the QUARTET (QRT) genes. Science. **264**: 1458-1460.
40. Twell, D., R. Wing, J. Yamaguchi, and S. McCormick, 1989, Isolation and expression of an anther-specific gene from tomato. Mol Gen Genet: 240-245.
41. Wilkinson, J., D. Twell, and K. Lindsey, 1997, Activities of CaMV 35S and nos promoters in pollen: implications for field release of transgenic plants. J Expt Bot. **48**: 265-275.
42. Schu, P., K. Takegawa, M. Fry, J. Stack, M. Waterfield, and S. Emr, 1993, Phosphatidylinositol 3-kinase encoded by yeast VPS34 gene essential for protein sorting. Science. **260**: 88-91.
43. Toker, A., 2004, Phosphoinositides and signal transduction. Cell Mol Life Sci. **59**: 761-779.
44. Simonson, A., A. Wurmser, S. Emr, and H. Stenmark, 2001, The role of phophoinositides in membrane transprt. Curr Opin Cell Biol. **13**: 485-492.
45. Kim, D., Y. Eu, Y. Kim, K. Pih, J. Jin, S. Kim, H. Stenmark, and I. Hwang, 2001, Trafficking of phosphatidylinositol 3-phosphate from the trans-golgi network to the lumen of the central vacuole in plant cells. Plant Cell. **13**: 287-301.
46. Meijer, H.J.G. and T. Munnik, 2003, Phospholipid-based signaling in plants. Annual Review Plant Biology. **54**: 265-306.

47. Gillooly, D., I. Morrow, M. Lindsay, R. Gould, N. Bryany, J. Gaullier, R. Parton, and H. Stenmark, 2000, Localization of phosphatidylinositol 3-phosphate in yeast and mammalian cells. EMBO J. **19**: 4577-4588.
48. Welters, P., K. Takegawa, E. SD., and M. Chrispeels, 1994, AtVPS34, a phosphatidylinositol 3-kinase of *Arabidopsis thaliana*, is an essential protein with homology to a calcium-dependent lipid binding domain. Proc Natl Acad Sci, USA. **91**: 11398-11402.
49. Monteiro, D., Q. Liu, S. Lisboa, G. Scherer, H. Quader, and R. Malhó, 2005, Phosphoinositides and phosphatidic acid regulate pollen tube growth and reorientation through modulation of [Ca2+]c and membrane secretion. J Expt Bot. **56**: 1665-1674.
50. Monteiro, D., P. Castanho Coelho, C. Rodrigues, L. Camacho, H. Quader, and R. Malhó, 2005, Modulation of endocytosis in pollen tube growth by phosphoinositides and phospholipids. Protoplasma. **226**: 31-38.
51. Gupta, R., J. Ting, L. Sokolov, S. Johnson, and S. Luan, 2002, A tumor suppressor homolog, AtPTEN1, is essential for pollen development in *Arabidopsis*. Plant Cell. **14**: 2495-2507.
52. Lobstein, E., A. Guyon, M. Férault, D. Twell, G. Pelletier, and S. Bonhomme, 2004, The putative Arabidopsis homolog of teast Vps52p is required for pollen tube elongation, localizes to golgi, and might be involved in vesicle trafficking. Plant Physiol. **135**: 1480-1490.
53. Tassa, A., M. Roux, D. Attaix, and D. Bechet, 2003, Class III phosphoinositide 3-kinase–Beclin1 complex mediates the amino acid-dependent regulation of autophagy in C2C12 myotubes. Biochem J. **376**: 577-586.

Chapter 3

AtFDC is a Novel FYVE-Domain-Containing Protein that Interacts with Autophagy Protein 6 (AtATG6) in *Arabidopsis thaliana*

Abstract

Phosphatidylinositol-3-phosphate (PI3P) plays key roles in the regulation of both constitutive protein trafficking, and stress-induced trafficking through the autophagy pathway. Proteins that contain high specificity PI3P-binding domains, including FYVE domains, which allow for peripheral association with membranes, mediate this biological activity. In yeasts and plants, the class III phosphatidylinositol-3-kinase complex (PI3K) produces PI3P. Here we show that Arabidopsis autophagy-related protein 6 (AtATG6), a subunit of the PI3K complex, interacts with AtFDC a novel FYVE-domain-containing protein. Bioinformatics analysis revealed that AtFDC is one of 15 *Arabidopsis* FYVE-domain-containing proteins. AtFDC also showed conservation of the canonical sequence R+HHC+XCG, which contains the “histidine switch.” In addition to eight conserved cysteines, which coordinate zinc ions, it was determined that AtFDC contained eight free thiol groups and bound zinc ions in the expected 2:1 ratio. AtFDC was found to peripherally associate with membranes and also exhibited punctate intracellular localization. Both properties are observed in other functional FYVE domain proteins. However, AtFDC did not display any lipid binding ability *in vitro*. Thus, AtFDC is the first of the non-PRAF (PH, RCC1, and FYVE) *Arabidopsis* FYVE domain proteins to be characterized, and the first novel ATG6 protein interaction partner identified in plants.

Introduction

Eukaryotic organisms respond to a wide variety of biotic and abiotic stress factors through the activation of lipid signaling pathways and through the production of phosphatidylinositol lipids. The myo-inositol head group of these lipids undergoes regulated modification by spatially separated substrate-specific phosphatidylinositol-lipid-kinases [1]. These phosphatidylinositol lipids play key roles in the regulation of transcription [2], activation of the autophagy pathway, pathogen response [3], polarized cell growth [4], cell signaling [5,6], root hair development [7] and in the maintenance of constitutive and stress induced vesicular trafficking processes, including the autophagy pathway [5,8,9]. The autophagy pathway allows cells to survive under hostile conditions by promoting internal degradation and recycling. Initiation of this process requires the activity of the class III phophatidylinositol-3-kinase (PI3K) complex, which catalyzes the formation of phosphatidylinositol-3-phosphate (PI3P) through the addition of a phosphate group to the 3 prime position of the myo-inositol head group [10].

PI3P is required for the continual sorting of newly synthesized proteins and their receptors to the endosome and vacuole [9,11,12]. PI3P also has established roles in trans-Golgi-to-vacuole/lysosome protein sorting [10], and regulation of the actin cytoskeleton [13,14]. Research conducted with *Daucus carrota* identified the essential lipid phosphatidylinositol-3-phosphate (PI3P) in plant cells [14,15]. Subsequently, PI3P has been found to have distinct regulatory roles during root nodule development in soybeans [16] and in the regulation of stomatal movements in response to abscisic acid signaling [17,18]. Although its role is not clearly defined, PI3P is also associated with sites of active transcription in the nucleus [19,20].

The yeast and mammalian PI3K complex is composed of at least three conserved subunits: Vps34, which is the catalytic subunit; Vps15, which is an activating kinase; and autophagy-related protein 6 (Atg6) [21]. Subsequent bioinformatics analysis has identified sequence-based homologues for each of

these three conserved components [22]. An additional component Atg14, which serves as a linker protein between Vps34 and Vps15 in yeast, lacks a sequence-based homologue in Arabidopsis. The involved of the Arabidopsis VPS34 homolog in PI3P synthesis was demonstrated in a 1994 study that analyzed *atvps34* mutants. Whereas *atvps34* homozygotes are not viable, heterozygous segregants produce reduced levels of PI3P [15]. The biological activity of PI3P is largely mediated by cytosolic proteins that contain highly specific PI3P-binding domains. These domains allow the effector proteins to become reversibly and peripherally associated with membranes [1,23-25]. The effector proteins then serve as receptors during cellular trafficking, as signaling components through interactions with small GTPases, or as docking/scaffold proteins for large macromolecular complexes [8,26].

One well-studied class of PI3K effector proteins contains evolutionarily conserved FYVE domains. The 60-80 amino acid FYVE domain was initially identified in four proteins: Fab1, YOTB, Vac1, and EEA1 [27-29]. The crystal structure of several of these FYVE-domain-containing proteins has been solved and consistent with earlier point mutation analysis, indicates that eight-highly conserved cysteine residues are responsible for coordinating two zinc ions [30]. This association stabilizes the anti-parallel beta sheets and is necessary for the functionally active conformation of the FYVE domain [29,30]. In addition, a conserved RHHCCG motif forms the PI3P-binding pocket and contains the histidine residues required for the “histidine switch” which allows for pH-dependent binding of the FYVE domain to PI3P [31,32]. Through association with PI3P, many FYVE-domain proteins localize to the PI3P-rich endosomal or Golgi membranes and serve important roles in endosomal fusion and protein sorting [23,26,29]. Additional proteins, such as Fab1, are active kinases, others, such as EEA1 and Vac1, associate with small GTPases, while members of the *Arabidopsis* PRAF family contain RCC1 (Regulator of Chromosomal Condensation 1) DNA binding motifs [6,33].

Studies have also confirmed the requirement for PI3K activity during the autophagy pathway in plants. Carbon-starved tobacco cells treated with the PI3K

inhibitor wortmannin are unable to form autophagic vesicles [34]. The most well-studied plant PI3K component homolog is ATG6 which been implicated in regulating the hypersensitive response during programmed cell death in tobacco [35]. Interestingly ATG6's role during the restriction of programmed cell death requires the activity of another PI3K component homolog, NtVPS34 [35,36]. This suggests that ATG6 functions in a PI3K complex in plants similar to other eukaryotic systems. The Arabidopsis ATG6 homolog also has an essential role during pollen development [37-39]. However, it is unclear whether AtATG6's role in pollen biology requires PI3K activity or PI3P production.

Due to the variety of ATG6's biological functions in plants and the lack of an Atg14 homolog, we wanted to identify additional AtATG6 interacting proteins. This would allow for a greater understanding of ATG6's role in plant-specific processes like pollen development, and could potentially identify novel PI3K components. To achieve this goal, a yeast two-hybrid assay was performed. Here we present the identification and characterization of a novel AtATG6-interacting protein termed AtFDC, or FYVE-domain-containing protein. Unlike the previously characterized Arabidopsis FYVE domain containing proteins, PARF [40], PARF-LP [20] (also termed PRAF4 [41]), and UVR8 (also termed PRAF9 [41]), which also contain PH and RCC1 domains, AtFDC contains only a canonical FYVE-domain. To date, AtFDC is the first of the non-PRAF FYVE-domain-proteins to be characterized and the first novel ATG6 protein interaction partner identified in plants.

Materials and Methods

Plasmid construction. Full-length *AtFDC* and *AtATG6* were amplified using Vent polymerase (New England Biolabs, Ipswich, MA) from full-length cDNA clones (U12263, U12843) obtained from ABRC (Arabidopsis Biological Resource Center). The primers were AtFDC Primer 1: 5'ATGCAACAGGG AGATTACAAT3', AtFDC Primer 2: 5'TCAATGTGCGCTAACGAGGAA3', ATG6 Primer 1: 5'ATGAGGAAAGAGGAGATTCCA3', ATG6 Primer 2: 5'CTAAGT TTTTTTACAGTAAGG3'. PCR products were incubated with 1 unit Taq

polymerase at 72^{o}C for 15 min (Promega, Madison, WI) and then ligated into TOPOPCRII (Invitrogen, Carlsbad, CA) following the manufacturer's instructions. In addition, *AtFDC* and *AtATG6* were amplified with and without their stop codons from full-length cDNA clones (U12263 and U12843) and ligated into the Gateway® pENTR/SD/TOPO vector (Invitrogen, Carlsbad, CA) (ATG6 see ref [38], AtFDC LP:5'CACC ATG CAA CAG GGA GAT TAC AAT3', FDC RPstop: 5'TCA ATG TGC GCT AAC GAG GAA3', AtFDC RPnostop: 5'ATG TGC GCT AAC GAG GAA3').

For the yeast two-hybrid assay, full length *ATG6* was amplified from U12843 with specific primers (ATG6-NdeILP: 5'CATATGAGGAAAGAGGAGATTCCA3', ATG6-SalIRPnostop:5' GTCGACAGTTTTTTTACAGTAAGGCTT3') that added mutagenic SalI and NdeI restriction sites. The PCR products were ligated into TOPOPCRII. TOPOPCRII:*ATG6* was digested with SalI and NdeI and the *ATG6* gene fragment was gel purified and then ligated into SalI- and NdeI-digested pAS1 vector (ABRC).

For overexpression of AtFDC and AtATG6 in *E.coli*, LR clonase™ recombination reactions (Invitrogen, Carlsbad, CA) were performed to transfer the *AtFDC* and *ATG6* cDNAs with stop codons from pENTR/SD/TOPO into pH9-GW [38]. For the yeast overexpression studies, the yeast vector pYL435 was obtained from ABRC and mutagenesis was performed as described previously [38]. LR clonase™ recombination reactions (Invitrogen, Carlsbad, CA) were performed to transfer the *AtFDC* cDNA with and without the native stop codon from pENTR/SD/TOPO into this modified pYL435 vector [38]. For overexpression of AtFDC in plants, LR clonase™ recombination reactions (Invitrogen, Carlsbad, CA) were performed to transfer the *AtFDC* cDNA with a stop codon from pENTR/SD/TOPO into pCHF3-GW, a 35S:His-tagged plant overexpression vector (gift from Jianming Li, University of Michigan; pCHF3-GW is pCHF3 modified with a Gateway® cassette).

Protein overexpression and purification. pH9-GW-*AtFDC* and pH9-GW-*AtATG6* were transformed into chemically competent BL21 protein over-

expression cells. Following growth to 0.4-0.6 OD_{600} nm in LB^{kan50} media, protein production was induced by addition of 1 mM IPTG. Cell cultures were harvested three hours post induction by centrifugation at 5,000 rpm for 10 min at $4^{o}C$, resuspended in lysis buffer (40 mM imidazole, 4 M NaCl, 160 mM Tris-Cl, pH 7.9) and subjected to sonication (3x20 sec pulse with 20 sec pause). The crude extract was then centrifuged at 5,000 rpm to pellet unbroken cells. The cleared lysate was applied to HisBind resin columns (Novagen, Darmstadt, Germany) and processed according to the manufacturer's instructions. 2 M urea was added to the lysis buffer to solubilize AtFDC; the urea was removed later by standard dialysis against 40 mM HEPES buffer. The protein concentration in each elution fraction was determined using a BCA protein assay kit (Pierce, Rockford, IL). A final solution of 1 mg/ml AtATG6 was prepared in 40 mM HEPES buffer, pH 7.5 (while AtFDC was soluble only to 0.5-0.8mg/ml)

Yeast two-hybrid screen and mating assay. pAS1:*AtATG6 was* transformed into haploid Y187 cells and transformants were identified by growth on SC–Trp media. Y187::pAS1:ATATG6 cell cultures were grown to mid-log phase and subjected to a second transformation with either an empty pACT vector (negative control) or the CD4-10 Arabidopsis yeast two-hybrid library (ABRC and NSF/DPE/USDA Collaborative research in plant biology program, research collaboration group in plant protein phosphorylation (USDA 92-37105-7675)) at a titer of $2.5x10^{9}$ pfu/ml. The cells were then plated onto interaction media SC-Leu/-Trp/-His/25 mM 3-AT and grown for five days at $30^{o}C$. A sample of this transformation was plated onto SC-Leu/-Trp to assess the total number of transformants screened in this study (approximately 3.4×10^{6} colonies). Eighty-seven medium to large colonies were re-streaked onto interaction media SC-Leu/-Trp/-His/25 mM 3-AT and tested for β-D-galactosidase activity using a 5-bromo-4-chloro-3-indolyl β-D-galactoside filter assay. The Y187::pAS1:*AtATG6*::empty pACT vector cells were negative for autoactivation.

Sixty clones showing strong activation (blue color) were grown in SC-Leu media to cause loss of the bait plasmid. Samples were then subjected to PCR using Taq polymerase (RP:5'CACTACAGGGATGTTTAATACCAC3',

LP:5'GCACAGTTGAAGTGAACTTGCGGG3'). To allow for sequencing of the pACT interacting gene the PCR products were purified in the following manner: 50 µl PEG (20% PEG 8000, 2.5 M NaCl) was added to a 50 µl PCR reaction and incubated at 37^{o}C for 15 min. The reaction was precipitated by centrifugation at 12,000rpm for 15 minutes (room temperature) and the pellet rinsed with 80% ethanol. Following drying the pellet was dissolved in 25 µl of water and then each product was sequenced using the PCR primers. Genes were identified using BLAST tools on the TAIR website (http://www.arabidopsis.org/).

Selected pACT interaction plasmids were isolated from cultures grown in SC-Leu media (causes loss of the initial ATG6 containing plasmid) to allow for mating studies. In brief, pelleted 3 ml yeast cultures were resuspended in 500 µL lysis buffer (0.1 M Tris-HCL pH 8.0, 50 mM EDTA, 1% SDS) and vortexed with glass beads. The solution was supplemented with 25 µL of 5 M NaCl and extracted with 400 µL TE-saturated phenol and with 400 µL phenol:chloroform (4:1). DNA was precipitated by the addition of 1 ml 95% ethanol, pelleted by centrifugation at 12,000 rpm for 5 minutes, rinsed with 70% ethanol, dried at room temperature, and resuspended in water. For the yeast mating assay, haploid Y190 yeast cells containing the pACT-*AtFDC* construct isolated from the yeast two-hybrid screen were mated with haploid Y187 cells containing either the pAS1-*AtATG6* construct or pAS1 empty vector control. The haploid and mated cell lines were streaked on interaction media and yeast growth was assayed for β-galactosidase activity.

Far western analysis. pH9-GW:*AtFDC*, pH9-GW:*AtATG6*, and pGEM7Zf :*SoGLO* [42] were linearized with an appropriate enzyme prior to *in vitro* transcription with SP6 RNA polymerase (Promega, Madison, WI). Radiolabeled protein probes were produced by addition of *in vitro* synthesized mRNA to a cell-free rabbit reticulocyte lysate (Promega, Madison, WI) translation system containing [^{35}S]methionine. Incorporation of the radiolabel was quantified via trichloroacetic acid precipitation as previously described [43].

Purified His6-tagged AtFDC, AtATG6 and AtPEX5 protein (gift from A. Liepman) were applied to methanol-activated PVDF membrane in duplicate (10

µg protein per spot). The membrane was then allowed to air dry before being probed for two hours at room temperature with $5x10^6$ TCA-precipitable counts of *in vitro* transcribed and translated AtATG6, AtFDC or SoGLO (positive control) in TBS-TWEEN with 3% BSA. The blots were then washed 3 times for 20 minutes in TBS-TWEEN, allowed to air dry and then exposed overnight to light-sensitive film.

Zinc-binding experiments. Protein concentration (mg/ml) was determined by measuring the absorbance at 276 nm of purified AtFDC:HIS6 protein and using the calculated extinction coefficient for AtFDC (1.004, http://www.expasy.ch/tools/protparam.html) to calculate the mg/ml protein. To generate Zn^{2+}-coordinated AtFDC, the protein was incubated with 2 mM DTT and 2 molar equivalents of Zn^{2+}, purified on a NAP5™ column (Amersham biosciences, Pittsburgh, PA) and eluted at a concentration of 20 µM into HEPES buffer with 20 µM NaCl (pH 7.5). The Ellman's assay [44] was performed in triplicate as follows: 600 µl guanidinium-HCl, 40 µl of 4 mg/ml Ellman's reagent (Sigma, St. Louis, MO) and 160 µl of 40 mM HEPES, pH 7.5 containing 0.2 µM AtFDC protein were combined, and after 10 min incubation at room temperature, the absorbance at 412 nm was measured. The number of free cysteines in AtFDC was calculated using the following equation [44]: OD_{412}nm = [µM protein] x (# of free cysteines) x 13,700. For the PAR/PCMB assay [45], a Zn^{2+} standard curve was generated by adding appropriate volumes of a 153 µM $ZnCl_2$ solution to get final Zn^{2+} concentrations from 0.5 -2.5 µM to a cuvette containing 8 µl of 10 mM PAR (Pyridyl Azo Resorcinol, Sigma, St. Louis, MO) in 40 mM HEPES buffer (pH 7.5). The solution was brought to a final volume of 800 µl with 40 mM HEPES (pH 7.5) and the absorbance at 500 nm measured using a spectrophotometer. For determination of AtFDC Zn^{2+} binding, 0.5µM purified AtFDC protein, in either the oxidized or reduced Zn^{2+} coordinated form was combined with 4.8 µL of 5 mM PCMB (para-chloromercuribenzoic acid, Sigma, St. Louis, MO) in 100 µM PAR solution, brought to a final volume of 800 µl with 40 mM HEPES, pH 7.5, and the OD_{500}nm recorded [45]. Control cuvettes were prepared containing 0.5µM purified AtFDC protein, in either the oxidized (H_2O_2-

treated) or reduced Zn^{2+}-coordinated reduced form without PCMB. Linear regression analysis was performed on the Zn^{2+} standard curve. The resulting equation was solved using the AtFDC absorbance at 500 nm, to calculate the molar ratio of AtFDC and Zn^{2+}.

Lipid blots. PIP strips™ (containing 100 pmol per spot of all eight phosphoinositides and other biologically active lipids) were purchased from Echelon Biosciences (Salt Lake City, UT). Each strip was incubated with TBS-Tween + 5% lipid-free BSA (Sigma, St. Louis, MO) and gently agitated for one hour at room temperature. Strips were then transferred into the same solution supplemented with 1.0 µg/ml AtFDC-HIS protein, PIP2-grip control protein (Echelon biosciences, Salt Lake City, UT), or no protein (negative control). The membrane was incubated with gentle rocking at room temperature for two hours and then washed 3 times (20 min each wash) with TBS-Tween buffer. Membranes were probed with anti-pentahis (Qiagen, Valencia, CA) primary antibody diluted 1:10,000 in TBS-Tween 20 with 5% lipid free BSA and then with a goat-anti-mouse-HRP-conjugated secondary antibody (Pierce, Rockford, IL) diluted 1:20,000 in TBS-Tween 20 with 5% lipid-free BSA. Protein was detected using chemiluminescent substrate according to the manufacturer's instructions (Millipore, Billerica, MA).

Plant analysis. Mutant *atfdc-1* (Salk_013246 line; ABRC) plants were grown in 16 hours light and 8 hours dark at 22^{o}C. For screening, DNA was extracted as previously described [38]. The presence of the T-DNA insert was determined by PCR, using the gene-specific primers suggested at http://signal.salk.edu/cgi-bin/T-DNAexpress (013246 LP:5'GCAACCTAGAGATCTGGCTACAA3', 013246 RP: 5'ACACGTGGCGGTATAATGAAC3'). The LBc1 primer was used to detect the T-DNA inserts in the SALK lines (LBc1: 5'GCCGATTTCGGAAGGAGGATC3'). PCR conditions used were 50-55^{o}C annealing, 25 cycles, 2 min. extension. For RT-PCR analysis, total RNA was extracted from leaf tissues of wild-type and *atfdc-1* plants using the RNeasy Plant Mini kit (Qiagen, Valencia, CA) with on-column DNase digestion, according to manufacturer's directions. RNA was

quantified using a spectrophotometer. RT-PCR was performed using the Access Quick RT-PCR kit (Promega, Madison, WI). PCR portion = 55^{o}C annealing, 23 cycles, 3 minute extension) with 50-100 ng RNA template and 100 ng *AtFDC* gene-specific primers or 10 ng β-tubulin gene-specific primers.(AtFDC primer1: 5'TTGAAGATTCCTATGGCGATG3', AtFDC primer2: 5'ACAGTGTCCAGAAGGGTGTTG3', At1g20100 RP: 5'GCTGCATCGGAAAGAGAAGAAGGA3', At1g20100 LP:5'CAATCTCTTGACGTCTGCAAGCTC3', β-tubulin primer 1:see ref [38],).

Expression of AtFDC in yeast. Yeast vector pYL435 was obtained from ABRC and QuikChange ® Mutagenesis (Stratagene, Cedar Creek TX) was used to modify the vector as previously described [38]. LR clonase™ recombination reactions (Invitrogen, Carlsbad, CA) were performed to transfer *AtFDC* from pENTR into this modified pYL435 vector. BY4742 yeast were transformed and grown on –Ura selective media. Protein production was induced by addition of galactose to the SC-Ura media (6.7 g/L yeast nitrogen base (YNB) without amino acids, 10 g/L ammonium sulfate, 0.67 g/L amino acids–Leu/–Ura, 24 mg/L Leu, pH 5.6, 20 g/l galactose).

For the membrane wash experiments, yeast cells were grown to mid-log phase in SC-Ura + 2% galactose, and harvested by centrifugation at 3,200 rpm for 5 min at 4^{o}C. Cells were resuspended to 10 OD_{660}/50 µL yeast protein prep buffer (0.3 M sorbitol, 0.1 M NaCl, 5 mM $MgCl_2$, 10 mM Tris-HCL pH 7.6) by adding acid washed glass beads to just below the meniscus and vortexing for three 1 min cycles, with a 2 min ice rest in between each burst. The solution was transferred to a new tube and the beads washed once with additional buffer. The solution was then centrifuged at 2,500 rpm (4^{o}C) to pellet unbroken cells. The initial supernatant fraction (S1) was resuspended using beads and centrifuged at 14,000 rpm for 30 min at 4^{o}C. The supernatant fraction (S2) was removed and stored at -70^{o}C for further analysis. The pellet fraction (P2) was resuspended in yeast protein prep buffer using beads and ultracentrifuged at 40,000 rpm for one hour at 4 ^{o}C yielding the final supernatant (S3) and pellet (P3). This pellet fraction

contained the largest fraction of AtFDC protein, when analyzed by western blot using a Penta-his antibody (Qiagen, Valencia, CA), as described above.

Membrane washes were performed by incubating equal volumes of resuspended P3 fraction with either 2% SDS, 250 mM NaCl, 500 mM NaCl, buffer (negative control) or following pH increase to 11 with NaOH. Samples were vortexed and homogenized 10 times with a micropestle before incubating on ice for 4 hours. Samples were then centrifuged at 40,000 rpm for 30 min. The supernatant (soluble) and pellet (insoluble) fractions were separated and resuspended to equal volumes in sample buffer. Samples were then analyzed by western blot using a Penta-his antibody (Qiagen, Valencia, CA).

BY4742:pYL435-AtFDC yeast were grown overnight in SC-Ura media containing 2% galactose to induce protein production. Cells were diluted to approximately $2x10^6$cells/ml and grown for an additional 6 hours (two doublings). Cells were fixed by addition of 0.1 volume 40% formaldehyde and incubation on ice for 2 hours. Cells were washed three times with solution A (100 mM potassium phosphate buffer, pH 7.5, 1.2 M sorbitol), resuspended to $1x10^8$ cells/ml (solution A with 2 µl/ml β-mercaptoethanol) and divided into 250 µl aliquots. To prepare spheroplasts, cell aliquots were incubated with 30 µl Zymolyase (stock solution – 10 mg/ml in 50 mM Tris HCl, 150 mM NaCl, 5 mM EDTA; pH 7.5) at 30°C for 30 minutes. Cell were then pelleted at 2,500 rpm and washed twice with solution A. Cells were transferred into 10 well glass slides treated with 1% polyethyleneamine solution (Sigma, St. Louis, MO) incubated at room temperature for 30 minutes, washed with 2% goat serum (Sigma, St. Louis, MO) in solution A, and allowed to dry. The slides were then placed in a -20°C methanol bath for 6 min, transferred to acetone at -20°C for 30 sec and dried at room temperature.

Slide-mounted yeast samples were incubated overnight in block buffer (solution A with 0.2% goat serum) containing anti-FLAG M2 antibody (1:5,000, Sigma). Slides were placed in a humidity chamber to prevent them from drying out. Slides were then washed three times with block buffer and incubated with rabbit anti-mouse-DTAF-conjugated secondary antibody (Jackson

Immunoreserach laboratories, West Grove, PA) for two hours at room temperature. Finally, slides were washed three times with block buffer, air dried, and then coverslips were mounted using Vector-shield (Sigma, St. Louis, MO). Samples were imaged using DIC and confocal fluorescence microscopy on a Leica TCF SP5 (software version 1.7) with a Leica 40X objective and 1.7 zoom factor. Microscope settings were as follows; standard Leica GFP protocol modified for excitation at 495 nm and reading of emissions from 498-624 nm.

Results

Identification of AtFDC, a novel ATG6 interaction partner. To identify proteins that directly interact with AtATG6, a yeast two-hybrid screen was performed. Full-length At*A*TG6 protein was fused to the Gal-4 DNA binding domain (pAS1) and screened against the CD4-10 yeast two-hybrid library. This library was generated using mRNA isolated from mature *Arabidopsis* leaves and roots, cloned into the pACT vector. From this screen, forty-six colonies showed strong β-galactosidase activity (data not shown). Following isolation of the pACT plasmids, each unknown gene was PCR amplified, sequenced and the locus was identified through BLAST searches against the Arabidopsis mRNA library (www.arabidopsis.org). Twenty-six percent of the colonies contained full-length cDNA corresponding to the At1g20110 locus. Bioinformatic analysis of the predicted full-length protein sequence identified an evolutionarily conserved FYVE domain within the protein. We designated this unknown protein as AtFDC, for FYVE-Domain-Containing protein. Interestingly, this locus was previously annotated as encoding a lipase [33], however the carboxyl terminal region, which contained the lipase domain, has been subsequently re-annotated as a separate locus, At1g20120.

Before proceeding with further analysis, it was important to confirm the interaction with ATG6, so yeast mating assays were performed. The pACT:*AtFDC* plasmid isolated in the yeast two-hybrid screen was transformed into haploid Y190 cells, which were then mated with haploid Y187 cells containing pAS1:*AtATG6* (Figure 3.1A-1) or a pAS1:EMPTY control (Figure 3.1A-

2). Only the pACT:*AtFDC*/pAS1:*AtATG6* diploids grew on interaction media (compare Figure 3.1A-1 to 3.1A-2 to 5). These colonies were also positive for β-galactosidase activity (Figure 3.1A right), confirming the interaction between AtFDC and AtATG6.

To eliminate the possibility that additional proteins may be mediating the interaction between AtATG6 and AtFDC in yeast, the interaction was tested *in vitro* using a far-western protein blot overlay assay (Figure 3.1B). Purified, membrane-bound his-tagged AtATG6:HIS and AtFDC:HIS proteins were probed with *in vitro* synthesized ^{35}S-labeled AtATG6 and AtFDC proteins. The interaction between AtPEX5:HIS, the peroxisome targeting signal 1 (PTS1) receptor, and glycolate oxidase, a PTS1-containing protein from spinach, was used as a positive control for these experiments (Figure 3.1B, bottom row, left). The membranes were then exposed to film (Figure 3.1B, left). A positive interaction was seen when bound AtATG6:HIS was probed with radiolabeled AtFDC, and vice versa (Figure 3.1B). This confirms that the two proteins were able to interact *in vitro* and that the interaction was direct.

Having established that AtFDC interacted with AtATG6, bioinformatic analyses were performed to further characterize AtFDC and to identify additional FYVE-domain-containing proteins in Arabidopsis. Protein sequence analysis revealed that AtFDC (Figure 3.2A), like other proteins with a FYVE domain, contained the eight conserved cysteines, which coordinate zinc ions, and the canonical sequence R+HHC+XCG, which binds the phosphate groups of PI3P [30,32]. To identify additional Arabidopsis FYVE domain containing proteins, amino acids 455-515 of AtFDC (which correspond to the predicted FYVE domain) or the full-length protein sequence were queried against the TAIR database. Fifteen separate loci containing both the conserved cysteine residues (green and red boxes) and the PI3P-binding motif (blue box) were identified (Figure 3.2C). One locus, At1g29800, lacked any EST or microarray data, suggesting it may be a pseudogene, so it was omitted from subsequent consideration.

To further analyze the protein sequence relationships, an un-rooted cladogram was generated (Figure 3.2B). The ClustalW alignment of all the FYVE-domain-containing proteins from Arabidopsis was analyzed using the Protdist and neighbor programs of the Phylip3.67 package (Figure 3.2B). The nine proteins that contain PH and RCC1 domains, in addition to a FYVE domain, share the highest protein sequence similarity (purple clade). Three of these proteins have been previously studied: PARF1 [40], PARF-LP1 [20] (also termed PRAF4 [41]), and UVR8 (also termed PRAF9 [41]). In addition, two FAB1-like proteins were identified (pink clade). Based on this sequence analysis, the protein that is most closely related to AtFDC is encoded by the At3g43230 locus. Unlike AtFDC, the FYVE domain from At3g43230 is located in the amino-terminal region and this protein also contains a DUF500 domain (Domain of Unknown Function). This combination of FYVE and DUF500 domains, which was only found in plants, is absent from AtFDC. These differences in protein structure suggested that AtFDC may be unique in Arabidopsis. In addition, comparison with the rice genome identified two sequence-based homologs for AtFCD1, both containing a single FYVE domain near the carboxyl terminus. The presense of rice proteins that share higher homology with AtFDC than any Arabidopsis proteins reinforces the notion that AtFDC has a functional role that is distinct from other Arabidopsis FYVE-domain-containing proteins.

Functional characterization of AtFDC. To further understand the physiological role of AtFDC, it was important to determine whether the FYVE domain was functional. All FYVE domains contain four pairs of cysteine residues, which each coordinate two Zn^{2+} ions in a $1C_2A$, $2C_2B$, $3C_2A$, $4C_2B$ manner [30]. This means that the first and third pairs coordinate one Zn^{2+} ion, and the second and fourth coordinate the second Zn^{2+} ion (Figure 3.2C). Therefore, a protein that coordinates Zn^{2+} ions in this manner must contain eight free thiol groups (eight coordinating cysteine residues). To determine the number of zinc-coordinating thiols present in the purified AtFDC protein, an Ellman's assay [44] was performed using oxidized and reduced forms of AtFDC. In proportion to the number of thiol groups, the Ellman's reagent, DTNB (5,5'-dithiobis(2-nitrobenzoic

acid)), produces a colormetric product that can be quantified by reading the absorbance of the solution at 412 nm [44]. To calculate the number of free thiol groups, Beers law was solved using a molar absorptivity of $\varepsilon_{412\ nm}$=13,700 M^{-1} cm^{-1} per free thiol group [44]. It was determined that approximately eight (8.13±0.324) free thiols were present in AtFDC, supporting the hypothesis that eight of the cysteines in the amino acid sequence may be involved in zinc ion coordination (data not shown).

The next step was to test whether AtFDC bound Zn^{2+} ions in the expected molar ratio. If four cysteines are required for each zinc ion, and AtFDC contains eight coordinating cysteines, a molar ratio of 2 M-Zn^{2+}:1 M-AtFDC would be expected. To experimentally determine the actual ratio, a PAR/PCMB assay was performed [45]. A Zn^{2+} standard curve was generated by incubating known concentrations of Zn^{2+} with PAR (pyridyl azo resorcinol) and recording the absorbance at 500 nm. Next, oxidized (without-zinc) or reduced (zinc-coordinated) AtFDC was incubated with or without PCMB (p-chloro mercury benzoic acid). PCMB releases bound Zn^{2+} molecules into the solution. As expected, there was no change in the absorbance when PCMB was added to oxidized AtFDC protein. Conversely, when PCMB was added to reduced (zinc-coordinated) AtFDC, the absorbance increased from 0.193 to 0.269 (average) indicating that Zn^{2+} ions were released into the solution (there was no change when just PCMB was added to the solution). By solving the linear equation from the standard curve (Abs at 500 nm = 0.075X + 0.115, where x is the Zn^{2+} in µM), it was determined that 0.5 µM AtFDC protein bound 1.03 ± 0.17 µM Zn^{2+}. This experimental ratio of 2.05±0.35 Zn^{2+} to 1 AtFDC protein is very close to the 2:1 ratio expected for a protein containing a zinc-binding FYVE domain.

Before directly testing the PI3P-binding capacities of AtFDC, it was first important to determine whether AtFDC was a cytosolic or membrane protein *in vivo*. To do this, a His-tagged form of AtFDC was constitutively expressed in Arabidopsis. Although multiple lines with kanamycin resistance were recovered and the transgene was detected by PCR, no AtFDC protein was observed by western blot (data not shown). Consequently, AtFDC was heterologously

expressed in wild-type BY4742 yeast cells, which, like all eukaryotic cells, contain PI3P-rich membranes. AtFDC-containing yeast cell lysates were subjected to two rounds of centrifugation and then ultracentrifugation, finally yielding an enriched membrane fraction (lane P3 in Figure 3.3A and 3.3B). During each step AtFDC was present only in the pellet fraction, with no detectable protein in the soluble fractions (Fig 3.3A, compare S-soluble and P-insoluble fractions). This indicated that AtFDC was associating with the membrane fraction.

To test whether AtFDC was peripherally associated with the yeast membranes, the membrane-enriched P3 fraction was used in standard salt-wash experiments. Treating the P3 membranes with detergent partially released AtFDC into the soluble fraction, as expected (Figure 3.3B). Incubations with high salt (500 mM NaCl) or high pH conditions completely released AtFDC into the soluble fraction, indicating AtFDC was most likely peripherally associated with the membranes (Figure 3.3B). In addition, because treatment with 250 mM NaCl was not sufficient to cause release, AtFDC was most likely associated with the membranes, rather than simply present in protein aggregates. To confirm that AtFDC associates with a membrane rather than simply forming aggregates in yeast, AtFDC protein localization was observed using indirect immunofluorescence. Analysis revealed that the AtFDC protein was present in one to two punctate dots per cell (Figure 3.3C); no signal was seen in control cells (Figure 3.3C, left). Thus, AtFDC was not simply aggregating in the cytosol, but rather AtFDC peripherally associated with an internal membrane in yeast.

Having determined that AtFDC peripherally associates with membranes in yeast, the functionality of the FYVE domain was tested using lipid blots. Purified zinc-coordinated AtFDC protein was incubated with a commercial membrane containing 15 different lipids including PI3P. Following binding, the membrane was probed with Penta-his antibody to see where the AtFDC protein bound. While the positive control bound as expected no lipid binding was observed for AtFDC (data not shown).

Analysis of *atfdc* mutants. To study the physiological function of AtFDC, the only available mutant line, a T-DNA insertional mutant (Salk_013246), was obtained from the ABRC stock center (Figure 3.4A). The T-DNA is located in a shared promoter region. Plants were grown under 16hr-day, 8hr-night conditions and screened by PCR for the presence of the T-DNA allele. The *atfdc-1* mutant allele segregated at the expected 1:2:1 ratio of wildtype: heterozygotes: homozygous mutants (data not shown). *atfdc-1* homozygous plants displayed no visible phenotype in comparison to wild-type segregants (Figure 3.4B). RT-PCR analysis was performed to determine the level of *AtFDC* transcript in the homozygous plants. Due to the location of the T-DNA the expression level of the other locus controlled by the promoter region (At1g20100) was also examined. The RNA levels of *AtFDC* and At1g20100 were unaffected by the presence of the T-DNA insert in *atfdc-1* homozygous plants as compared to wild type (Figure 3.4C). Thus, this line is not suitable for further *atfdc* mutant analysis.

Discussion

In this study we provide evidence that Arabidopsis ATG6 interacts with AtFDC, an Arabidopsis FYVE-domain-containing protein. The interaction was initially identified in a yeast two-hybrid screen using ATG6 as “bait” (Figure 3.1A) and subsequently confirmed by far-western analysis (Figure 3.1B). AtFDC, which was not bound to PI3P, directly interacted with ATG6 in the far-western analysis suggesting that the interaction between the two proteins may not require PI3P binding. However, zinc ions were present so it is possible that the interaction with ATG6 requires zinc association of AtFDC. Further characterization of AtFDC indicated it was able to bind zinc ions in the ratio previously reported [30] for a FYVE-domain-containing protein. This suggested that AtFDC contains a functional FYVE domain (able to bind to PI3P), a conclusion supported by the high level of amino acid conservation in the FYVE-domain region of the protein (Figure 3.2C). In addition, AtFDC was peripherally associated with a membrane when heterologously expressed in yeast (Figure 3.3B), and further subcellular localization indicated association with an internal

punctate structure (Figure 3.3C), possibly the nucleus or endosome. These data indicate that AtFDC interacts peripherally with an internal membrane component *in vivo,* consistent with the hypothesis that it functions as a PI3P-binding protein. However, AtFDC did not display any lipid binding in a lipid blot assay (data not shown). This may be due, in part, to the limitation of the lipid blot assay used. Alternatively, AtFDC may require additional protein interactions to facilitate its membrane and PI3P interaction, perhaps AtATG6. In addition, since purification of AtFDC required treatment with solubilizing agents, the altered conformation of AtFDC may not allow for PI3P binding, although it could coordinate zinc. In summary, it appears that AtFDC interacts with AtATG6, binds zinc ions, and associates with an internal cellular structure, strongly suggesting an ability to interact with a membrane component, most likely PI3P.

To our knowledge, this is the first report of an ATG6 homolog interacting with a FYVE-domain-containing protein. Consequently our understanding of the physiological function of ATG, allows us to hypothesize a functional role for AtFDC. In mammalian cells, Beclin 1 (the ATG6 homolog) is reported to be both membrane associated and cytosolic [46]. Since no cytosolic localization of AtFDC was observed, either by fractionation (Figure 3.3A, B) or indirect immunofluorescence (Figure 3.3C), AtFDC is most likely associated with the membrane pool of ATG6 (unpublished data). In yeast, the PI3K complex is composed of the three common subunits Vps34, Vps15 and Atg6, and it is localized to membranes, including the Golgi, via the myristolation of VPS15 [47,48]. In addition Atg14, a protein that “links” Vps34 and Atg6 in yeast, is required for the kinase to be active in the autophagy pathway [21]. An alternative subunit (Vps38) functions in place of Atg14 in the vacuolar protein sorting pathway, which also delivers cargo to the yeast vacuole [21]. Bioinformatic analyses show that AtFDC has no significant homology with yeast ATG14 (data not shown), which is to be expected as Atg14 has no identifiable lipid-binding domains [48]. Also, since mammalian Beclin 1 is able to directly interact with the Vps34 catalytic subunit, it is entirely possible that Arabidopsis lacks an ATG14

homolog [46]. Thus, it is most likely that AtFDC is not serving the same role as yeast Atg14.

Arabidopsis ATG6 contains an evolutionarily conserved nuclear export signal, and although the functionality of this signal has not been tested in plants, the mammalian homolog Beclin 1 requires the signal for its function as a tumor suppressor [49]. A truncated form of Beclin 1 that lacked this signal accumulated in the nucleus [49]. Recently, a number of reports have shown that the nuclei of yeast and mammalian cells contain PI3P [2,20,50]. While nuclear pools of PI3P could be the product of a class I or class II kinase complex in mammalian systems, immunolocalization of the soybean VPS34 (class III) homolog in root tissue revealed a strong signal in the nucleus with a predominant signal seen in the nucleolus [19,20,51]. The PI3K complex also co-localizes with transcription sites and is thought to be present in fibrillar structures [19,50].There are other reports of nuclear-localized FYVE-domain-containing proteins including ALFY, a FYVE-domain-containing protein that localizes to the nuclear envelope [52]. Therefore, it is possible that AtATG6 functions in a class III PI3K in the nucleus, as it does on the trans-Golgi network and endosome [46,53], and that AtFDC associates with the nuclear pool of ATG6 and PI3P. Thus, AtFDC may be involved in ATG6-mediated PI3P signaling in the nucleus.

It's also possible that AtFDC is directly involved in vacuolar protein trafficking as an effecter protein for the class III PI3K complex. This is supported by the localization of AtFDC to punctuate internal structures (Figure 3.3). These internal structures could represent endosomes or the *trans*-Golgi network, both of which have PI3P-rich membranes [50,54]. AtFDC could associate with the membrane, perhaps aided by a protein-protein interaction with ATG6 and then, like other FYVE-domain-containing proteins, recruit additional components to the membrane [9,11]. This hypothetical function could be stress-related via the autophagy pathway, or non-stress related, such as during endosomal protein trafficking in a manner similar to ScVps27 [9,26]. These suggestions are not mutually exclusive, as yeast Atg6 is present in both autophagic and non-autophagic PI3K complexes [21]. Unfortunately, no additional information

regarding a stress or non-stress related function, can be gained from existing microarray data because mRNA transcript levels for AtFDC do not change under the tested stress conditions, including carbon deprivation and osmotic stress. It is possible that AtFDC is post-translationally regulated by the activity of the PI3K signaling and the presence of PI3P similar to other FYVE domain proteins.

Since AtFDC is the first reported FYVE-domain-containing protein to interact with any PI3K component, it could have a completely novel, potentially plant-specific, role. For example, several recent studies have shown that AtATG6 is essential for pollen germination in Arabidopsis [37-39]. The process of pollen germination is unique to plants, while later stages, including pollen tube growth, are similar to other polarized cell growth, such as axon growth and guidance. The overall process of pollen germination through pollen tube growth requires phosphatidylinositol-lipid-based signaling for regulation of extensive membrane trafficking to the growing tip and for endocytosis events [4]. Perhaps the interaction between AtATG6 and AtFDC is important during pollen germination, explaining why such an interaction has not previously been reported in other systems. Transcript for AtFDC is enriched in pollen, as is transcript for AtATG6, supporting the notion that the two proteins could both be present and interacting in pollen [55]. However, since the precise cellular role of ATG6 in pollen germination has not been established, it remains unclear whether AtATG6 functions in an autophagic or non-autophagic manner during this process. Therefore, the role of AtFDC is likewise unclear, though it raises some interesting questions regarding both the exact role of AtATG6 in the PI3K complex and the potential protein effectors required for its function during pollen germination.

In conclusion, AtATG6 interacts with AtFDC, a novel FYVE-domain-containing protein. AtFDC is the first of the non-PRAF-domain-containing proteins characterized in Arabidopsis and one of 15 FYVE-domain-containing proteins in the proteome. While PRAF proteins appear to have functional roles in DNA binding and chromatin condensation, it is likely that AtFDC is involved in PI3K-mediated protein trafficking pathways, such as the autophagy pathway, and that the function of AtFDC is mediated through its interaction with AtATG6. It

remains to be seen whether AtFDC, like ATG6, is also involved in pollen germination.

Acknowledgments

We thank Dr. Ursula Jakob and Dr. Amy Chang for their helpful comments throughout this project. Dr Marianne Amenta-Ilbert and Dr. Sumin Han provided invaluable assistance with the zinc-binding and yeast experiments respectively. Thanks to the Arabidopsis Biological Resource Center for the T-DNA seed stocks [56]. NHL was partially supported by the NIH-funded Cellular Biotechnology Training Program at the University of Michigan. This work will be submitted to Autophagy.

Table 3.1. Potential AtATG6 interaction partners identified by Yeast two hybrid. # = number of clones, % = percent of all clones with this gene

Protein Description	Locus	#	%	Functional class	Pred Loc	Note
zinc finger (FYVE type)	AT1G20110.1	12	13.8	DNA/RNA/LIPID/ZINC binding	unknown	
PP2A 4 serine/threonine protein phosphatase	AT2G42500.2	5	5.7	catalytic subunit of phosphatase 2A.	cytoplasm or nucleus	
zinc finger (B-box type) family protein	AT1G06040.1	4	4.6	DNA/RNA/LIPID/ZINC binding	cytoplasm or nucleus	*partial
avirulence-responsive protein	AT3G28940.1	3	3.4	Response to bacterium	unknown	
bZIP transcription factor	AT1G42990.1	3	3.4	DNA/RNA/LIPID/ZINC binding	unknown	
expressed protein	AT5G26740.2	3	3.4	unknown	endomembrane	
protease inhibitor/seed storage/lipid	AT4G12545.1	3	3.4	similar to AIR1	endomembrane	
thioredoxin family	AT1G08570.1	3	3.4	cell redox homeostasis	unknown	
expressed protein	AT1G08380.1	2	2.3	unknown	unknown	
fasciclin-like arabinogalactan-protein	AT1G03870.1	2	2.3	cell adhesion	membrane	
lactoylglutathione lyase	AT1G80160.1	2	2.3	Carbohydrate metabolism	endomembrane	
(UBA)/TS-N domain-containing protein	AT1G04850.1	2	2.3	unknown	cytoplasm	*partial
zinc finger (B-box type) family	AT4G27310.1	2	2.3	DNA/RNA/LIPID/ZINC binding	cytoplasm	
lipase family protein	AT5G14180.1	2	2.3	Triacylglycerol lipase 2	endomembrane	
SEUSS transcriptional co-regulator	AT1G43850.1	2	2.3	organ/flower development	nucleus	*partial
expressed protein	AT4G38750.1	2	2.3	unknown	endomembrane	
glutathione S-transferase	AT2G30870.1	2	2.3	glutathione trasnfer activity	cytoplasm	
SIT4 phosphatase	AT1G07990.1	2	2.3	phosphatase (putative)	endomembrane	
scarecrow-like transcription factor 1	AT1G21450.1	2	2.3	Transcriptional regulation	nucleus	
nodulin MtN21 family protein	AT3G28050.1	1	1.1	unknown	membrane	
nitrogen regulation family protein	AT5G67220.1	1	1.1	Nitrogen regulation	mitochondria	
acyl carrier family protein	AT4G25050.1	1	1.1	Fatty acid biosynthesis	chloroplast	
annexin 3	AT2G38760.1	1	1.1	annexin - Calcium ion binding	cytosol and cell surface	
caldesmon-related / Poly-adenylate binding protein	AT1G52410.2	1	1.1	Calcium ion binding	chloroplast	
expressed protein	AT5G12230.1	1	1.1	unknown	unknown	*partial
formate--tetrahydrofolate ligase	AT1G50480.1	1	1.1	Folic acid biosynthesis	unknown	
hypothetical protein	AT3G45820.1	1	1.1	unknown	unknown	
malate dehydrogenase related	AT1G04410.1	1	1.1	Malate dehydrogenase	unknown	
metallothionein-like protein	AT1G07610.1	1	1.1	copper response	cytoplasm	
oxygen-evolving protein 3	AT4G05180.1	1	1.1	Photosynthesis	thylakoid membrane	*partial
phytochrome A	AT2G37680.1	1	1.1	Photomorphopgenesis	cytoplasm or nucleus	
proton-dependent oligopeptide transport	AT1G72140.1	1	1.1	oligopeptide transport	membrane	
Trypsin protease inhibitor	AT1G73260.1	1	1.1	unknown	mitochondrian	

Figure 3.1. AtATG6 interacts with a novel FYVE-domain-containing protein.

A) Haploid Y187 cells expressing an AtATG6-Gal-4 binding domain fusion (3) were mated with haploid Y190 cells expressing either a AtFDC-Gal-4 activation domain fusion (4) or an empty vector control (5). When haploid and mated cell lines were streaked onto interaction media, only the diploids containing both AtATG6 and AtFDC (1) grew, unlike the control AtATG6 and empty pACT vector diploids (B). Yeast growth was also assayed for β-galactosidase activity; only the diploids in 1 were positive (right). 1:AtFDC/AtATG6 diploid, 2:AtATG6/Empty vector diploid, 3:AtATG6 haploid, 4:AtFDC haploid and 5:Empty vector haploid. B) Polyvinylidene fluoride (PVDF) membrane-bound AtPEX5, AtFDC, and AtATG6 (columns) were probed with ^{35}S-methionine-labeled AtATG6, AtFDC or SoGLO (rows). Binding was seen between AtFDC and AtATG6. The known interaction between AtPex5 and SoGLO was used as a positive control. As expected there was no binding between SoGLO or PEX5 and either AtFDC or AtATG6. The data are summarized in the table (right).

A

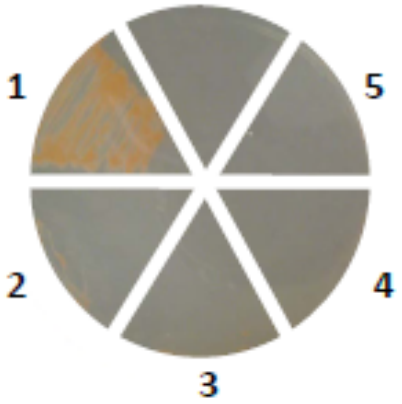

Quad	β-Gal activity
1:AtATG6/AtFDC diploid	Positive
2: AtATG6/ empty vector diploid	Negative
3: AtATG6 haploid	Negative
4: AtFDC haploid	Negative
5: Empty vector haploid	Negative

B

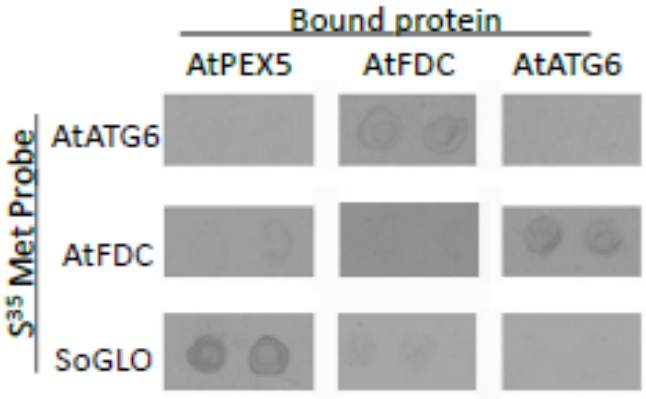

Figure 3.2. AtFDC is one of fifteen Arabidopsis FYVE-domain-containing proteins, all of which have a conserved FYVE domain.

A) AtFDC is a 601-amino acid protein that contains a FYVE domain (amino acids 455-515) in the carboxyl terminus (inset in A). The canonical sequence RR/KHH-CXXC-G is underlined and the four pairs of Zn^{2+}-coordinating cysteine residues are shown in red. B) Position-specific iterative BLAST using amino acids 455-515 of AtFDC (FYVE domain) identified fourteen additional FYVE-domain-containing proteins. This unrooted cladogram was generated using the full-length protein sequence from all FYVE-domain proteins aligned by Clustal W and then further analyzed using the Phylip 3.67 package (Protdist and Neighbor programs). Nine PRAF proteins, which all contain PH, RCC1 and FYVE domains, can be seen in the left-most clade (purple). The upper clade (pink) includes At4g14270 and At4g33240, the two FAB1 homologues that contain putative phosphatidylinositol-4-phosphate 5-kinase domains. C) All proteins contain the expected four pairs of cysteine residues (shown in green and red boxes), and conserved RR/KHH-CXXC-G motif.

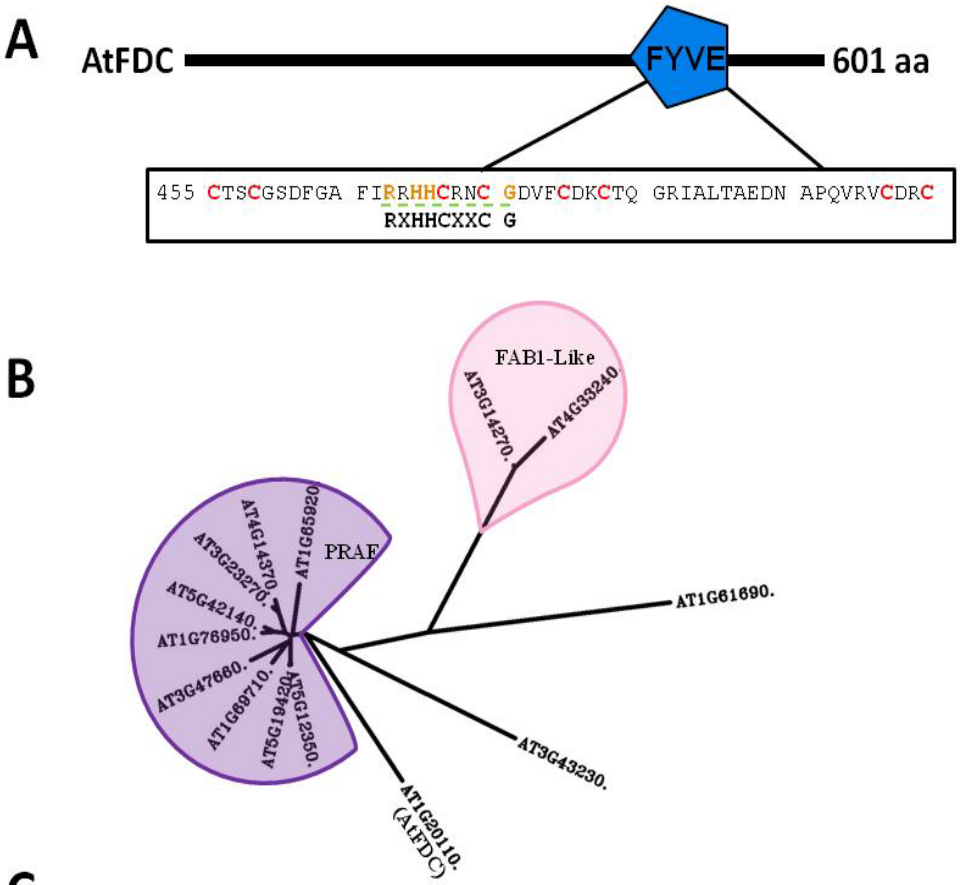
A
AtFDC
FYVE
601 aa
455 CTSCGSDFGA FIRRHHCRNC GDVFCDKCTQ GRIALTAEDN APQVRVCDRC
RXHHCXXC G
B
FAB1-Like
AT3G14270.
AT4G33240.
PRAF
AT4G14370.
AT1G65920.
AT3G23270.
AT5G42140.
AT1G76950.
AT3G47660.
AT1G69710.
AT5G19420.
AT5G12350.
AT1G61690.
AT3G43230.
AT1G20110.
(AtFDC)
C
AT5G19420. GMDQSM-CSGC-RQPFN-FK--RKRHN-CYNC-G-LVF-CHSC-SNKKSLKACMAPNPNKPY----RV-CDRC-FNKLK 742
AT5G12350. GMDQSM-CSGC-RQPFS-FK--RKRHN-CYNC-G-LVF-CHSC-TSKKSLKACMAPNPNKPY----RV-CDKC-FNKLK 719
AT5G42140. GTEQSQ-CSAC-RQAFG-FT--RKRHN-CYNC-G-LVH-CHSC-SSKKSLKAALAPNPGKPY----RV-CDSC-HSKLS 684
AT4G14370. GADQSV-CSGC-RQAFG-FT--RKRHN-CYNC-G-LVH-CHAC-SSKKALKAALAPTPGKPH----RV-CDAC-YTKLK 1598
AT1G76950. GAEQSQ-CSTC-RLAFG-FT--RKRHN-CYNC-G-LVH-CHSC-SSKKAFRAALAPSAGRLY----RV-CDSC-YVKLS 695
AT3G23270. GADQSI-CSGC-RQAFG-FT--RKRHN-CYNC-G-LVH-CHAC-SSKKALKAALAPTPGKPH----RV-CDAC-YSKLK 662
AT1G65920. LNDQTA-CSSC-KSAFG-FT--RKKHN-CYNC-G-LLF-CNAC-SSKKAVNASLAPNKSKLS----RV-CDSC-FDHLW 695
AT1G69710. GSEHSL-CAGC-RNPFN-FR--RKRHN-CYNC-G-LVF-CKVC-SSRKSLRAALAPDMNKPY----RV-CYGC-FTKLK 701
AT3G47660. GTDSTK-CSGC-RHPFN-YM--RKLHN-CYNC-G-SVF-CNSC-TSKKSLAAAMAPKTNRPY----RV-CDDC-YIKLE 699
AT3G43230. DSLAST-CMQC-STPFTAITCG--RHH-CREC-G-GIF-CRNC-SKGRC-LMPSRFRERNPQ----RV-CDSC-YERLD 238
AT1G29800. DSAASA-CMLC-SVRFHPIMCS--RHH-CRYC-G-GIF-CRDC-SKGKS-LVPVKFRVSDPQ----RV-CDVC-FVRLE 248
AT4G33240. DQSCPV-CYEC-DAQFT-VFN--RRHH-CRLC-G-RVF-CAKC-AANSIPSPSDETKDSHEEPERIRV-CNYC-YKQWE 103
AT3G14270. DQSCRV-CYEC-DCQFT-LIN--RRHH-CRHC-G-RVF-CGKC-TANSIPFAPSDLRTPREDWERIRV-CNYC-FRQWE 106
AT1G61690. VVDASH-CQGC-SSQFT-FIN--RKHH-CRRC-G-GLF-CGTC-TQQRLSL-RGQGDS--P----VRI-CEFC-KKIEE 79
AT1G20110. DEAVSK-CTSC-GSDFGAFI---RRHH-CRNC-G-DVF-CDKC-TQGRI---ALTAEDNAPQ---VRV-CDRC-MAEVS 682
-------C--C----------RKHH-C--C-G-----C--C----------C--C------

Figure 3.3. AtFDC is a peripheral membrane protein.

A) Step-wise soluble and insoluble (pellet) fractions were prepared from yeast cells expressing AtFDC-FLAG (BY4742:pYL435-AtFDC) and analyzed by western blot using an anti-Flag antibody. AtFDC was only detectable in the insoluble (P2 and P3) fractions and not the soluble fractions (S2 and S3). Whole cell extract is shown in the first lane (WC). B) Enriched membranes (P3) were incubated with 2% SDS, 250 mM NaCl, 500 mM NaCl, high pH conditions (pH 11) or in buffer (control). Soluble (S) and insoluble (P) fractions were prepared by ultracentrifugation and analyzed by western blot using an anti-FLAG antibody. AtFDC was detected in the soluble fractions under high salt and at high pH. C) Yeast cells expressing AtFDC (BY4742:pYL435-AtFDC) were processed for indirect immuno-fluorescence and probed using anti-FLAG M2 primary and DTAF-conjugated secondary antibodies. Samples were imaged using DIC (top) and confocal laser microscopy (bottom). Two representative images are shown (middle and right). Signal was detected in one to two small punctate dots per cell, indicating that AtFDC associates with an intracellular structure. No signal was detected from control cells (left).

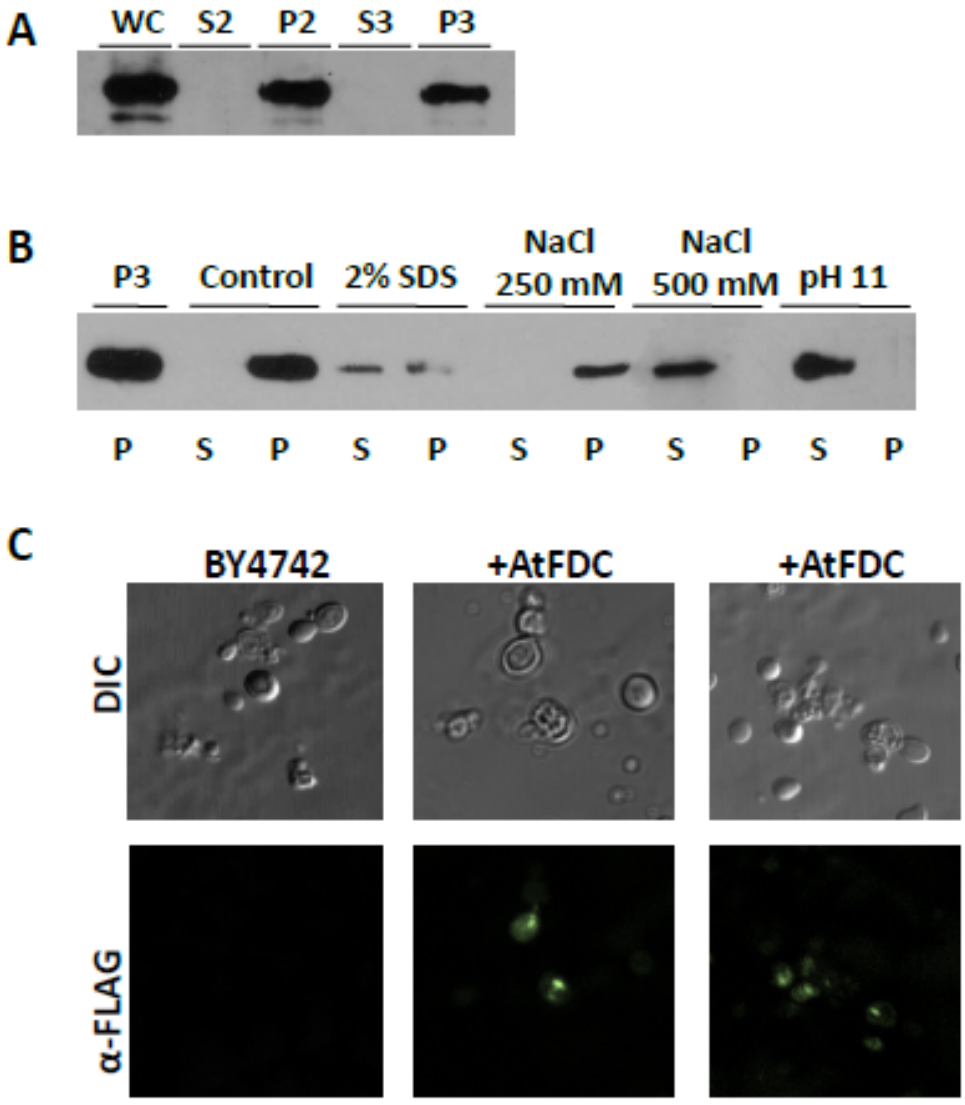
A
WC
S2
P2
S3
P3
B
P3
Control
2% SDS
NaCl
250 mM
NaCl
500 mM
pH 11
P S P S P S P S P S P
C
BY4742
+AtFDC
+AtFDC
DIC
α-FLAG

Figure 3.4. *atfdc-1* plants have no visible phenotypes and mRNA level was unaffected.

A) One T-DNA insertional mutant line for *AtFDC* (Salk_013246) was available. In this line the T-DNA (triangle with arrow) is located 390 bp upstream of the translation initiation site for *AtFDC (lower line)* and 139 bp upstream of the coding region of *At1g20100 (top line),* indicating potential disruption of both genes. At1g20120 is downstream of *AtFDC* and contains a lipase domain; the two were once annotated as a single gene. Exons are shown in red, terminating exons are shown in yellow, introns are grey hashed lines, arrows indicate the direction of each gene/T-DNA. B) Wild-type (left) and homozygous *atfdc-1 (*right) plants were grown under normal conditions and examined for any phenotypic differences. None were observed. C) RT-PCR was performed on mRNA samples from Wt and *AtFDC-1* using primers specific for *AtFDC (top)*, At1g20100 (middle) and β-tubulin (bottom – served as control). No differences were seen in the transcript levels of either *AtFDC* or At1g20100 indicating the T-DNA insert does not disrupt production of full-length transcript.

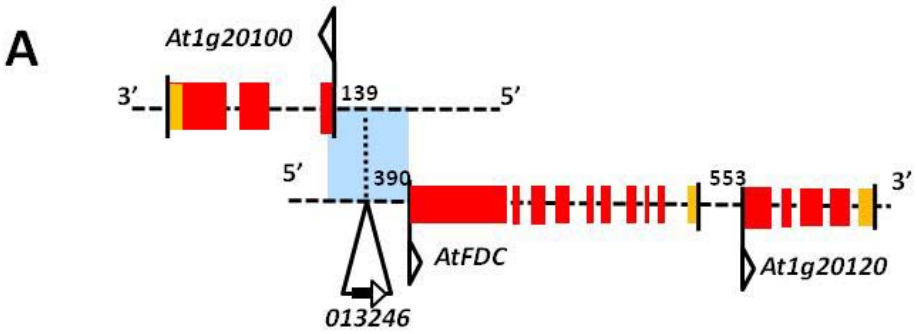
A
At1g20100
3'
139
5'
5'
390
553
3'
AtFDC
At1g20120
013246

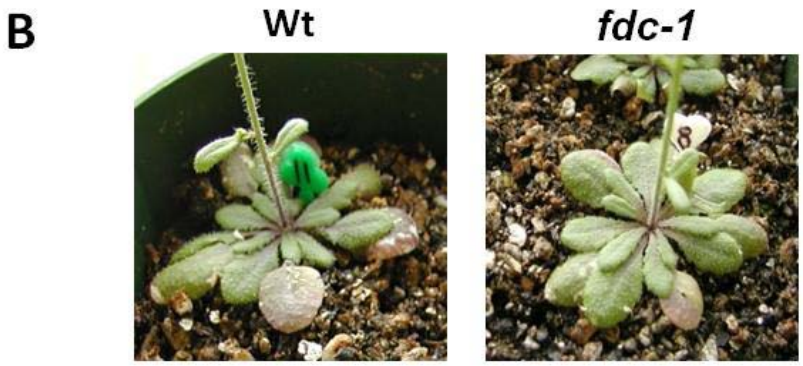
B
Wt
fdc-1

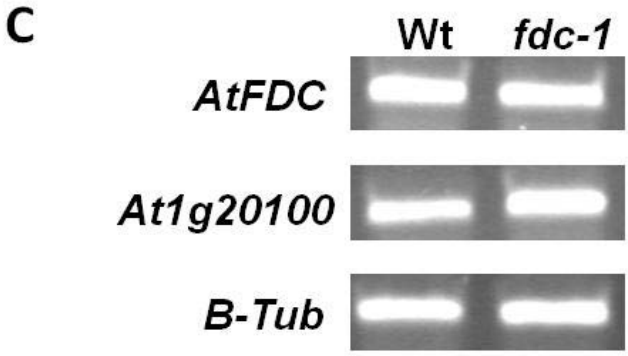
C
Wt
fdc-1
AtFDC
At1g20100
B-Tub

Literature cited

1. Burd, C.G. and S.D. Emr, 1998, Phosphatidylinositol(3)-phosphate signaling mediated by specific binding to RING FYVE domains. Mol Cell. **2**: 157-162.
2. Gonzales, M.L. and R.A. Anderson, 2006, Nuclear phosphoinositide kinases and inositol phospholipids. J Cell Biochem. **97**: 252-260.
3. Yilmaz, O., T. Jungas, P. Verbeke, and D.M. Ojcius, 2004, Activation of the phosphatidylinositol 3-kinase/Akt pathway contributes to survival of primary epithelial cells infected with the periodontal pathogen Porphyromonas gingivalis. Infect Immun. **72**: 3743-3751.
4. Monteiro, D., Q. Liu, S. Lisboa, G.E. Scherer, H. Quader, and R. Malho, 2005, Phosphoinositides and phosphatidic acid regulate pollen tube growth and reorientation through modulation of $[Ca^{2+}]c$ and membrane secretion. J Exp Bot. **56**: 1665-1674.
5. Toker, A., 2002, Phosphoinositides and signal transduction. Cell Mol Life Sci. **59**: 761-779.
6. Gillooly, D.J., A. Simonsen, and H. Stenmark, 2001, Cellular functions of phosphatidylinositol 3-phosphate and FYVE domain proteins. Biochem J. **355**: 249-258.
7. Anthony, R.G., et al., 2004, A protein kinase target of a PDK1 signalling pathway is involved in root hair growth in Arabidopsis. EMBO J. **23**: 572-581.
8. Meijer, H.J. and T. Munnik, 2003, Phospholipid-based signaling in plants. Annu Rev Plant Biol. **54**: 265-306.
9. Simonsen, A., A.E. Wurmser, S.D. Emr, and H. Stenmark, 2001, The role of phosphoinositides in membrane transport. Curr Opin Cell Biol. **13**: 485-492.
10. Schu, P.V., K. Takegawa, M.J. Fry, J.H. Stack, M.D. Waterfield, and S.D. Emr, 1993, Phosphatidylinositol 3-kinase encoded by yeast *VPS34* gene essential for protein sorting. Science. **260**: 88-91.
11. Nice, D.C., T.K. Sato, P.E. Stromhaug, S.D. Emr, and D.J. Klionsky, 2002, Cooperative binding of the cytoplasm to vacuole targeting pathway proteins, Cvt13 and Cvt20, to phosphatidylinositol 3-phosphate at the pre-autophagosomal structure is required for selective autophagy. J Biol Chem. **277**: 30198-30207.
12. Wurmser, A.E. and S.D. Emr, 2002, Novel PtdIns(3)P-binding protein Etf1 functions as an effector of the Vps34 PtdIns 3-kinase in autophagy. J Cell Biol. **158**: 761-772.
13. Yin, H.L. and P.A. Janmey, 2003, Phosphoinositide regulation of the actin cytoskeleton. Annu Rev Physiol. **65**: 761-789.
14. Dove, S.K., C.W. Lloyd, and B.K. Drobak, 1994, Identification of a phosphatidylinositol 3-hydroxy kinase in plant cells: association with the cytoskeleton. Biochem J. **303**: 347-350.

15. Welters, P., K. Takegawa, S.D. Emr, and M.J. Chrispeels, 1994, AtVPS34, a phosphatidylinositol 3-kinase of *Arabidopsis thaliana*, is an essential protein with homology to a calcium-dependent lipid binding domain. Proc Natl Acad Sci U S A. **91**: 11398-11402.
16. Hong, Z. and D.P. Verma, 1994, A phosphatidylinositol 3-kinase is induced during soybean nodule organogenesis and is associated with membrane proliferation. Proc Natl Acad Sci U S A. **91**: 9617-9621.
17. Jung, J.Y., Y.W. Kim, J.M. Kwak, J.U. Hwang, J. Young, J.I. Schroeder, I. Hwang, and Y. Lee, 2002, Phosphatidylinositol 3- and 4-phosphate are required for normal stomatal movements. Plant Cell. **14**: 2399-2412.
18. Park, K.Y., J.Y. Jung, J. Park, J.U. Hwang, Y.W. Kim, I. Hwang, and Y. Lee, 2003, A role for phosphatidylinositol 3-phosphate in abscisic acid-induced reactive oxygen species generation in guard cells. Plant Physiol. **132**: 92-98.
19. Bunney, T.D., P.A. Watkins, A.F. Beven, P.J. Shaw, L.E. Hernandez, G.P. Lomonossoff, M. Shanks, J. Peart, and B.K. Drobak, 2000, Association of phosphatidylinositol 3-kinase with nuclear transcription sites in higher plants. Plant Cell. **12**: 1679-1688.
20. Drobak, B.K. and B. Heras, 2002, Nuclear phosphoinositides could bring FYVE alive. Trends Plant Sci. **7**: 132-138.
21. Kihara, A., T. Noda, N. Ishihara, and Y. Ohsumi, 2001, Two distinct Vps34 phosphatidylinositol 3-kinase complexes function in autophagy and carboxypeptidase Y sorting in *Saccharomyces cerevisiae*. J Cell Biol. **152**: 519-530.
22. Bassham, D.C., M. Laporte, F. Marty, Y. Moriyasu, Y. Ohsumi, L.J. Olsen, and K. Yoshimoto, 2006, Autophagy in development and stress responses of plants. Autophagy. **2**: 2-11.
23. Gaullier, J.M., A. Simonsen, A. D'Arrigo, B. Bremnes, H. Stenmark, and R. Aasland, 1998, FYVE fingers bind PtdIns(3)P. Nature. **394**: 432-433.
24. Kutateladze, T.G., K.D. Ogburn, W.T. Watson, T. de Beer, S.D. Emr, C.G. Burd, and M. Overduin, 1999, Phosphatidylinositol 3-phosphate recognition by the FYVE domain. Mol Cell. **3**: 805-811.
25. Hurley, J.H. and S. Misra, 2000, Signaling and subcellular targeting by membrane-binding domains. Annu Rev Biophys Biomol Struct. **29**: 49-79.
26. Katzmann, D.J., C.J. Stefan, M. Babst, and S.D. Emr, 2003, Vps27 recruits ESCRT machinery to endosomes during MVB sorting. J Cell Biol. **162**: 413-423.
27. Yamamoto, A., D.B. DeWald, I.V. Boronenkov, R.A. Anderson, S.D. Emr, and D. Koshland, 1995, Novel PI(4)P 5-kinase homologue, Fab1p, essential for normal vacuole function and morphology in yeast. Mol Biol Cell. **6**: 525-539.
28. Peterson, M.R., C.G. Burd, and S.D. Emr, 1999, Vac1p coordinates Rab and phosphatidylinositol 3-kinase signaling in Vps45p-dependent vesicle docking/fusion at the endosome. Curr Biol. **9**: 159-162.

29. Dumas, J.J., E. Merithew, E. Sudharshan, D. Rajamani, S. Hayes, D. Lawe, S. Corvera, and D.G. Lambright, 2001, Multivalent endosome targeting by homodimeric EEA1. Mol Cell. **8**: 947-958.
30. Misra, S. and J.H. Hurley, 1999, Crystal structure of a phosphatidylinositol 3-phosphate-specific membrane-targeting motif, the FYVE domain of Vps27p. Cell. **97**: 657-666.
31. Lee, S.A., R. Eyeson, M.L. Cheever, J. Geng, V.V. Verkhusha, C. Burd, M. Overduin, and T.G. Kutateladze, 2005, Targeting of the FYVE domain to endosomal membranes is regulated by a histidine switch. Proc Natl Acad Sci U S A. **102**: 13052-13057.
32. Kutateladze, T.G., 2006, Phosphatidylinositol 3-phosphate recognition and membrane docking by the FYVE domain. Biochim Biophys Acta. **1761**: 868-877.
33. Jensen, R.B., T. La Cour, J. Albrethsen, M. Nielsen, and K. Skriver, 2001, FYVE zinc-finger proteins in the plant model *Arabidopsis thaliana*: identification of PtdIns3P-binding residues by comparison of classic and variant FYVE domains. Biochem J. **359**: 165-173.
34. Matsuoka, K., D.C. Bassham, N.V. Raikhel, and K. Nakamura, 1995, Different sensitivity to wortmannin of two vacuolar sorting signals indicates the presence of distinct sorting machineries in tobacco cells. J Cell Biol. **130**: 1307-1318.
35. Patel, S. and S.P. Dinesh-Kumar, 2008, Arabidopsis ATG6 is required to limit the pathogen-associated cell death response. Autophagy. **4**: 20-27.
36. Liu, Y., M. Schiff, K. Czymmek, Z. Tallóczy, B. Levine, and S.P. Dinesh-Kumar, 2005, Autophagy regulates programmed cell death during the plant innate immune response. Cell. **121**: 567-577.
37. Fujiki, Y., K. Yoshimoto, and Y. Ohsumi, 2007, An Arabidopsis homolog of yeast ATG6/VPS30 is essential for pollen germination. Plant Physiol. **143**: 1132-1139.
38. Harrison-Lowe, N.J. and L.J. Olsen, 2008, Autophagy Protein 6 (ATG6) is required for pollen germination in *Arabidopsis thaliana*. Autophagy. **4**: 339 - 348
39. Qin, G., et al., 2007, Arabidopsis AtBECLIN 1/AtAtg6/AtVps30 is essential for pollen germination and plant development. Cell Res. **17**: 249-263.
40. Heras, B. and B.K. Drobak, 2002, PARF-1: an *Arabidopsis thaliana* FYVE-domain protein displaying a novel eukaryotic domain structure and phosphoinositide affinity. J Exp Bot. **53**: 565-567.
41. van Leeuwen, W., L. Okresz, L. Bogre, and T. Munnik, 2004, Learning the lipid language of plant signalling. Trends Plant Sci. **9**: 378-384.
42. Brickner, D.G., J.J. Harada, and L.J. Olsen, 1997, Protein transport into higher plant peroxisomes. In vitro import assay provides evidence for receptor involvement. Plant Physiol. **113**: 1213-1221.
43. Olsen, L.J., S.M. Theg, B.R. Selman, and K. Keegstra, 1989, ATP is required for the binding of precursor proteins to chloroplasts. J Biol Chem. **264**: 6724-6729.

44. Ellman, G.L., 1959, Tissue sulfhydryl groups. Arch Biochem Biophys. **82**: 70-77.
45. Graumann, J., H. Lilie, X. Tang, K.A. Tucker, J.H. Hoffmann, J. Vijayalakshmi, M. Saper, J.C. Bardwell, and U. Jakob, 2001, Activation of the redox-regulated molecular chaperone Hsp33--a two-step mechanism. Structure. **9**: 377-387.
46. Kihara, A., Y. Kabeya, Y. Ohsumi, and T. Yoshimori, 2001, Beclin-phosphatidylinositol 3-kinase complex functions at the *trans*-Golgi network. EMBO Rep. **2**: 330-335.
47. Stack, J.H., D.B. DeWald, K. Takegawa, and S.D. Emr, 1995, Vesicle-mediated protein transport: regulatory interactions between the Vps15 protein kinase and the Vps34 PtdIns 3-kinase essential for protein sorting to the vacuole in yeast. J Cell Biol. **129**: 321-334.
48. Kametaka, S., T. Okano, M. Ohsumi, and Y. Ohsumi, 1998, Apg14p and Apg6/Vps30p form a protein complex essential for autophagy in the yeast, *Saccharomyces cerevisiae*. J Biol Chem. **273**: 22284-22291.
49. Liang, X.H., J. Yu, K. Brown, and B. Levine, 2001, Beclin 1 contains a leucine-rich nuclear export signal that is required for its autophagy and tumor suppressor function. Cancer Res. **61**: 3443-3449.
50. Gillooly, D.J., I.C. Morrow, M. Lindsay, R. Gould, N.J. Bryant, J.M. Gaullier, R.G. Parton, and H. Stenmark, 2000, Localization of phosphatidylinositol 3-phosphate in yeast and mammalian cells. EMBO J. **19**: 4577-4588.
51. Vermeer, J.E., W. van Leeuwen, R. Tobena-Santamaria, A.M. Laxalt, D.R. Jones, N. Divecha, T.W. Gadella, Jr., and T. Munnik, 2006, Visualization of PtdIns3P dynamics in living plant cells. Plant J. **47**: 687-700.
52. Simonsen, A., H.C. Birkeland, D.J. Gillooly, N. Mizushima, A. Kuma, T. Yoshimori, T. Slagsvold, A. Brech, and H. Stenmark, 2004, Alfy, a novel FYVE-domain-containing protein associated with protein granules and autophagic membranes. J Cell Sci. **117**: 4239-4251.
53. Yan, Y. and J.M. Backer, 2007, Regulation of class III (Vps34) PI3Ks. Biochem Soc Trans. **35**: 239-241.
54. Raiborg, C., B. Bremnes, A. Mehlum, D.J. Gillooly, A. D'Arrigo, E. Stang, and H. Stenmark, 2001, FYVE and coiled-coil domains determine the specific localisation of Hrs to early endosomes. J Cell Sci. **114**: 2255-2263.
55. Honys, D. and D. Twell, 2003, Comparative analysis of the Arabidopsis pollen transcriptome. Plant Physiol. **132**: 640-652.
56. Alonso, J.M., et al., 2003, Genome-wide insertional mutagenesis of *Arabidopsis thaliana*. Science. **301**: 653-657.

Chapter 4

NHL57 is a Senescence-Associated Peroxisomal Protein with a Novel SFL PTS1 Tripeptide

Abstract

Peroxisomes are dynamic organelles with biochemical functions that are tightly attenuated to developmental cues including the process of senescence. To understand the physiological changes during plant senescence, proteomic analysis was conducted on peroxisomes isolated from dark-induced senescent *Arabidopsis* leaves. Here we report on NHL57, a protein with a novel SFL Peroxisomal Targeting Signal 1 (PTS1) tripeptide, which was enriched in the senescent peroxisome. NHL57 transcript levels increase during dark-induced and natural senescence. Furthermore, *nhl57* homozygous mutant plants lacked full-length transcript and exhibited retarded degradation of chlorophyll during dark-induced senescence. When transiently expressed in tobacco leaves, YFP-NHL57 co-localized with a CFP-SKL peroxisomal marker as expected and in vitro import experiments determined that the SFL tripeptide was necessary, but not sufficient for targeting. In addition, deletion of the SFL tripeptide severely disrupted the ability of NHL57 to bind to the PTS1 receptor, PEX5. We also present data on NHL60, a putative NHL57 homolog, which lacks the SFL tripeptide. This work expands our current knowledge of the amino acid variants allowable in a functional PTS1 signal and suggests an exciting link between chlorophyll degradation and peroxisome physiology during senescence.

Introduction

Peroxisomes are biochemically diverse organelles that are present in almost all eukaryotes. Initially named for their role in hydrogen peroxide metabolism, peroxisomes are also responsible for the β-oxidation of fatty acids [1], synthesis of bile and plasmalogen in mammals [2], production of jasmonic acid in plants [3] and the breakdown of methanol in the methylotrophic yeast *Pichia pastoris* [4]. Within plants multiple classes of peroxisomes have been described, differentiated by their specialized metabolic functions and corresponding enzyme complement [5]. In leguminous species, which form *Rhizobium*-containing root nodules, peroxisomes are essential for nitrogen assimilation [6]. In photosynthetic tissues, metabolites from the carbon salvage pathway, photorespiration, are actively shuttled between peroxisomes, chloroplasts and mitochondria. In the cotyledons of oil-rich species, such as pumpkins or *Arabidopsis thaliana*, fats are broken down for use in carbohydrate synthesis via the glyoxylate cycle in glyoxysomes [5]. During plant senescence in sweet potato, key glyoxylate cycle enzymes are up-regulated presumably to facilitate energy production during the cessation of photosynthetic activity and chlorophyll degradation, through the breakdown of membrane lipids [7].

Despite these different classifications and diverse functions, it is important to remember that peroxisomes are not static organelles. Due to the unifying mechanisms that control biogenesis and protein import, they have the essential ability to alter their biochemical functions in response to abiotic and biotic cues [5,8]. One cue of particular interest is the onset of programmed cell death during plant senescence [9,10]. Characterized by the degradation of chlorophyll [11], plant senescence is a complex process controlled by key plant hormones [12,13], their respective signaling components, and transcription factors such as WRKY53 [14]. Multiple transcriptome profiling experiments have revealed the complexity of the process. The expression of hundreds of genes encoding protein degradation machinery and transporters for ions are altered during senescence [15-17]. Chloroplasts are the first organelles to undergo structural changes, while mitochondria and nuclei remain largely intact until the later stages

of senescence, just prior to tonoplast rupture and cell death [9,11]. However, despite research using various plant species showing the up-regulation of glyoxylate cycle enzymes [7,18], increases in catalase activity [19], and identification of senescence-induced peroxidases [20], little is known about the changes that occur in the non-enzymatic protein complement in peroxisomes during senescence.

Unlike chloroplasts and mitochondria, peroxisomes do not contain DNA, so all peroxisomal proteins are nuclear encoded and post-translationally targeted to the peroxisome [8,21]. As shown in Figure 4.1, proteins destined for the peroxisomal matrix primarily contain one of two recognized targeting signals; an extreme carboxyl terminal tripeptide, Peroxisomal Targeting Signal 1 (PTS1), or an amino terminal nonapeptide, Peroxisomal Targeting Signal 2 (PTS2) [22]. Cargo proteins containing a PTS1 or PTS2 are bound by their corresponding cytosolic receptor, PEX5 or PEX7, respectively [23]. While some essential peroxisomal enzymes such as thiolase contain a PTS2 signal [24], the vast majority of peroxisomal proteins are targeted via a PTS1 [25].

The canonical PTS1, Serine-Lysine-Leucine (SKL) was initially identified in firefly luciferase [26-28]. Provided the residues are accessible for binding to the Trico peptide repeat of PEX5, this SKL tripeptide is sufficient for peroxisomal targeting of reporter proteins [28,29]. Work in yeast, plant, and mammalian systems has identified many functional amino acid variants refining the definition to a more inclusive (**S**/A/C/P), (**K**/R/H/N/S), (**L**/M/I/V) motif [25,29-31]. Unlike SKL, multiple PTS1 tripeptide variants are necessary for import of their native proteins but lack sufficiency when fused to reporters [32]. In such cases, the poorly conserved amino acid residues directly upstream of the tripeptide, often referred to as auxiliary moieties, have been found to be essential for the functionality of the PTS1 signal [29,31,33]. In addition, several PTS1 tripeptides exhibit species-specific functionality, including GKI, which is a PTS1 in *Candida albicans*, but not in *Saccharomyces cerevisiae* [34].

Recently our ability to both identify novel proteins and correlate their expression with changes in peroxisomal function has been aided by the use of

proteomics [35]. While it was previously possible to predict peroxisomal targeting for novel proteins with experimentally tested tripeptide variants, prediction of additional novel signals was complicated by many factors, including species specificity and the lack of consensus among accessory residues. In addition, without a physiological context, such as senescence association, prediction of protein function is hampered, especially for the large number of proteins annotated simply as “expressed” or “of unknown function” in the *Arabidopsis* genome. Now, by analyzing the protein complement of the peroxisome during different developmental stages, the physiological significance of novel proteins can be better understood. Here we report on the novel protein NHL57 that was identified in a proteomic analysis of peroxisomes isolated from senescent *Arabidopsis* leaves. We show that NHL57, a previously uncharacterized protein, is enriched during plant senescence. In addition, NHL57 contains a novel PTS1 tripeptide, SFL that is necessary but not sufficient for peroxisomal targeting. This is the first time that phenylalanine has been reported in a functional PTS1 tripeptide. In addition, we present data on NHL60, a putative NHL57 homolog, which may be useful in understanding the use of NHL57’s accessory residues for prediction of PTS1 functionality.

Materials and Methods

Peroxisome proteomics. For isolation of dark-induced senescent peroxisomes, 4-week-old wild-type *Arabidopsis* plants were detached below the rosette and transferred to a dark growth chamber for 2 to 4 days. Peroxisomes were isolated as previously described [35]. Protein concentration was quantified using the sensitive Lowry method [36]. For purity analysis, peroxisomal proteins (10 µg) were precipitated using the chloroform methanol method [37]. Organelle purity was determined both by western blot using an α-V-DAC antibody (generous gift from Thomas Elthon, University of Nebraska) and by silver staining [38] for observation of the P-subunit of glycine decarboxylase. High- and low-purity standards were defined and used as internal controls for the analyses. High-purity samples were submitted to the Michigan State University Proteomics

Facility. For detailed information regarding the proteomic methods and algorithms used for analysis of MS/MS results see [39]. Following protein identification using the TAIR6 *Arabidopsis* database, all peptides present in the senescent peroxisome protein samples, with an ID probability of at least 90%, were examined using the Scaffold software program (Proteome Software Inc, Portland Oregon). Peptides with increased frequency in the senescent samples compared to non-senescent wild-type peroxisomes were selected for further examination. The criteria for selection of a candidate protein were as follows; either senescence-specific or senescence-enriched (>2 fold), previously unreported as a peroxisomal protein (designation based upon data available at the Araperox database ref [25]), reproducible identification between trial and full-scale MS analysis runs and a novel targeting signal; either a new variant of a PTS1 or a PTS2 signal, or no identifiable signal.

RT-PCR. Dark-induced senescence leaves were harvested as above and frozen in liquid nitrogen. For heat shock experiments, whole plants were transferred to a 42°C growth chamber for 2 hours and then returned to room temperature. Leaves were harvested before, immediately after and at 2, 4, 6, 8 and 24hrs post heat shock. For spatial profiling, leaves were harvested from three, five or seven week old wild-type plants corresponding to pre-bolt, early flowering and late flowering stages of development respectively. RNA was extracted using Trizol reagent (Invitrogen, Carlsbad, CA) In brief, samples were weighed, ground in liquid nitrogen, and 10 vol of Trizol reagent added. Tissue was pelleted, and 0.2 vol of chloroform was added to the cleared supernatant fraction. Samples were vortexed, centrifuged, and the upper aqueous phase transferred to a new tube. RNA was precipitated by addition of 0.25 ml isopropanol and 0.25 ml of 0.8 M sodium citrate/1.2 M NaCl solution. Following centrifugation, RNA pellets were dried, resuspended in water, and RNA was DNAse-treated using RQ1 Rnasefree-Dnase (Promega, Madison WI), per manufacturer's directions. RT-PCR was performed using the Access Quick (Promega, Madison, WI) RT-PCR kit (RT=52°C for 45 min, then PCR portion = 52°C annealing, 22 cycles, 2 minute extension) with 100 ng RNA template and

100 ng gene-specific primers or 25 ng β-tubulin gene-specific primers. (*NHL57* primer A: 5'ATGAAAGCCGCCGTTTTCCGT 3', *NHL57* primer B: 5'ACGGCGCGTGAGACGCGTGACTTC3' *NHL57* primer C: 5'GCCTAAGTATCTTCAATGGCCAGA3', *NHL57* primer D: 5'TTATAGGAAAGAAGTACCCGCGAG3', β-tubulin primer 1: 5'ATACAGAACAAGAACTCGTCTTAC3', β-tubulin primer 2: 5'CTCTTCTTCTTCAACATCATACTC3')

Genotyping and chlorophyll assays. Seeds from SALK Lines 024636 and 088755 were obtained from ABRC (*Arabidopsis* Biological Resource Center) and grown under 16 hr light and 8 hr dark conditions. Plant DNA extractions and screening PCR were performed as previously reported [40] using the following primers (*NHL57* primer S FOR: 5'GAAGTCACGCGTCTCACGCGCCGT3', *NHL57* primer S REV: 5'TCCCTGCACTTCGCTCATCTTCTC3', *NHL60* primer S FOR: 5'GAAGTTCTAGGAGCTGTTAATGGT3', *NHL60* primer S REV: 5'CTTGTCCCGGCAAGTCCACGATGC3'). Chlorophyll assays were performed as follows: for dark-induced senescence experiments, 4-6 week-old wild-type or *nhl57* mutant *Arabidopsis* plants were harvested and transferred to a dark growth chamber. Leaves were harvested at one-day intervals for four days, weighed, and ground in two volumes of water until uniform consistency. Dilutions of each sample were prepared (1:6, 1:10, and 1:30) in water to a total volume of 150 µL. Next, 600 µL of acetone were added, samples were centrifuged at full speed in a microcentrifuge for two min, to pellet any white tissue and the OD of the supernatant was measured at 652 nm (80% acetone served as blank). The chlorophyll concentration (mg/gfw) was calculated using an extinction coefficient of 34.5 [41]. Leaves were imaged prior to extraction.

Plasmid construction. Full-length *NHL57* and *NHL60* were amplified using Vent polymerase (New England Biolabs, Ipswich, MA) from full-length cDNA clones (U14219, U20102) obtained from ABRC, (*NHL57* Primer 1: 5'GCTAATTTAGTCGACATGAAAGCCGCCGTTTTC3', *NHL57* Primer 2: 5'GCCAGAACGTCTAGATTATAGGAAAGAAGTACCCGC3', *NHL60*Primer 1: 5'GCGTCTGCAGTCGACATGGAAATCTCTTCTTTCCCA3', *NHL57* Primer 2:

5’GCCAGAACGTCTAGACTATAGAGTTCTTGTCCCGGC3’), PCR products were incubated with 1 unit Taq polymerase at 72°C for 15 min (Promega, Madison, WI) and then ligated into TOPOPCRII (Invitrogen, Carlsbad, CA) following the manufacturer’s instructions. Quik-Change® site-directed mutagenesis (Stratagene, Cedar creek, TX) was used to introduce a stop codon upstream of the SFL to generate the TOPOPCRII-*NHL57*ΔSFL constructs using the following primers (*NHL57*-FOR-Minus SFL: 5'GGCCTCGCGGGTACTTGACTTTCCTATAATCTAG3’, *NHL57*-REV-Minus SFL: 5'CTAGATTATAGGAAAGTCAAGTACCCGCGAGGCC3'). YFP was amplified using mutagenic primers which added the SFL, SKL or a stop, from the peYFP-C1 vector (BD Biosciences Clontech, Mountain view, CA) using Go Taq (Promega, Madison, WI) and then ligated into TOPOPCRII (Invitrogen, Carlsbad, CA) following the manufacturer’s instructions (YFP-FOR: 5’GTCGACACCATGGTGAGCAAGGGCGAG3’, YFP-REV-No signal: 5’CTGGCATGGACGAGCTGTACAAGTGATCAGA3’, YFP-REV-SFL: 5’CATGGACGAGCTTACAAGTCCTTCCTGTGATCTAGA3’, YFP-REV-SKL: 5’CATGGACGAGCTGTACAAGTCCAAGCTGTGATCTAGA3’).

For expression in tobacco, *NHL57* and *NHL60* were sub cloned into pCAM-YFP-C1 (gift from Nielson lab, University of Michigan, Ann Arbor, MI), TOPOPCRII clones were digested with SalI and XbaI, gel purified using a QIAEXII kit (Qiagen, Valencia, CA) and ligated using T4 DNA ligase (Promega, Madison, WI) per manufacturer’s directions.

***In vitro* import experiments and far-westerns.** The following constructs: TOPOPCRII-*NHL57*, TOPOPCRII-*NHL60*, TOPOPCRII-YFP-NS, TOPOPCRII-YFP-SFL, TOPOPCRII-YFP-SKL, and pGEM7Zf:SoGLO, were linearized with an appropriate restriction enzyme prior to *in vitro* transcription with SP6 RNA polymerase (Promega, Madison, WI). For TOPOPCRII-*NHL57*ΔCt, an internal NdeI recognition-site was used so that the translation product lacked the final 53aa compared to the full-length protein. Radiolabeled protein probes were produced by addition of in vitro synthesized mRNA to a cell-free rabbit reticulocyte lysate (Promega, Madison, WI) translation system containing

[^{35}S]methionine. Incorporation of the radiolabel was quantified via trichloroacetic acid precipitations as previously described [42]. Glyoxysomes were prepared as previously reported [43]. For import experiments, 5x10^5 TCA precipitable counts were incubated with 250 µg fresh glyoxysomes under import conditions (25°C, + 5 mM ATP), control samples were incubated on ice. Samples were digested with proteinase K (10-20 µg/ml) and processed as previously reported [42].

The level of import was quantified using a BioRad phosphoimager and BioRad Quantity One 1-D Analysis Software volume analysis tools. Import was normalized to the no-protease control lane (indicates total protein added to the import reaction). Each experiment was repeated a minimum of four times and the average level of import (± S.D.) was calculated. For experiments shown in Figure 4.6, the amount of protein in the negative control was subtracted from each individual reaction; the average of these adjusted values (± S.D.) is shown. Duplicate aliquots of purified His-tagged AtATG6 and AtPEX5 proteins (10 µg each) were applied to methanol-activated PVDF membrane. The membranes were allowed to air dry before being probed for two hours at room temperature with 5x10^5 TCA-precipitable counts of *in vitro* transcribed and translated NHL57, NHL57ΔSFL or SoGLO (positive control) in TBS-TWEEN with 3% BSA. The blots were then washed 3 times for 20 min in TBS-TWEEN, allowed to air dry, and then exposed overnight to light-sensitive film.

Subcellular localization. Tobacco (*Nicotiana benthamiana*) plants were grown in 12 hours light/12 hours dark for 5-6 weeks. Agrobacterium containing pCAM-YFP-*NHL57*, pCAM-YFP-*NHL60*, pCAM-YFP-empty, pCHF1-CFP-SKL, a PTS1 positive control kindly provided by Dr. Jianping Hu (Michigan State University, Lansing, MI), or the p19 plasmid were grown overnight at 30°C. Cultures were then diluted 1:10 with fresh media and grown to 0.6-0.8 OD_{600nm}. Cells were pelleted at 5,000 rpm and then gently resuspended to 0.1 OD_{600nm} in water. Cells were combined (p19, PTS1 control and one of the three pCAM vectors) and co-infiltrated using a 1 ml syringe (no needle). Leaves were imaged after 48 hours using brightfield and confocal fluorescence microscopy on a Leica TCF SP5 (software version 1.7) with a Leica 40X objective. Microscope settings

were as follows: eYFP - excitation at 514 nm, emission from 525-566 nm, CFP- excitation at 458 nm, emission from 470-498 nm. To observe nuclei, small pieces of tobacco leaves were transferred into a petri dish and 4', 6-diamidino-2-phenylindole (1 µg/ml, DAPI) solution was applied. Samples were incubated either at 4°C overnight or at room temperature for 1 hr and then imaged on a Leica TCF SP5 with excitation at 405 nm, emission from 431-456 nm.

Results

Proteomic identification. To identify proteins present in senescent peroxisomes, high purity organelles were isolated from *Arabidopsis* leaves undergoing dark-induced senescence. To validate that the experimental conditions did induce senescence, the expression level of a known senescence responsive-gene, YSL4, was measured using RT-PCR [44]. We selected YSL4 because it is the peroxisomal isoform of aspartate amino transferase (ASP3) and should show induction at the protein level during our proteomic analysis. As shown in Figure 4.2A, YSL4 expression increased during the 4 days of dark treatment, indicating senescence was induced in the leaf tissue. Representative images of the leaves at each stage during senescence are shown in Figure 4.2B. As expected, progressive yellowing of the leaves indicated the characteristic senescence-associated degradation of chlorophyll [45]. In addition, the total chlorophyll concentration was determined. As can be seen in Figure 4.2B, the chlorophyll levels decreased steadily during the 4 days of dark treatment, indicating that senescence was induced.

Having established experimental conditions that induced senescence, peroxisomes were isolated and subjected to peptide sequencing using Mud-PIT mass spectrometry (for complete description of the proteomic methods see [35]). The Scaffold program (Proteome Software Inc. Portland, Oregon) was used to determine the total spectral counts for each peptide present in the senescent-peroxisome protein samples. Proteins whose corresponding peptides showed increased frequency in the senescent samples as compared to wild-type peroxisomes [35] were selected for further examination. The full-length amino

acid sequences were then examined for the presence of a predicted PTS1 or PTS2 signal and further analyzed for the presence of conserved functional domains. In addition, the expression profile for each associated gene was analyzed using Genevestigator (https://www.genevestigator.ethz.ch/gv/index.jsp) to identify those with specific senescence association rather than those with more pleiotropic function. Additional information regarding the proteins identified in the senescent peroxisomal proteomics will be made available as part of the *Arabidopsis* 2010: Understanding Peroxisomal Protein Networks project (see the project website - URL: http://www.peroxisome.msu.edu/) and related publications.

NHL57, a novel 57 kDa protein of unknown function, was selected for further study. NHL57 was predicted to be cytosolic despite having a low pI of 5.7. NHL57 showed a two-fold enrichment in senescent peroxisomes and appeared to be senescence-regulated at the transcript level, based on microarray data. In addition, sequence analysis revealed a novel extreme carboxyl terminal SFL tripeptide, a potential variant of the canonical PTS1 tripeptide, SKL (Figure 4.2C). For these reasons, we selected NHL57 for further investigation.

Senescence association. First, it was important to determine whether NHL57 was induced by senescence as the proteomic data suggested. To do this RT-PCR was performed to measure *NHL57* expression during dark-induced senescence. As can be seen in Figure 4.3A, the *NHL57* expression pattern was comparable to that seen for YSL4, with a steady increase in mRNA transcript levels over the 4-day treatment. This indicated that *NHL57* expression was induced during senescence and that NHL57 was regulated at the transcriptional level. Because we had been prematurely inducing senescence in detached leaves, we next tested whether *NHL57* expression showed a similar response profile during the natural age-induced process of senescence. To do this, leaves were harvested from alternating positions (youngest to oldest) from healthy 24-day-old plants and RT-PCR was performed. At this age, while the large young leaves are photosynthetic and pre-senescent, the smaller old leaves, which are shaded by the new rosette growth, are visibly senescing (Figure 4.3B top). As

shown in Figure 4.3B, as the age of the leaf tissue increased there was a corresponding increase in the *NHL57* transcript level. At 24 days, *NHL57* expression was highest in the oldest leaves that are actively undergoing senescence, as indicated by the YSL4 expression level. Therefore the expression level of *NHL57* was up-regulated during senescence, regardless of whether the process is abiotically, or developmentally induced.

To further investigate the role of *NHL57*, a spatial expression profile was generated. Leaves, roots, cauline leaves and flowers were harvested from plants at three developmental time points (pre-bolt, early bolting and late flowering). RT-PCR revealed that *NHL57* expression levels in green leaves of pre-bolt, early flowering, and late flowering plants was very low compared to the levels seen in yellow leaves during the advanced stages of flowering (Figure 4.3C). This further supports our data that indicate *NHL57* expression levels respond to natural senescence cues in leaves (Figure 4.3A). A notable increase in the expression level of *NHL57* was observed in roots from early and late flowering plants compared to roots of pre-bolt plants. This may indicate a role for NHL57 in senescent roots. In addition to expression in senescing leaf tissues, high levels of *NHL57* mRNA transcript were present in flowers, which may suggest a role in stress response during the transition to flowering.

Protein targeting. Having established that NHL57 is senescence associated, we next wanted to determine whether NHL57 is a peroxisomal protein. To do this, amino-terminal eYFP-NHL57 fusion constructs were generated and transiently co-expressed with a CFP-SKL peroxisomal marker in tobacco leaves (Figure 4.4). As expected, the free eYFP control showed a diffuse pattern indicating it was cytosolic. There was no co-localization with the punctate CFP-SKL peroxisomal marker when the channels were overlaid. In contrast, many punctate structures were observed in the eYFP-NHL57 expressing cells. Overlaying the channels showed clear co-localization of the eYFP-NHL57 with the peroxisomal CFP-SKL marker, confirming that NHL57 was localized to the peroxisome. Additionally, since the eYFP construct is an amino-terminal fusion,

this suggests that the carboxyl terminus, which ends with the SFL tripeptide, contains the targeting signal.

To determine whether the SFL tripeptide present at the extreme carboxyl terminus of NHL57 is responsible for its peroxisomal localization, *in vitro* import experiments were performed. Briefly, radiolabeled proteins were incubated with isolated peroxisomes under standard import conditions [42]. Following import, protease and non-protease treated samples were visualized using autoradiography (Figure 4.5). While the no-protease control indicates the total protein added to the import (Lane 1), the presence of radiolabeled proteins following protease treatment is indicative of protease protection due to import into peroxisomes (Lane 2). A control import reaction conducted at the non-permissive temperature of 4°C confirmed that sufficient protease was present to degrade all of the protein in the reaction (Lane 3). Full-length radiolabeled NHL57 (Figure 4.5A) and GLO (glycolate oxidase) a known PTS1 containing protein, were imported. Full-length NHL57 and GLO were both protease-protected, indicating they successfully imported into peroxisomes (Figure 4.5B, Lane 2, rows 1 and 4 respectively). As expected, import did not occur at the non-permissive temperature of 4°C (Figure 4.5B, Lane 3, rows 1 and 4 respectively). For all experiments, the level of import was quantified using a phosphorimager. The ratio between the total protein (lane 1) and the imported or negative control (lanes 2 and 3, respectively) was defined as the relative import level. The relative import level for each protein, and the associated standard deviation, is shown on the right. Approximately 12% of the total NHL57 protein was imported, which is comparable to the 13% observed for GLO.

To address whether the carboxyl terminal region of NHL57 is required for import, amino acids 449-501 were deleted (Figure 4.5A). This removed the SFL tripeptide and 50 upstream residues, including those that may serve as accessory residues. The resultant protein, termed NHL57ΔCt, ended with an HNI tripeptide. As shown in figure 4.5B, NHL57ΔCt was not imported into peroxisomes, indicated by the lack of protease-protected protein in Lane 2. When quantified, the relative import seen at the permissive and non-permissive

temperatures was equivalent (2.9±1.9 vs. 1.9±1.5), indicating complete protease accessibility due to loss of peroxisomal targeting. To determine whether the SFL tripeptide alone was necessary for import, a premature stop codon was introduced. This resulted in the deletion of the final three amino acids of NHL57 and an AGT tripeptide at the extreme carboxyl terminus (Figure 4.5A). This truncated protein, termed NHLΔSFL, was not imported into peroxisomes (Figure 4.5B, Lane 2, row 3). There is no statistically significant difference between the relative import ratios at the permissive and non-permissive temperatures (4.3±1.5 vs. 3.3±1.1). These data indicate that the SFL tripeptide is necessary for peroxisomal targeting of NHL57. Due to its location at the carboxyl terminus it is most likely a new variant of a PTS1.

Despite its similarity to the SKL signal, it is important to confirm the designation of the SFL tripeptide as a PTS1 variant. If the tripeptide serves as a PTS1, then NHL57 should directly interact with the PTS1 receptor PEX5. To address this question His-tagged purified Pex5 and ATG6 (negative control) were bound to PVDF membrane, and then the membrane was probed with radiolabeled GLO (positive control), or full-length NHL57. As can be seen in Figure 4.5C, full-length NHL57 bound to PEX5 indicating it directly interacts with the PTS1 receptor. Since we previously showed that removal of the SFL prevents import, it was important to determine whether this was due to loss of PEX5 binding. When tested, NHL57ΔSFL showed either no binding or greatly reduced binding to PEX5 (Figure 4.5C). None of the proteins interacted with ATG6, which was used as a negative control because it is not a peroxisomal protein and should have no association with PEX5 [46]. Thus, NHL57 imported via the PTS1 pathway, as predicted, and removal of the SFL tripeptide prevented its interaction with PEX5.

Having established that the SFL tripeptide was a functional PTS1 signal that was necessary for import of NHL57, we next wanted to establish whether it was also sufficient for peroxisomal targeting. To do this, in vitro imports were performed using eYFP as a reporter protein. Either an SKL (eYFP-SKL, positive control) or SFL (eYFP-SFL) tripeptide was fused to the carboxyl terminus of the

eYFP protein (Figure 4.6A). In addition, unaltered eYFP, lacking a PTS1 signal, (eYFP) was used as a control. As expected, the eYFP-SKL protein successfully imported into peroxisomes (Figure 4.6B) and the eYFP protein remained protease accessible. However, eYFP-SFL also remained protease accessible, indicating it was not imported into peroxisomes (lack of a band in Lane 2 Row 2). This suggests that the SFL tripeptide, while necessary, was not sufficient for peroxisomal import. GLO and the eYFP-SKL controls imported at comparable levels (Figure 4.6C). In addition, there was no statistically significant difference between the YFP-SFL and the negative control eYFP, further indicating that the SFL tripeptide was not sufficient for targeting (Figure 4.6C).

Signal conservation. Since the SFL tripeptide was necessary, but not sufficient to direct import, it is possible that additional residues are required to assist the targeting of SFL-containing proteins. Accessory residues have previously been suggested to play a role in targeting of some peroxisomal proteins [29]. To search for potential accessory residues in NHL57, bioinformatic techniques were used to identify nineteen proteins from both *Arabidopsis* and other photosynthetic species with significant homology to NHL57 in the last 50 amino acids (Figure 4.7B). Of the nineteen selected, two proteins from *Brassica rapa* showed the highest level of sequence conservation with retention of the SFL and only three total amino acid substitutions in the 17 preceding residues. All of the proteins share significant identity over the final 30-33 amino acids indicating high conservation of the signal region. Next, the full-length protein sequences were compared. Due to the availability of only partial EST sequence data for some of the proteins, it was impossible to determine whether they share significant homology outside of the 150-200 amino acids translated from the annotated mRNA sequences. For those proteins whose full length mRNA sequences are available, three proteins, two from *Brassica rapa* and two from *Vitis vinifera*, share at least 70% overall identity, indicating they may be protein homologs of NHL57. While the two potential homologues from *Brassica rapa* proteins show conservation of the SFL, the *Vitis vinifera* proteins contain an AFL. Due to the high overall sequence homology with NHL57, the AFL variant seen in

the *Vitis vinifera* protein may be a functional signal. Interestingly, one protein from *Curcuma longa* appears to be only 138 amino acids long, perhaps suggesting a modified function.

All nineteen protein sequences were compared to identify a potential consensus sequence in the 20 terminal amino acids (Figure 4.7A). These residues may be required for SFL function and therefore predictive of successful peroxisomal targeting for other novel PTS1 variants. To determine whether these residues are indicative of novel PTS1 function, we selected an *Arabidopsis* protein with high homology to NHL57 for further study. Unlike NHL57, this protein (NHL60), has an RTL tripeptide at its extreme carboxyl terminus (Figure 4.7B). In addition, unlike the *Brassica rapa* and *Vitis vinifera* proteins, NHL60 does not appear to be a functional protein homolog; the overall percent sequence identity is only 55% due to significant sequence divergence in the amino-terminal region of the proteins. The two proteins share 60% identity in the last 50 amino acids and 75% identity in the last 20 amino acids, indicating possible retention of accessory residues alongside a novel targeting signal. In fact, there are just three amino acid substitutions in the putative accessory residue region. To test whether NHL60 is peroxisomally targeted, an in vitro import assay was performed. Full-length NHL60 was incubated with peroxisomes under import conditions. While GLO successfully imported into peroxisomes, full-length NHL60 did not, as seen by the lack of protease protected protein (Figure 4.8B). Thus, the RTL tripeptide was not a functional PTS1 despite retention of the same accessory residues present in NHL57. This also implies that the upstream consensus sequence was not a good indicator of peroxisomal targeting. However, accessory residues may function with more conserved signals, such as the AFL present in the *Vitis vinifera* NHL57 homolog.

Since NHL60 was not a peroxisomal protein, we wanted to determine its subcellular localization. Amino-terminal eYFP-fusion constructs were generated and transiently co-expressed in tobacco leaves with a CFP-SKL peroxisomal marker protein. Once again, the free eYFP was seen diffuse throughout the cell, while the CFP-SKL peroxisomal marker displayed a characteristic punctate

(peroxisomal) localization pattern (Figure 4.8C). The eYFP-NHL60 fluorescent signal was observed in one large punctate structure per cell, suggesting a possible nuclear localization for NHL60. As expected, there was no co-localization with a CFP-SKL peroxisomal marker. Co-localization of the eYFP-NHL60 signal with DAPI-stained nuclei supported this suggestion (Figure 4.8C). Further examination of the NHL60 amino acid sequence revealed a potential monopartite nuclear localization signal [47], consisting of KKRPRK, between amino acids 48-54 (Figure 4.8A). This signal is present in the divergent amino terminal region where NHL60 and NHL57 have the lowest sequence identity. We predict that this signal is responsible for the nuclear targeting of NHL60. As expected this signal is completely absent from NHL57

Mutant analysis. To assess the physiological role of NHL57, seeds from a mutant line (SALK_024636), which contains a T-DNA insertion at base 687 in the *NHL57* coding region, were obtained and plants were screened for homozygous progeny (Figure 4.9A). Despite annotation as a homozygous line, wild-type, heterozygous and homozygous progeny were recovered (data not shown). Both Col-0 and the SALK line wild-type siblings were used for phenotypic comparisons. To determine whether this line represented a loss-of-function allele, RT-PCR was performed on *nhl57* homozygous plants to test for the presence of both full-length and truncated *NHL57* mRNA transcripts. RNA was extracted from 4-week-old plants and probed either with primer pair A-B to detect a truncated transcript, or primers A-C to detect the full-length transcript. As shown in Figure 4.9B, while some truncated transcript was present, no full-length transcript was detected in the *nhl57* homozygous plants. This strongly suggests that mutant plants do not produce full-length protein.

Prior to bolting, *nhl57* homozygous plants did not display any obvious phenotypes. Unlike other peroxisomal mutants [48,49] *nhl57* homozygous plants did not exhibit sucrose-dependant germination phenotypes and successfully set seed. However, during natural senescence, the plants appeared slightly greener than their wild-type siblings. To explore this phenotypic observation, whole plants were detached and placed in the dark for four days under high humidity.

Individual leaves were removed in a position-specific manner, photographed, and the total chlorophyll was extracted. As seen in Figure 4.9C, leaves from *nhl57* or wild-type plants showed similar levels of chlorophyll through to the second day of dark treatment. During days 3 and 4, leaves from *nhl57* homozygous plants contained significantly more chlorophyll than wild-type leaves. While wild-type plants retain just 24% of their chlorophyll content by day 3, *nhl57* homozygous plants retain 36%. This indicates that *nhl57* homozygotes maintained significantly more chlorophyll during dark-induced senescence, compared to wild type.

Discussion

In this study, we present data on the identification and characterization of a novel peroxisomal protein, NHL57. Initially identified through proteomic techniques, examination of the amino acid sequence revealed a novel PTS1 tripeptide, SFL, at the carboxyl terminus (Figure 4.2). *In vivo* analysis revealed co-localization of eYFP-NHL57 with a CFP-SKL peroxisomal marker confirming peroxisomal localization (Figure 4.4). This was further supported by *in vitro* protein import assays (Figure 4.5). Loss of peroxisomal targeting upon deletion of the carboxyl-terminal region (SFL and 50 aa) or the SFL alone indicated that the SFL was necessary for peroxisomal targeting (Figure 4.5B). PEX5-binding assays showed that NHL57 directly interacted with the PTS1 cytosolic receptor, PEX5 (Figure 4.5C). Furthermore, removal of the SFL tripeptide prevented this binding (Figure 4.5), consistent with the observed loss of peroxisomal targeting when the SFL was absent during *in vitro* protein import assays. In addition, tagging of the non-peroxisomal protein eYFP with an SFL tripeptide indicated that, unlike the major PTS1, SKL, SFL was not sufficient for peroxisomal targeting (Figure 4.6). Taken together, these data suggest that the SFL tripeptide should be considered a new, minor PTS1.

This is the first time it has been demonstrated that the SFL tripeptide is a functional PTS1, so it is important to consider what this new information can tell us about PTS1 signals. The SFL tripeptide varies from the major PTS1 tripeptides, SRL and SKL by a single amino acid substitution [50,51]. Unlike the

previously characterized PTS1 variants, which have a basic residue in the second position, phenylalanine is a non-polar hydrophobic amino acid. In addition, this is first time that an aromatic amino acid has been seen in a targeting tripeptide [50] and is contrary to data suggesting that the second residue must be capable of hydrogen bonding [30]. We believe these data allow us to expand plant peroxisomal targeting signal predictions to include new variants with a phenylalanine in the second position. It is also possible that larger, polar hydrophobic aromatic residues, such as tryptophan, can replace the phenylalanine and serve as functional PTS1 signals.

In our we study we identified proteins from 16 different photosynthetic organisms that share high amino acid sequence identity with NHL57 within the final 30 amino acids (Figure 4.7). While many of these proteins show conservation of the SFL signal, several contain other degenerate tripeptides that, like SFL, are similar to other major PTS1 signals. For example, the ARL tripeptide can target the GUS reporter protein to peroxisomes in plants [32]. In addition both ARL and a second tripeptide AKL bind to PEX5 in the yeast two-hybrid system [52]. In fact, AKL is the tripeptide found in glycolate oxidase, which was used as a control in the *in vitro* import assays (Figure 4.5 and 4.6). Two of the proteins identified in *Vitis vinifera* contain an AFL tripeptide at the extreme carboxyl terminus. Since this a single amino acid variant from the established ARL and AKL major PTS1 signals, there is a strong possibility that these two proteins are also peroxisomally targeted. Full sequence alignment with NHL57 suggests that the proteins from *Vitis vinifera* may be functional homologues of NHL57 lending further support to the hypothesis that they are also peroxisomally targeted.

The SFL was not sufficient (Figure 4.6C) for targeting, suggesting additional amino acid residues were required to facilitate PEX5 binding. Recent attention has been focused on the importance of the upstream residues in PTS1 function. Consequently, we examined the upstream residues of NHL57 and identified proteins with significant homology in this region. Following identification of homologs, we chose to test whether the upstream residues could predict

peroxisomal targeting of proteins with tripeptides that have more than one amino acid substitution from a known major PTS1. NHL60, an *Arabidopsis* protein, has an RTL tripeptide. To our knowledge, neither arginine nor threonine has been reported in functional plant PTS1 proteins. These changes reverse the usual amino acid characteristics of an uncharged residue followed by a basic amino acid. In addition, NHL60 shares high overall similarity with NHL57 suggesting the two could function redundantly if both were targeted to peroxisomes. However, as can be seen in Figure 4.8, unlike YFP-NHL57, YFP-NHL60 did not target to peroxisomes, but rather co-localized with DAPI-stained nuclei. While it is possible that a weak peroxisomal PTS1 will be masked by a nuclear localization signal *in vivo*, it is unlikely that even low efficiency peroxisomal import would not be observed *in vitro*. In addition, since both microarray and RT-PCR data (data not shown) indicate that NHL60 is not induced during senescence, it is possible that the two proteins have very different biological functions. These data suggest that the upstream residues seen in NHL57, while necessary for import, may only be useful in predicting peroxisomal targeting when the final tripeptide is only one amino acid substitution away from a major PTS1. In fact, these accessory residues can be found in non-peroxisomal proteins, like NHL60, when additional tripeptide substitutions are seen.

NHL57 was initially identified as a senescence-enriched protein in proteomics analyses performed using organelles isolated from dark-induced senescent tissue (Figure 4.2). We showed that *NHL57* gene expression was induced during both dark-induced and natural senescence (Figure 4.3A and B). This suggested that NHL57 is senescence-associated and that it responds to both the developmentally programmed switch to catabolism and the environmentally stimulated programmed cell death. In addition to the observed senescence response, *NHL57* mRNA transcript levels were also spatially regulated, as evidenced by the high transcript levels in floral organs (Figure 4.3C). Microarray data suggest that *NHL57* expression levels are induced three-fold during senescence (Genevestigator) supporting the RT-PCR data. Additional stress conditions including both osmotic and hydrogen peroxide stress show two-

fold up-regulation of *NHL57*. Therefore, NHL57 may respond to a broad range of stress conditions.

Despite its senescence association, it is difficult to determine the biological role of NHL57 due to its lack of any identifiable functional domains. To understand the physiological significance of NHL57, homozygous mutant plants were studied during dark-induced senescence. The loss of NHL57 resulted in retarded degradation of chlorophyll during the later stages of dark-induced senescence (Figure 4.9C/D) compared to wild-type. This was not observed with NHL60 homozygous mutant plants (data not shown). Why the loss of a peroxisomally localized protein leads to slowed degradation of a cellular component in chloroplasts is unclear. It is possible that NHL57 has a direct role in the modulation of chlorophyll degradation. In humans, phytanic acid, a derivative of the phytol side-chain of chlorophyll, is degraded in the peroxisome through α-oxidation [53]. While experimental data currently limits oxylipin producing enzymes to plant defense and oxidative stress prevention [54], plant oxygenase enzymes may also degrade chlorophyll derivatives [11,55]. NHL57 may play a role in the shuttling of metabolic intermediates between the chloroplasts and peroxisomes [56] perhaps for the targeted degradation of membrane lipids via the β-oxidation pathway [1,9]. Unlike other species, *Arabidopsis* peroxisomes do not revert to glyoxysomes during senescence [57]. Therefore, NHL57 is not likely to be involved in the switch to gluconeogenesis.

There are established links between several key plant hormones and their ability to regulate the longevity of photosynthetic potential during senescence [58]. While cytokinins increase longevity of leaf tissue during senescence [9,59], exogenous application of jasmonic acid promotes premature degradation of chlorophyll and rapid loss of photosynthetic potential in leaf tissue [60]. The first three steps of jasmonic acid biosynthesis have been localized to the chloroplast, but the final steps involved in the conversion of 12-oxo-phytodienoic acid into jasmonic acid occur in peroxisomes [61,62]. Perhaps the enzymatic potential of peroxisomes is impaired during senescence in NHL57 homozygotes, leading to reduced jasmonic acid production and, in turn, retarded chlorophyll degradation.

A similar phenotype was observed in rice plants when over-expression of OsDOS (a Jasmonic acid-repressed nuclear protein) resulted in delayed senescence that was characterized by retarded degradation of chlorophyll [13,63].

In conclusion, NHL57 contains a novel minor PTS1 tripeptide, SFL, that is necessary, but not sufficient for peroxisomal targeting. These data expand our current knowledge about the amino acid variants allowable in a functional PTS1 in plants. They also demonstrate the importance of the PTS1 tripeptide in PEX5 receptor binding. In addition, NHL57 is a novel senescence-associated protein. Understanding the link between NHL57 and delayed chlorophyll degradation may provide important insights into the role of peroxisome physiology during plant senescence.

Acknowledgements

We thank Dr. Sigrun Reumann (U of Stavanger, Norway) and Dr. Jianping Hu (MSU) for their commitment to the 2010 proteomics project and the MSU proteomics core for their assistance with the proteomic analysis. Dr. Sheng Quan (MSU) and Gregg Sobocinski provided technical assistance with the tobacco infiltrations and confocal spectroscopy, respectively. Thanks also go to Jennifer Rothstein, an undergraduate who worked on the project, and to the Arabidopsis Biological Resource Center for the T-DNA seed stocks. NHL was partially supported by the NIH-funded Cellular Biotechnology Training Program at the University of Michigan. This project was funded by a grant from the NSF to Dr. Laura Olsen (University of Michigan).

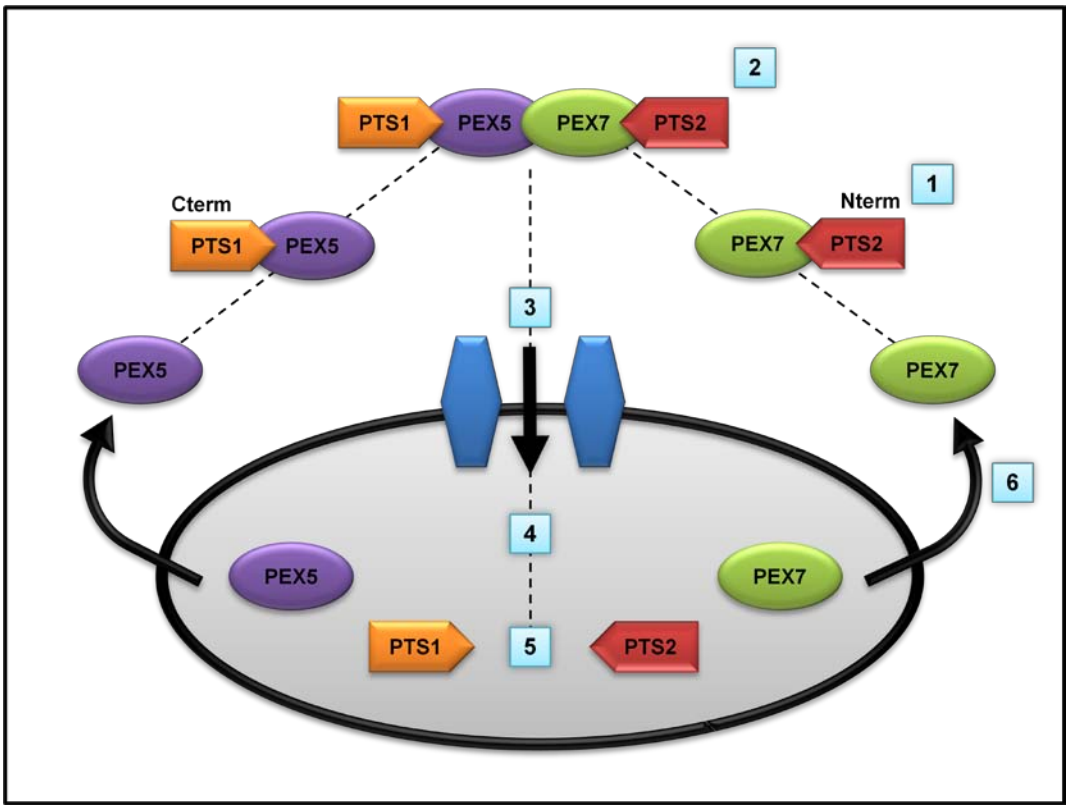

Figure 4.1. Model of peroxisome protein import pathways: *Arabidopsis* receptor recycling

1) Proteins targeted to the peroxisomal matrix containing a PTS1 or PTS2 signal bind to PEX5 or PEX7, respectively. 2) A receptor-cargo-protein complex is formed between cargo-bound PEX5 and PEX7. 3) The complex docks at the peroxisomal membrane. Yellow hexagons represent an extensive membrane-associated complex composed of PEX2-4, PEX8, PEX10, PEX12 to 14 and PEX22; in addition, PEX1, PEX6 and PEX15 are thought to be involved in receptor recycling. 4) The receptor-cargo-protein complex is translocated into the peroxisomal lumen. 5) Receptor and cargo proteins dissociate, and PTS2 proteins are proteolytically processed to their mature form. 6) Receptors are exported to the cytosol for further rounds of import.

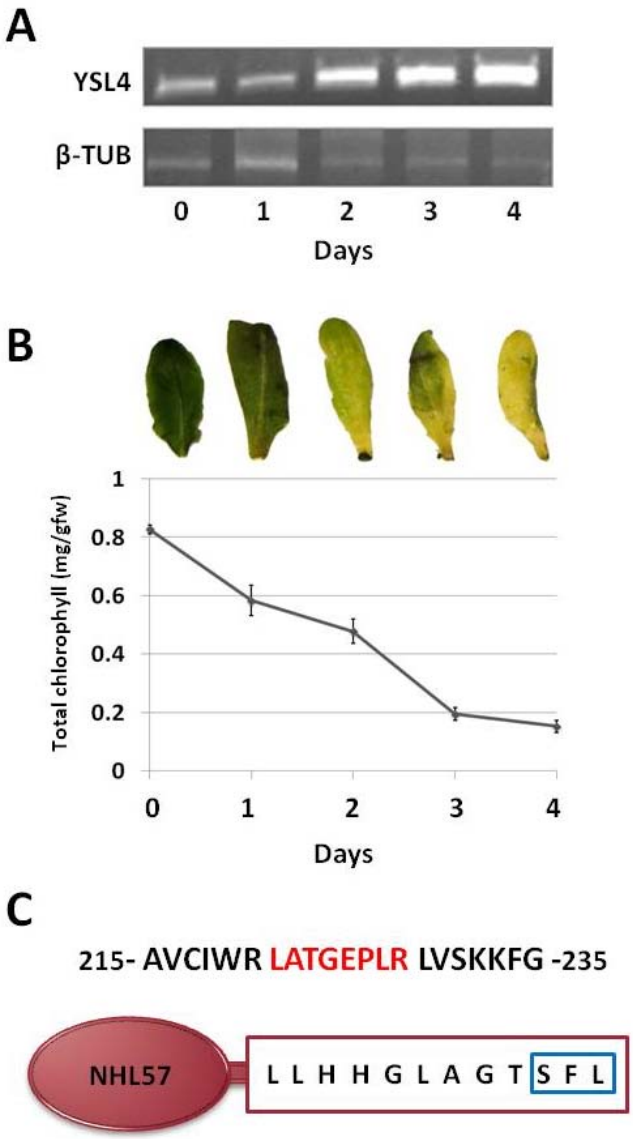

Figure 4.2. NHL57 was identified in senescent peroxisomes and contains a novel putative PTS1 tripeptide

A) Wild-type plants were detached at the base and dark-treated for four days. RT-PCR was performed to assess the expression of YSL4, a known senescence responsive gene. As expected YLS4 was induced over the course of treatment. No change was seen in the β-tubulin mRNA level control. B) Quantification of the total chlorophyll (mg/g fresh weight) in leaves from detached wild-type plants subjected to 4 days dark-treatment. The characteristic degradation of chlorophyll can be seen in the representative leaf images. C) The NHL57 peptide fragment identified in the proteomics study is indicated in red. Below is the carboxyl terminal region of NHL57 containing the novel SFL tripeptide (blue square).

Figure 4.3. *NHL57* is a senescence-associated gene.

A) Wild-type plants were detached at the base and dark-treated for four days. RNA was extracted and RT-PCR performed. *NHL57* expression levels steadily increased similar to YSL4. No change was seen in the β-tubulin mRNA level control. B) Leaves from 28-day-old plants were harvested from youngest (green) to oldest (yellow) and RNA was extracted. Shown are five representative leaves. As can be seen, while β-tubulin expression is unchanged, *NHL57* expression is up regulated as the leaves underwent natural senescence. C) RNA was extracted from different tissues at three developmental stages. Increased expression of *NHL57* was seen in flowers (early and late), in addition to yellow leaves (Lf, green leaf, Rt, root, Cl, cauline leaf, Flr, flower, Ylf, yellow leaf). D) *eYFP-NHL57* was co-infiltrated into tobacco leaves with the peroxisomal marker *eCFP-SKL*. Free-eYFP has a cytosolic localization, while eYFP-NHL co-localizes with eCFP-SKL. This indicates that NHL57 is a peroxisomal protein.

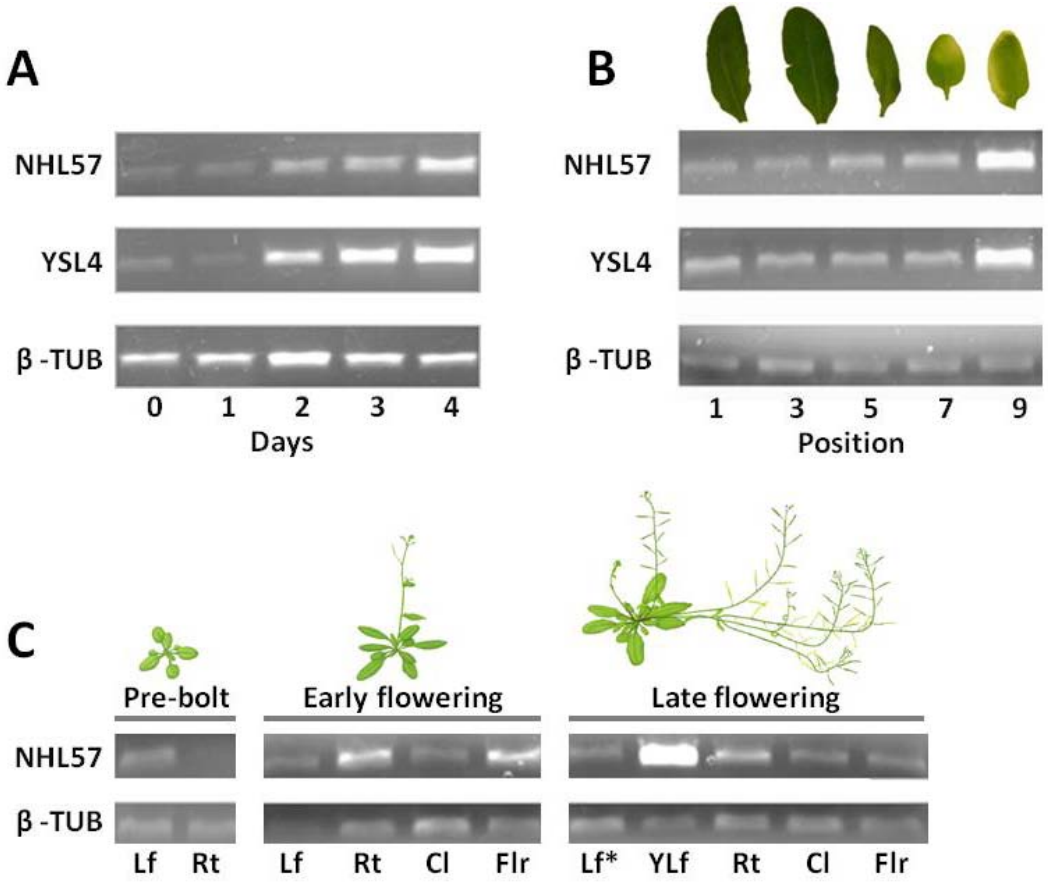
A
NHL57
YSL4
β -TUB
0 1 2 3 4
Days
B
NHL57
YSL4
β -TUB
1 3 5 7 9
Position
C
Pre-bolt
Early flowering
Late flowering
NHL57
β -TUB
Lf Rt
Lf Rt Cl Flr
Lf* YLf Rt Cl Flr

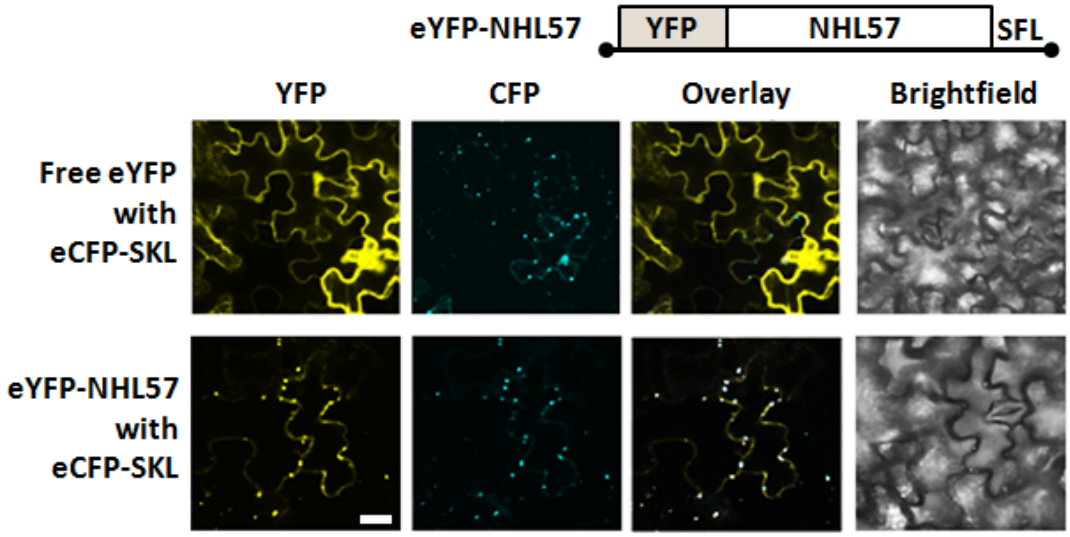

Figure 4.4. NHL57 is a peroxisomal protein

eYFP-NHL57 was co-infiltrated into young tobacco leaves with the peroxisomal marker *eCFP-SKL* and the helper gene *p19*. Free-eYFP has a cytosolic localization. eYFP-NHL co-localizes with eCFP-SKL, indicating that NHL57 is a peroxisomal protein. Representative images of tobacco epidermal cells are shown. The same localization was seen in mesophyll cells. Scale bar represents 25 µM.

Figure 4.5. The carboxyl-terminal region and tripeptide SFL of NHL57 are necessary for import into peroxisomes and for PEX5 binding

A) Diagram indicating the carboxyl-terminal sequences and total amino acid lengths of the NHL57 variants tested. NHL57ΔCt lacks the final 53 aa, while NHL57ΔSFL lacks only the final three amino acids. B) Radiolabeled full-length NHL57, NHL57ΔCt, NHL57ΔSFL, and GLO proteins were incubated with peroxisomes under import conditions. The left lane (no protease, 25°C) shows the total protein added to each import reaction, center lane the protein that was protease protected due to import (protease, 25°C), and the right lane a protease-treated negative control (protease, 4°C). Both GLO (positive control) and NHL57 were protease-protected, indicating they were peroxisomal. Neither NHL57ΔCt nor NHL57ΔSFL were protease-protected, indicating these truncations impeded transport into peroxisomes. The average import over a minimum of five experiments and the associated standard deviation are shown on the right (imported protein/total protein). C) The SFL tripeptide is required for NHL57 binding of the PTS1 receptor PEX5 through a direct protein-protein interaction. Radiolabeled NHL57, NHL57ΔSFL and GLO proteins were incubated with PVDF membranes on which purified HIS:PEX5 and HIS:ATG6 (negative protein control) were bound. An interaction was observed between PEX5 and NHL57 (top). Removal of the SFL prevented this interaction (middle). The interaction between GLO and PEX5 was used as a positive control (bottom); no proteins interacted with FDC (negative control).

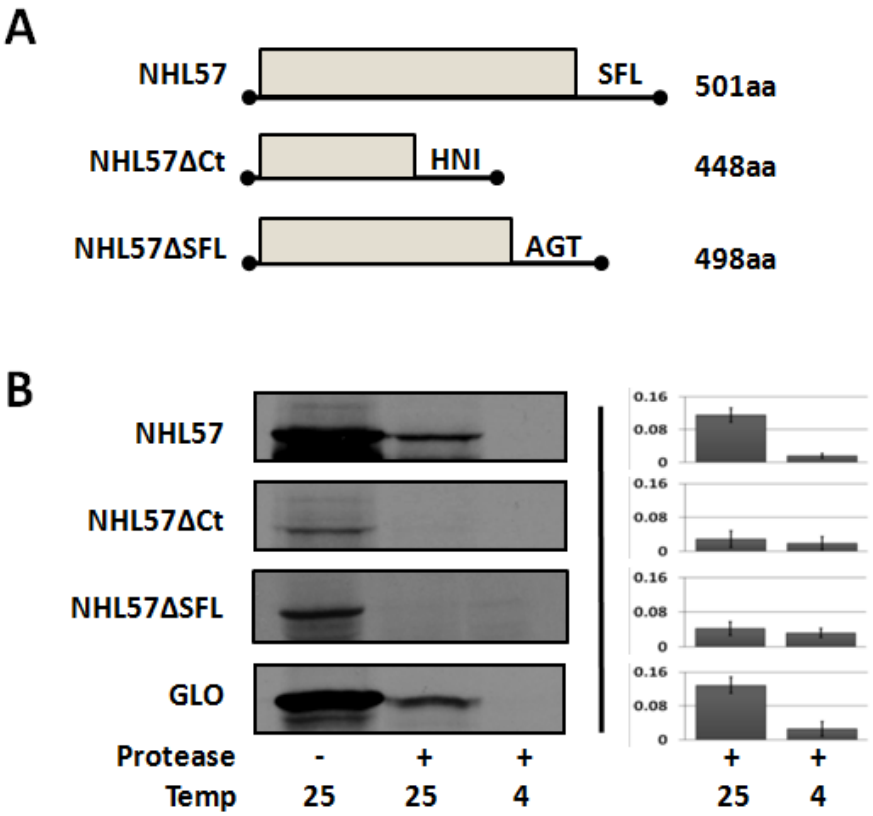
A
NHL57
SFL
501aa
NHL57ΔCt
HNI
448aa
NHL57ΔSFL
AGT
498aa
B
NHL57
NHL57ΔCt
NHL57ΔSFL
GLO
Protease - + + + +
Temp 25 25 4 25 4
0.16
0.08
0
C
PEX5
ATG6
NHL57
NHL57ΔSFL
GLO

Figure 4.6. Carboxyl terminal SFL tripeptide was not sufficient for peroxisomal targeting

A) Three eYFP proteins were tested for their ability to import into peroxisomes: eYFP fused to either an SKL or SFL tripeptide, and free eYFP, which lacked a targeting signal. The total amino acids and the carboxyl-terminal sequences of the variants are indicated. B) eYFP, eYFP-SKL, eYFP-SFL and GLO were incubated with peroxisomes under import conditions. Both GLO (positive control) and the eYFP-SKL were protease-protected, indicating they are peroxisomal. Neither the free eYFP control nor the eYFP-SFL fusion protein were protease-protected, indicting they were not peroxisomal. Therefore, the SFL tripeptide was not sufficient for targeting. C) The average import over a minimum of five experiments (protease protected protein/total protein) and associated standard deviation for each eYFP protein fusion and GLO are shown. The difference between the average import ratio for the free eYFP control and the eYFP-SFL fusion protein is not statistically significant.

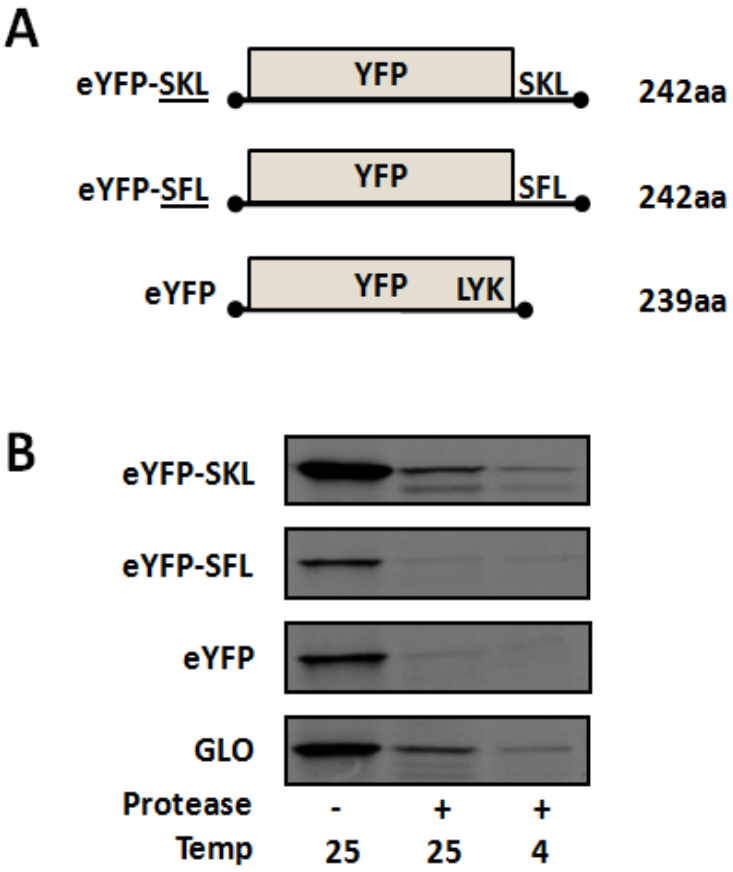
A
eYFP-SKL
YFP
SKL
242aa
eYFP-SFL
YFP
SFL
242aa
eYFP
YFP
LYK
239aa
B
eYFP-SKL
eYFP-SFL
eYFP
GLO
Protease
-
+
+
Temp
25
25
4
C
Relative import
0.12
0.08
0.04
0.00
GLO
SKL
SFL
eYFP

Figure 4.7. Conserved carboxyl terminal motif is present in putative SFL-variant PTS1-containing homologues

A) The final 20 amino acids (left to right) at the carboxyl termini of 19 different sequences with significant homology to NHL57 were aligned and the frequency of each amino acid determined. Blue boxes indicate the amino acids that showed no substitutions, these are shown as the consensus sequence. Below is a second consensus showing those amino acids that are present in at least 14 of the sequences at that position. NHL57 is shown for comparison. Amino acid substitutions at each of the 20 positions are shown from left to right. The frequency of each substitution (percentage and number of sequences) is indicated vertically. Variants in the tripeptide are indicated in the right three columns. B) Alignment of the final 30-33 amino acids of the sequences analyzed in A. Each grouping represents progressively more divergent amino acid sequences. Each consensus sequence shown summarizes all the sequences above it.

A

Position	20	19	18	17	16	15	14	13	12	11	10	9	8	7	6	5	4	3	2	1	Position
NHL57	A	R	D	T	I	S	H	N	L	L	H	H	G	L	A	G	T	S	F	L	NHL57
Consensus		R			I		H			L	H					G					Consensus
Majority		R	D		I	A	H	N	L	L	H	H		L	A	G	T		F	L	Majority

Number of sequences (19 total)	19	18	17	16	15	14	13	12	11	10	9	8	7	6	5	4	3	2	1	Percentage of sequences
19		R			I		H			L	H					G				100
18								N	L					A						95
17			D									H				T		F		89
16																			L	84
15	A												G							79
14						A								L						74
13																	S			68
10			A																	53
5					S									H						26
4																	A			21
2	TV		E	HN									N						F	11
1				TQS DR				K	X			NR	CV		S		N-	GR	TL	V	5

B

Name/Species	Amino acid sequence	
AtNHL57	LPE-NVLRSVNAMKA RDT ISHNLLHH GLAGT SFL-	33
Brassica rapa 1	LPE-NGLRSVSAMKA RDD ISHNLLHH GLAGT SFL-	33
Brassica rapa 2	LPE-NGLRSVTAMKA RDA ISHNLLHH GLAGT SFL-	33
(with all above)	*** * ****.**** ** ******** ***** ***	
CONSENSUS	RD ISHNLLHH GLAGT SFL	
Manihot esculenta	IPE-NALRSVGAIQA RDH IAHNLLHH GLAGT SFL-	33
Malus domestica	VPE-VALRSTSSMKA RDA IAHNLLHH GLAGT SFL-	33
Prunus persica	VPE-VALRSQSSMKA RDA IAHNLLHH GLAGT SFL-	33
Glycine max	VPE-VALRSMSSMKT RDA IAHNXLHH GLAGT SFL-	33
(with all above)	:** *** :::: ** *:** *** ***** ***	
CONSENSUS	RD I HN LHH GLAGT SFL	
Populus trichocarpa	VPE-VALRSASSMKA RDA IAHNLLHH CHAGT SFL-	33
Physcomitrella patens	LPENINFPI-TAMQA RDA IAHNLLHN VHAG- SFL-	32
Lycopersicon esculentum	IPE-VVVRSMNAMKV RDQ IAHKLLHH NHSGT SFL-	33
(with all above)	:** . :::. ** *:*: ** : :* ***	
CONSENSUS	RD I HN LH GT SFL	
More divergent sequences		
Arachis stenosperma	VPE-IALRSMTSMKA RDA IAHNLLHH GLAGT SFV-	33
Solanum lycopersicum	LPE-IQLRSTNARLA RDA IAHNLLHH NHAGT SLL-	33
Centaurea maculosa	VPE-AALRSANAMKV RDS IAHNLLHH NHAGT SFLS	34
Vitis vinifera	IPE-NGLRSASSAQA RDR IAHDLLHH GLAGN AFL-	33
Vitis vinifera2	IPE-IPLRSTTSMKA RDA IAHNLLHH GLAGT AFL-	33
Curcuma longa	VPE-NSIRSVSASQA REN IAHNLLHH GLAGT AFF-	33
Zingiber officinale	VPE-NSIRSVSASQA REN IAHNLLHH GLAGT AFF-	33
Gossypium hirsutum	VAE-DGLRSVSSLKA RDA IAHNLLHH GLAGT GFL-	33
AtNHL60	VPE-NNIRSASAVNT RDH ISHNLLHR GLAGT RTL-	33
(overall)	:.* . : . *: *:*. **. :* .	
CONSENSUS	R I H LH G	

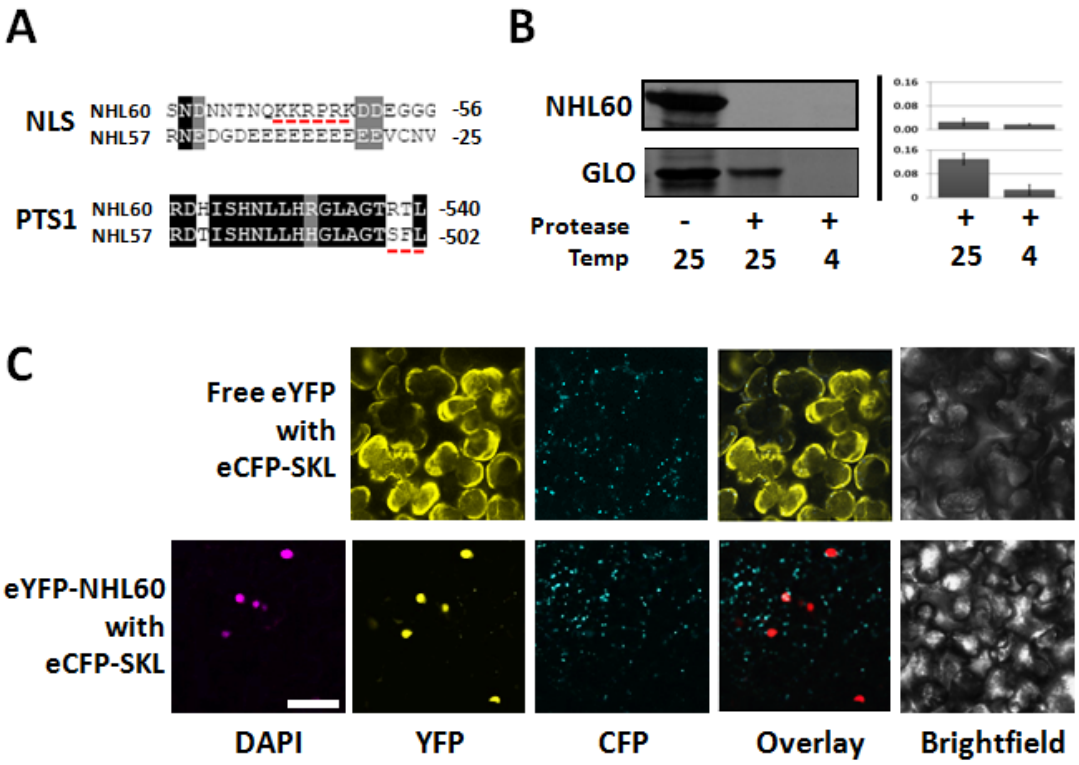

Figure 4.8. NHL60 is a non-peroxisomal sequence-based homologue of NHL57

A) Amino acid sequence alignment of NHL57 and NHL60 indicate the location of the putative PTS1 and nuclear localization signal. NHL60 has an RTL tripeptide while NHL57 has an SFL (top underlined). There is significant amino acid conservation in the upstream residues. The putative NLS in NHL60 is not conserved in the NHL57 amino acid sequence. B) NHL60 and GLO were incubated with peroxisomes under standard import conditions. NHL60 was not protease-protected, indicating it is not peroxisomal. As expected, GLO was protease protected. The corresponding quantitation is shown on the right. C) eYFP-NHL60 was co-infiltrated into tobacco leaves with the peroxisomal marker eCFP-SKL. One punctate structure per cell was observed (eYFP-NHL), which co-localized with the DAPI-stained nuclei, indicating NHL60 is a nuclear protein. No co-localization was observed with the eCFP-SKL peroxisomal marker. Free eYFP was cytosolic. Scale bar presents 60 µM.

Figure 4.9. NHL57 homozygotes have a senescence-associated phenotype

A) Diagram indicating the T-DNA insertion site in *atnhl57-1* (SALK_024636) at bp 687, and the locations of RT-PCR (A, B, C) and screening (s) primers. The black line represents a single exon; NHL57 has no introns. B) RT-PCR was performed on RNA extracted from wild-type or *nhl57* homozygous plants using two primer sets; one to detect truncated transcript upstream of the T-DNA insertion site (A-B) and a second set that span the T-DNA insertion site to detect full-length transcript (A-C). While truncated transcript was detected in homozygotes, no full-length transcript was detected, indicating this is most likely a loss-of-function allele. Representative images of *atnhl57-1* plants at 7, 21 and 42 days post-germination are shown. C) Wild-type and *nhl57* homozygous plants were detached at the base and dark-treated for four days. Leaves were removed at each time point. Leaves from *nhl57* homozygous plants retained higher chlorophyll content at days 3 and 4 as compared to wild-type plants. D) Quantification of the chlorophyll in mutant (dark grey), and wild-type (light grey) leaves. A statistically significant difference between mutant and wild-type plants can be seen in the chlorophyll levels at 3 and 4 days (asterisk, p=0.034). Bars indicate standard deviation over four experiments.

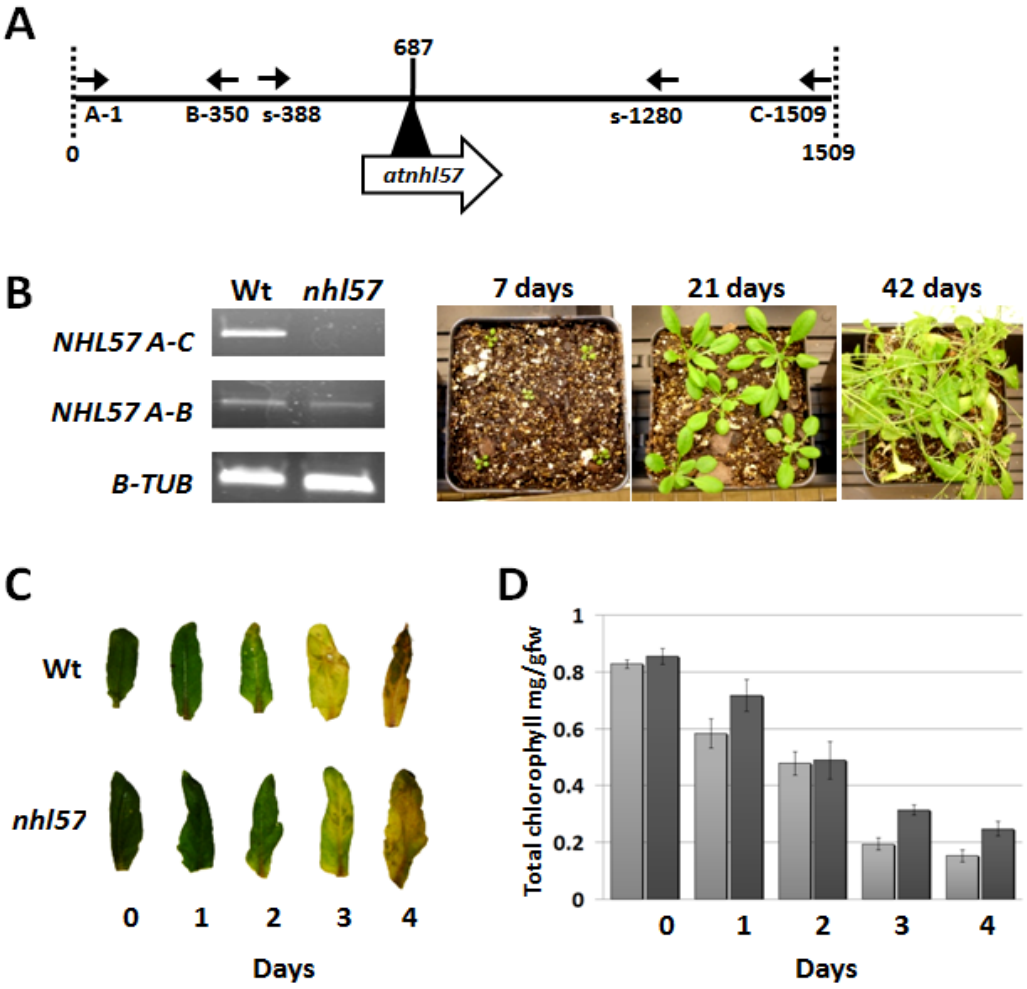
A
687
A-1
B-350
s-388
s-1280
C-1509
0
1509
atnhl57
B
Wt
nhl57
NHL57 A-C
NHL57 A-B
B-TUB
7 days
21 days
42 days
C
Wt
nhl57
0
1
2
3
4
Days
D
Total chlorophyll mg/gfw
1
0.8
0.6
0.4
0.2
0
0
1
2
3
4
Days

Literature cited

1. Poirier, Y., V.D. Antonenkov, T. Glumoff, and J.K. Hiltunen, 2006, Peroxisomal beta-oxidation--a metabolic pathway with multiple functions. Biochim biophys acta. **1763**: 1413-1426.
2. Vandenbosch, H., R.B.H. Schutgens, R.J.A. Wanders, and J.M. Tager, 1992, Biochemistry of peroxisomes. Annu Rev Biochem. **61**: 157-197.
3. Stintzi, A. and J. Browse, 2000, The Arabidopsis male-sterile mutant, opr3, lacks the 12-oxophytodienoic acid reductase required for jasmonate synthesis. Proc Natl Acad Sci U S A. **97**: 10625-10630.
4. van der Klei, I.J., H. Yurimoto, Y. Sakai, and M. Veenhuis, 2006, The significance of peroxisomes in methanol metabolism in methylotrophic yeast. Biochim biophys acta. **1763**: 1453-1462.
5. Michels, P.A., J. Moyersoen, H. Krazy, N. Galland, M. Herman, and V. Hannaert, 2005, Peroxisomes, glyoxysomes and glycosomes (review). Mol Membr Biol. **22**: 133-145.
6. Webb, M.A. and E.H. Newcomb, 1987, Cellular compartmentation of ureide biogenesis in root-nodules of cowpea (*Vigna unguiculata* (L) Walp). Planta. **172**: 162-175.
7. Chen, H.J., W.C. Hou, W.N. Jane, and Y.H. Lin, 2000, Isolation and characterization of an isocitrate lyase gene from senescent leaves of sweet potato (Ipomoea batatas cv. Tainong 57). J Plant Physiol. **157**: 669-676.
8. Olsen, L. and J. Harada, 1995, Peroxisomes and their assembly in higher plants. Ann Rev Plant Physiol Plant Mol Biol. **16**: 123-146.
9. Lim, P.O., H.J. Kim, and H.G. Nam, 2007, Leaf senescence. Annu Rev Plant Biol. **58**: 115-136.
10. Simeonova, E., A. Sikora, M. Charzynska, and A. Mostowska, 2000, Aspects of programmed cell death during leaf senescence of mono- and dicotyledonous plants. Protoplasma. **214**: 93-101.
11. Hoertensteiner, S., 2006, Chlorophyll degradation during senescence. Annu Rev Plant Biol. **57**: 55-77.
12. Wingler, A., A. von Schaewen, R.C. Leegood, P.J. Lea, and W.P. Quick, 1998, Regulation of leaf senescence by cytokinin, sugars, and light - Effects on NADH-dependent hydroxypyruvate reductase. Plant physiology. **116**: 329-335.
13. Lim, P.O. and H.G. Nam, 2005, The molecular and genetic control of leaf senescence and longevity in Arabidopsis, in Curr Topics Devel Biol 67. 49-83.
14. Miao, Y., T. Laun, P. Zimmermann, and U. Zentgraf, 2004, Targets of the WRKY53 transcription factor and its role during leaf senescence in Arabidopsis. Plant MolBiol. **55**: 853-867.
15. Guo, Y., Z. Cai, and S. Gan, 2004, Transcriptome of Arabidopsis leaf senescence. Plant Cell Environ. **27**: 521-549.

16. Lin, J.F. and S.H. Wu, 2004, Molecular events in senescing Arabidopsis leaves. Plant J. **39**: 612-628.
17. Breeze, E., E. Harrison, T. Page, N. Warner, C. Shen, C. Zhang, and V. Buchanan-Wollaston, 2008, Transcriptional regulation of plant senescence: from functional genomics to systems biology. Plant Biol. **10**: 99-109.
18. De Bellis, L., P. Picciarelli, L. Pistelli, and A. Alpi, 1990, Localization of glyoxylate-cycle marker enzymes in peroxisomes of senescent leaves and green cotyledons. Planta. **180**: 435-439.
19. Zimmermann, P., C. Heinlein, G. Orendi, and U. Zentgraf, 2006, Senescence-specific regulation of catalases in *Arabidopsis thaliana* (L.) Heynh. Plant Cell Environ. **29**: 1049-1060.
20. Abeles, F.B., L.J. Dunn, P. Morgens, A. Callahan, R.E. Dinterman, and J. Schmidt, 1988, Induction of 33-Kd and 60-Kd peroxidases during ethylene-induced senescence of cucumber cotyledons. Plant physiology. **87**: 609-615.
21. Lazarow, P.B. and Y. Fujiki, 1985, Biogenesis of peroxisomes. Annu Rev Cell Biol. **1**: 489-530.
22. Subramani, S., A. Koller, and W.B. Snyder, 2000, Import of peroxisomal matrix and membrane proteins. Annu Rev Biochem. **69**: 399-418.
23. Brown, L.A. and A. Baker, 2008, Shuttles and cycles: transport of proteins into the peroxisome matrix. Molecular Membrane Biology. **25**: 363-375.
24. Glover, J.R., D.W. Andrews, S. Subramani, and R.A. Rachubinski, 1994, Mutagenesis of the amino targeting signal of *Saccharomyces cerevisiae* 3-ketoacyl-CoA thiolase reveals conserved amino acids required for import into peroxisomes in vivo. J Biol Chem. **269**: 7558-7563.
25. Reumann, S., C. Ma, S. Lemke, and L. Babujee, 2004, AraPerox. A database of putative Arabidopsis proteins from plant peroxisomes. Plant physiology. **136**: 2587-2608.
26. Keller, G.A., S. Krisans, S.J. Gould, J.M. Sommer, C.C. Wang, W. Schliebs, W. Kunau, S. Brody, and S. Subramani, 1991, Evolutionary conservation of a microbody targeting signal that targets proteins to peroxisomes, glyoxysomes, and glycosomes. J Cell Biol. **114**: 893-904.
27. Gould, S.G., G.A. Keller, and S. Subramani, 1987, Identification of a peroxisomal targeting signal at the carboxy terminus of firefly luciferase. J Cell Biol. **105**: 2923-2931.
28. Gould, S.J., G.A. Keller, N. Hosken, J. Wilkinson, and S. Subramani, 1989, A conserved tripeptide sorts proteins to peroxisomes. J Cell Biol. **108**: 1657-1664.
29. Brocard, C. and A. Hartig, 2006, Peroxisome targeting signal 1: is it really a simple tripeptide? Biochim biophys acta. **1763**: 1565-1573.
30. Sommer, J.M., Q.L. Cheng, G.A. Keller, and C.C. Wang, 1992, In vivo import of firefly luciferase into the glycosomes of *Trypanosoma brucei* and mutational analysis of the C-terminal targeting signal. Mol Biol Cell. **3**: 749-759.

31. Mullen, R.T., M.S. Lee, C.R. Flynn, and R.N. Trelease, 1997, Diverse amino acid residues function within the type 1 peroxisomal targeting signal. Implications for the role of accessory residues upstream of the type 1 peroxisomal targeting signal. Plant physiology. **115**: 881-889.
32. Hayashi, M., M. Aoki, A. Kato, M. Kondo, and M. Nishimura, 1996, Transport of chimeric proteins that contain a carboxy-terminal targeting signal into plant microbodies. Plant J. **10**: 225-234.
33. Lametschwandtner, G., C. Brocard, M. Fransen, P. Van Veldhoven, J. Berger, and A. Hartig, 1998, The difference in recognition of terminal tripeptides as peroxisomal targeting signal 1 between yeast and human is due to different affinities of their receptor Pex5p to the cognate signal and to residues adjacent to it. J Biol Chem. **273**: 33635-33643.
34. Aitchison, J.D., W.W. Murray, and R.A. Rachubinski, 1991, The carboxyl-terminal tripeptide Ala-Lys-Ile is essential for targeting *Candida tropicalis* trifunctional enzyme to yeast peroxisomes. J Biol Chem. **266**: 23197-23203.
35. Reumann, S., et al., 2007, Proteome analysis of Arabidopsis leaf peroxisomes reveals novel targeting peptides, metabolic pathways, and defense mechanisms. The Plant cell. **19**: 3170-3193.
36. Ma, C.L., M. Haslbeck, L. Babujee, O. Jahn, and S. Reumann, 2006, Identification and characterization of a stress-inducible and a constitutive small heat-shock protein targeted to the matrix of plant peroxisomes. Plant physiology. **141**: 47-60.
37. Wessel, D. and U.I. Flugge, 1984, A method for the quantitative recovery of protein in dilute-solution in the presence of detergents and lipids. Anal Biochem. **138**: 141-143.
38. Blum, H., H. Beier, and H.J. Gross, 1987, Improved silver staining of plant-proteins, RNA and DNA in polyacrylamide gels. Electrophoresis. **8**: 93-99.
39. Reumann, S., et al., Manuscript submitted, In-depth proteome analysis of Arabidopsis leaf peroxisomes combined with in vivo subcellular targeting verification uncovers low-abundance proteins with metabolic and regulatory functions.
40. Harrison-Lowe, N.J. and L.J. Olsen, 2008, Autophagy protein 6 (ATG6) is required for pollen germination in *Arabidopsis thaliana*. Autophagy. **4**: 339 - 348
41. Arnon, D.I., 1949, Copper enzymes in isolated chloroplasts - polyphenoloxidase in *Beta vulgaris*. Plant physiology. **24**: 1-15.
42. Crookes, W.J. and L.J. Olsen, 1998, The effects of chaperones and the influence of protein assembly on peroxisomal protein import. J Biol Chem. **273**: 17236-17242.
43. Harrison-Lowe, N.J. and L.J. Olsen, 2005, Isolation of glyoxysomes from pumpkin cotyledons. Curr Protoc Cell Biol: 3.19.11-3.19.18.
44. Yoshida, S., M. Ito, I. Nishida, and A. Watanabe, 2001, Isolation and RNA gel blot analysis of genes that could serve as potential molecular markers for leaf senescence in *Arabidopsis thaliana*. Plant Cell Physiol. **42**: 170-178.

45. Ougham, H., S. Hortensteiner, I. Armstead, I. Donnison, I. King, H. Thomas, and L. Mur, 2008, The control of chlorophyll catabolism and the status of yellowing as a biomarker of leaf senescence. Plant Biol. **10**: 4-14.
46. Cao, Y. and D.J. Klionsky, 2007, Physiological functions of Atg6/Beclin 1: a unique autophagy-related protein. Cell Res. **17**: 839-849.
47. Kalderon, D., B.L. Roberts, W.D. Richardson, and A.E. Smith, 1984, A short amino-acid sequence able to specify nuclear location. Cell. **39**: 499-509.
48. Hayashi, M., K. Toriyama, M. Kondo, and M. Nishimura, 1998, 2,4-dichlorophenoxybutyric acid-resistant mutants of Arabidopsis have defects in glyoxysomal fatty acid beta-oxidation. The Plant cell. **10**: 183-195.
49. Woodward, A.W. and B. Bartel, 2005, The Arabidopsis peroxisomal targeting signal type 2 receptor PEX7 is necessary for peroxisome function and dependent on PEX5. Mol Biol Cell. **16**: 573-583.
50. Reumann, S., 2004, Specification of the peroxisome targeting signals type 1 and type 2 of plant peroxisomes by bioinformatics analyses. Plant physiology. **135**: 783-800.
51. Mano, S., M. Hayashi, M. Kondo, and M. Nishimura, 1997, Hydroxypyruvate reductase with a carboxy-terminal targeting signal to microbodies is expressed in Arabidopsis. Plant & cell physiology. **38**: 449-455.
52. Kragler, F., G. Lametschwandtner, J. Christmann, A. Hartig, and J.J. Harada, 1998, Identification and analysis of the plant peroxisomal targeting signal 1 receptor NtPEX5. Proceedings of the National Academy of Sciences of the United States of America. **95**: 13336-13341.
53. Wierzbicki, A.S., 2007, Peroxisomal disorders affecting phytanic acid alpha-oxidation: a review. Biochem Soc Trans. **35**: 881-886.
54. de Leon, I.P., A. Sanz, M. Hamberg, and C. Castresana, 2002, Involvement of the Arabidopsis alpha-DOX1 fatty acid dioxygenase in protection against oxidative stress and cell death. Plant J. **29**: 61-72.
55. Hamberg, M., A. Sanz, and C. Castresana, 1999, alpha-oxidation of fatty acids in higher plants - Identification of a pathogen-inducible oxygenase (PIOX) as an alpha-dioxygenase and biosynthesis of 2-hydroperoxylinolenic acid. J Biol Chem. **274**: 24503-24513.
56. Schnarrenberger, C. and C. Burkhard, 1977, Invitro interaction between chloroplasts and peroxisomes as controlled by inorganic-phosphate. Planta. **134**: 109-114.
57. Charlton, W.L., B. Johnson, I.A. Graham, and A. Baker, 2005, Non-coordinate expression of peroxisome biogenesis, beta-oxidation and glyoxylate cycle genes in mature Arabidopsis plants. Plant Cell Reports. **23**: 647-653.
58. Nooden, L.D., J.J. Guiamet, and I. John, 1997, Senescence mechanisms. Physiol Plant. **101**: 746-753.
59. Gan, S.S. and R.M. Amasino, 1995, Inhibition of leaf senescence by autoregulated production of cytokinin. Science. **270**: 1986-1988.

60. He, Y.H., H. Fukushige, D.F. Hildebrand, and S.S. Gan, 2002, Evidence supporting a role of jasmonic acid in Arabidopsis leaf senescence. Plant physiology. **128**: 876-884.
61. Afitlhile, M.M., H. Fukushige, M. Nishimura, and D.F. Hildebrand, 2005, A defect in glyoxysomal fatty acid beta-oxidation reduces jasmonic acid accumulation in Arabidopsis. Plant Physiol Biochem. **43**: 603-609.
62. Delker, C., B.K. Zolman, O. Miersch, and C. Wasternack, 2007, Jasmonate biosynthesis in *Arabidopsis thaliana* requires peroxisomal beta-oxidation enzymes - Additional proof by properties of pex6 and aim1. Phytochemistry. **68**: 1642-1650.
63. Kong, Z.S., M.N. Li, W.Q. Yang, W.Y. Xu, and Y.B. Xue, 2006, A novel nuclear-localized CCCH-type zinc finger protein, OsDOS, is involved in delaying leaf senescence in rice. Plant physiology. **141**: 1376-1388.

Chapter 5
Conclusions and Future Directions

When I began my thesis, I was interested in furthering my understanding of how plants respond to abiotic and biotic stress. During my research I investigated two stress-related processes, autophagy and senescence, through the study of three very different proteins, ATG6, FDC and NHL57. Five years ago, little was known about the function of ATG6 in plants and neither FDC nor NHL57 had been experimentally investigated. Because of my work, we have a greater understanding of the complex interactions between stress biology, reproductive physiology and peroxisome metabolism.

Each of the three data chapters presented in this thesis contributes to our knowledge of plant stress biology in a different way. The research presented in Chapter 2 provides a link between the autophagy pathway and pollen development through the examination of ATG6 function in *Arabidopsis thaliana*. Chapter 3 describes the identification of a plant FYVE-domain-containing protein (FDC) as an ATG6 interacting partner, suggesting such proteins may serve as effectors in ATG6-PI3K-mediated signaling in *Arabidopsis.* Finally, Chapter 4 shows how proteomics techniques were used to investigate the role of peroxisomes during senescence. This led to the identification of NHL57, a senescence-associated protein, which furthered our understanding of PTS1 proteins and suggested a connection between peroxisomes and chlorophyll degradation

Autophagy-related Protein 6 (ATG6)

When I entered graduate school, research into the autophagy pathway was just beginning in plant model systems. This provided the opportunity to investigate the physiological roles this pathway serves in a very different eukaryotic system. My work began with an investigation into the role of ATG6 during plant growth and development. As expected, heterozygous *atg6* mutant plants displayed developmental phenotypes consistent with those reported in mammalian systems. However, my initial intention of isolating *atg6* homozygous plants and examining them for stress-related phenotypes led me in an unexpected direction. As presented in Chapter 2, no homozygous *atg6* plants were ever recovered. Initially I spent time clearing the coats of *atg6-2* seeds, which had failed to germinate and examining embryos, looking for developmental phenotypes. Further investigation, and a several-year period spent working as a microscopist, geneticist, and pollen biologist, revealed that ATG6 was in fact required for pollen germination. While researchers have always presumed that the process of reproductive development is inherently stressful, due to the increased levels of protein synthesis, trafficking, intracellular signaling and rapid metabolite consumption, a link between the autophagy pathway and pollen development had never been proposed.

To date, there have several publications on the role of ATG6 during pollen development, but it is still unclear whether ATG6 is functioning in an autophagy-dependent or -independent manner. As in other eukaryotic systems, *Arabidopsis* ATG6 is presumed to function as a subunit in the class-III PI3K complex. This PI3K complex is expected to have both constitutive and inducible intracellular trafficking functions in all cell types including pollen grains. However, almost nothing is known about the specific role of the PI3K complex, or its product lipid PI3P, during pollen germination. It is known that high levels of intracellular trafficking are required for pollen tube growth and development. Perhaps loss of ATG6 causes perturbation of the PI3K signaling pathway, preventing delivery of the membrane and protein components necessary for initiation of pollen tube growth. It is unlikely that polarization is affected as *qrt1(-/-)/atg6(+/-)* tetrads show

correct polarization of the generative nuclei. Since almost five percent of the *atg6* pollen grains displayed initiation of pollen tube growth, there may be unidentified environmental factors that can mitigate the loss of ATG6 function. To date, researchers have yet to determine the precise cause of the *atg6* pollen germination phenotype. Having spent several years focused on an area outside of the expertise of my lab and distant from general plant stress biology, I chose to defer this question to the pollen biologists.

However, before I leave Chapter 2, I must admit that there is one outstanding question that still intrigues me - the question I had when I began the project; Is ATG6 required for development post-fertilization? I attempted to answer this question by taking advantage of our ability to generate whole plants from single cells. I attempted to regenerate diploid homozygous plants from isolated *atg6-2* haploid microspores. This method should have bypassed the pollen germination phenotype and allowed me to examine *atg6-2* embryos and plants. However, despite the recovery of multiple microspore embryos, none could be coaxed into adulthood. While this leaves the question unanswered, it in part suggests that an *atg6* homozygous plant is not viable. Future researchers could address this question by using a pollen-specific promoter to complement just the *atg6* pollen germination phenotype, and then observing any subsequent growth and development phenotypes. Current research is focused on understanding the role of ATG6 and the PI3K complex in the regulation of programmed cell death during the hypersensitive response. Due to the heterozygote phenotype and my brief experiment with microspore culture, I predict that ATG6 is also required for normal growth and development.

FYVE-Domain Containing protein (FDC)

To understand the role of ATG6 in plant growth and development, I completed a yeast two-hybrid screen. Initially I thought this would aid in the identification of an ATG14 functional homologue, since none was evident from bioinformatic analysis. However, when analyzing the data from two separate screens, using the double transformation and mating methods, I was intrigued by the number of zinc finger proteins, including those predicted to bind phosphatidylinositol-3-phosphate (PI3P). At the time, there was no direct evidence that ATG6 was part of a PI3K complex in plants, but the identification of a PI3P-binding protein (FDC) as an ATG6 interaction partner suggested that this function was conserved. Ultimately, I selected FDC for further study. While FDC's function had not been experimentally investigated, it was one of fourteen Arabidopsis FYVE-domain-containing proteins and was the first non-PRAF type characterized. Had I known then that FDC would be biochemically challenging to work with I may have selected an alternate protein despite the interesting biological question. While I was unable to reconstitute PI3P binding *in vitro*, I was able, through a variety of experiments, to support the hypothesis that FDC has all the expected characteristics of a functional PI3P-binding protein, including zinc binding and membrane association.

This is the first time that a PI3K-complex subunit has been shown to directly interact with a PI3P-binding protein. Potential implications for this interaction are discussed in Chapter 3. Unfortunately, the lack of a suitable FDC mutant line made loss-of-function analysis problematic and genetic analysis of the ATG6-FDC interaction essentially impossible. In addition, since *FDC* is a member of a gene family, RNAi techniques would require monitoring of the transcript levels of multiple family members, some of which may function redundantly with *FDC*. However, mutant analysis could yield important insights into the purpose of the ATG6-FDC interaction. For example, FDC may also function during pollen development, or serve as an effecter protein in response to specific plant stresses.

Several attempts were made to determine FDC function *in planta,* including analysis of the available mutant line and the construction of stable eYFP over-expression lines and GUS reporter fusions. However, all yielded negative results so these experiments were not included in Chapter 3. I will note one potential exception, a yeast complementation was performed with a *ScVPS27* deletion strain to test whether FDC could function in place of Vps27 during endosomal trafficking. While FDC did not completely complement the Vps27 phenotype, a slight effect was observed when an untagged form of FDC was highly over-expressed. What this means may become apparent as more members of the family are investigated and additional ATG6 interacting partners are identified and studied. Examination of additional novel partners identified in the yeast two-hybrid screens may reveal additional roles for ATG6 and the PI3K complex in plant stress biology.

Chapter 4

Having spent the majority of my graduate research either working with haploid pollen or doing *in vitro* biochemistry with PI3P binding proteins, my final project pulled me closer to my initial goals of adding to our understanding of plant stress responses. I had the opportunity to participate in a collaborative project focused on the proteomic identification of peroxisomal proteins during the process of senescence. As mentioned in Chapter 1, and detailed in Figure 1.7, peroxisomes are responsible for a variety of essential functions during plant senescence. This requires an alteration of the protein complement. This final project initially allowed me to gain first-hand experience with the preparation of high-purity organelles, and later with the analysis and interpretation of the proteomics data. As detailed in Chapter 4, this analysis led to the identification and characterization of a novel peroxisomal protein, NHL57. By analyzing the targeting signal present in NHL57, I was able to extend our current definition of acceptable PTS1 amino acid substitutions to include phenylalanine. This allows for further *in silco* predictions of functional targeting signals. In addition, the necessity of the SFL PTS1 for protein import and PEX5 binding was

demonstrated. This clearly supports the hypothesis that removal of the PTS1 tripeptide prevents protein import due to loss of interaction with the receptor. In addition, by also examining the targeting of NHL60, I was also able to demonstrate that conservation of the upstream residues is not enough to ensure functionality of novel PTS1 signals. I suggest a “rule of thumb” that proteins with these conserved upstream residues, containing a phenylalanine in the second position, and confirmed acceptable amino acids in the first and third positions, may contain functional signals.

Analysis of NHL57 also provides additional evidence that the peroxisomal protein complement undergoes significant changes during senescence (enzymatically detailed in chapter 1). NHL57 is the first non-enzymatic peroxisomal protein reported to have a senescence-associated phenotype (with the exception of the PEX proteins). Consequently, I find the functional role of NHL57 interesting. Following its identification, I confirmed the senescence association of NHL57 and that the mRNA level increased during dark-induced senescence. Examination of the *nhl57* mutant plants revealed a chlorophyll degradation phenotype. Why does loss of this protein affect the degradation of chloroplast metabolites? It is possible, though unlikely, that the function of NHL57 does not require its peroxisomal localization at all. This possibility could be tested by accessing the phenotype of *nhl57* mutant plants expressing an NHL57ΔSFL deletion construct. In Chapter 4, I detailed several possible explanations for this phenotype including altered jasmonic acid levels and the possible contribution of α-oxidation enzymes to phytanic acid degradation. The level of jasmonate metabolites should be tested in these mutant plants to determine if they are lower than the levels in senescing wild-type plants. In addition, future work could entail a more detailed examination of the degradation patterns of chloroplast proteins, including Rubisco and chlorophyll a/b binding proteins. This would separate a defect that is specific to chlorophyll degradation from a broader retardation of chloroplast senescence indicated by altered protein degradation. Study of additional novel peroxisomal proteins identified in the

proteomic-screen may also help elucidate the basis of the molecular biology behind this phenotype.

Finally, my work with NHL60 is interesting from a functional standpoint. NHL60 shares high sequence conservation with NHL57, but is actually a nuclear protein, and analysis of NHL60 mutants did not have any obvious phenotypes. It would be interesting, albeit complex, to address whether these two proteins are performing similar functions in two different cellular compartments. The first step would be to determine if their functions are interchangeable with respect to peroxisomes and the chlorophyll degradation phenotype. To determine whether the two proteins function in a similar manner, NHL60 could be targeted to the peroxisome by mutation of the carboxyl terminus signal on NHL60 to create an SFL PTS1. If this modified form of *NHL60* was placed under control of the *NHL57* native promoter and expressed in the *nhl57* mutant background, we could assess whether a peroxisome-localized NHL60 could function in place of NHL57. Of course this is hardly a simple experiment, as NHL60 may also need the putative NLS inactivated to prevent targeting to the nucleus, and a potential NHL60 over-expression phenotype. Ultimately, understanding the function of NHL57 would elucidate the biochemical connections between chloroplast and peroxisomal metabolism during senescence.

Summary

Like the work of many fellow graduate students, my research took a series of unexpected turns that led me to completion of my graduate work. Each of the three projects presented in this thesis focuses on different aspects of plants and their response to biotic and abiotic factors. Together they comprise a unique perspective on plant stress biology and provide a foundation for future work in pollen biology, lipid signaling, and senescent peroxisomes.

Appendices

Isolation of Glyoxysomes from Pumpkin Cotyledons

Abstract

Peroxisomes are single-membrane bound organelles found in virtually all eukaryotes. In plants, there are several classes of peroxisomes. Glyoxysomes are found in germinating seedlings and contain enzymes specific for the glyoxylate cycle, including isocitrate lyase and malate synthase. After seedlings become photosynthetic, leaf peroxisomes participate in reactions of the photorespiration pathway and contain characteristic enzymes such as glycolate oxidase and hydroxypyruvate reductase. As leaves begin to senesce, leaf peroxisomes are transformed back into glyoxysomes. Root peroxisomes in the nodules of legumes, for example, sequester enzymes such as allantoinase and uricase, which contribute to nitrogen metabolism in these tissues. Thus, peroxisomes participate in many metabolic pathways and contain specific enzyme complements, depending on the tissue source. All peroxisomes contain catalase to degrade hydrogen peroxide and enzymes to accomplish β-oxidation of fatty acids. Glyoxysomes can be isolated from pumpkin cotyledons by standard differential centrifugation and density separation, as described in this article.

Introduction

In the late 1960's, cell biologists determined that the spherical particles observed in plant cell electron micrographs were in fact classes of a distinct and vital organelle, the peroxisome [1] (see Figure A.4). Peroxisomes derive their name from their critical function in the metabolism of hydrogen peroxide. For example, the degradation of hydrogen peroxide is catalyzed by the matrix protein catalase, arguably the most abundant peroxisomal enzyme (Figure A.5). Catalase is also a major constituent of the distinctive peroxisomal core or crystalline inclusion that is sometimes observed in plant peroxisomes [2]. Peroxisomes are small organelles that are bound by a single phospholipid membrane. They can range in size from 0.5-1.5 μm. Although they have been observed in a variety of shapes, they are most commonly spherical. While all plant peroxisomes have some enzymes in common (e.g., catalase, thiolase), they are typically divided into several classes based upon their physiological roles, as defined by spatial and temporal parameters [3,4]. For example, cotyledons of oilseeds, such as pumpkins, contain a special class of peroxisomes, called glyoxysomes. These sequester all of the enzymes required for the glyoxylate cycle to supply the growing seedling with energy. In contrast, peroxisomes found later in leaf development have a partially different enzyme complement, because of their function in other pathways, including photorespiration[5].

An interesting feature of peroxisomes is their lack of an organellar genome. This means that nuclear genes encode all constituent proteins. Peroxisomal proteins are synthesized in the cytoplasm and post-translationally translocated into peroxisomes [6]. The biogenesis of peroxisomes most likely involves the growth and division of pre-existing peroxisomes [5,7]. Intense study has elucidated the molecular machinery (PEX proteins) required for the interrelated processes of peroxisome biogenesis and protein import. Import of peroxisomal matrix proteins occurs through two receptor-mediated import pathways. Each pathway is defined by one of two Peroxisome Targeting Signals

(PTS1, PTS2) on the cargo proteins that the receptors recognize and transport. Thus, there are two cytosolic receptors (Pex5p, Pex7p) that recognize the targeting signals and bind to the cargo proteins [8-10]. *In vitro* protein import assays have been invaluable in studies of the dynamics of peroxisomal protein import – addressing questions about the interactions between the receptors and cargo proteins, the energy requirements, the roles of protein chaperones, and the molecular mechanisms of translocation [6,9,11-14]. The success of these assays relies on the reproducible purification and manipulation of intact peroxisomes and the presences of the relevant protein cargo, receptors and other biochemical constituents.

In addition to questions of organelle biogenesis, peroxisome biochemistry and function has received recent attention. Many previously uncharacterized enzymes, including alanine aminotransferase, alanine:glyoxylate aminotransferase, and sarcosine oxidase, have been localized to plant peroxisomes [15-17]. A role for peroxisomal β-oxidation in auxin metabolism has been extensively studied (e.g., [18-20]). An isozyme of 12-oxophytodienoate reductase, OPR3, which catalyzes the final step of jasmonate biosynthesis, also possesses a peroxisomal targeting signal – suggesting a role for peroxisomes in jasmonic acid signaling [21,22]. Thus, peroxisomes have many critical physiological functions throughout the life cycle of plants.

Materials and Methods

The isolation of organelles is essential for a variety of biochemical procedures. The following protocol delineates the efficient isolation and purification of glyoxysomes from cotyledons. It has been used, with minor modifications, to isolate peroxisomes from multiple plant tissues and species. In addition, effective means to quantify and determine the integrity of the isolated organelles are discussed.

Equipment

- Sorvall RC5C floor centrifuge or equivalent
- Sorvall HB-6 swinging bucker rotor or equivalent
- Waring blender (2 speed) and 500 ml blender cup
- UV spectrophotometer
- BCA (or other) protein assay reagents (if desired)
- Miracloth
- Small, soft paintbrush (natural hair)
- Four 15 ml Corex tubes
- Several 250ml beakers
- Funnel
- Eight 50 ml polypropylene centrifuge tubes

Plant growth

Germinate pumpkin seeds (or desired organelle source) in the dark at 22-25^{o}C; the temperature should be optimized for the particular tissue source. The seedlings are ready for harvest when they are about 5-8 cm tall. Seeds that have just begun to germinate can also be harvested, as long as the seed coat is removed prior to grinding.

- Germination and growth routinely takes 5-7 days, depending on the time of year (shorter during the summer months).
- It should be sufficient to plant 75 ml of pumpkin seeds to be able to harvest the 25-35 g of tissue needed for this protocol. This amount may

need to be adjusted for other plants, depending on seed and seedling sizes and/or desired tissue source.

- Typically, seeds are placed on about 2 cm of medium coarse vermiculite and sprinkled with a thin layer of vermiculite (just enough to cover the seeds). They are then watered liberally and the flat is covered loosely with plastic wrap to maintain high humidity for germination.
- The seedlings can be watered 3-4 days after planting to promote germination.

Equipment Preparation

Keep all equipment and solutions cold (4°C) for the duration of the procedure.

- Pre-cool centrifuge rotor and centrifuge to 4°C.
- Weigh one 250 ml beaker and place on ice.
- Pre-cool the blender cup in a 4°C refrigerator.
- Chill an additional beaker, funnel, four 15 ml Corex tubes and eight 50 ml polypropylene centrifuge tubes on ice.

Solution Preparation

Keep all solutions and materials on ice throughout the procedure.

- Grinding Buffer: Prepare 170 ml of 1X Grinding Buffer with BSA (1 mg/ml) by adding 85 ml of 2X Grinding Buffer to 85 ml distilled water. Add 170 mg BSA to the buffer; mix well.
- Resuspension Buffer: Prepare 20 ml 1X Resuspension Buffer from 2X Resuspension Buffer; 10 ml 2X Resuspension Buffer plus 10 ml distilled water.
- Percoll Gradient: Place 1.5 ml 2 M Sucrose solution in a 15 ml Corex tube. Carefully add 10 ml 28% Percoll/1X Resuspension Buffer solution, being very careful not to mix the sucrose and Percoll layers.

Protocol

1. Record the age and growth conditions of the pumpkin seedlings. Suitable plants are shown in Figure A.1.

2. Harvest the pumpkin cotyledons in dim room light. Manually separate the cotyledons from the hypocotyls. For very small seedlings, remove the seed coat and radicle as well. Place the cotyledons into the pre-weighed chilled beaker. Reweigh the beaker and record the tissue weight. Be sure to keep the tissue cold. Avoid exposure to bright lights as this will induce greening. Normal room lighting can be resumed during the first centrifugation step.

3. Put the tissue and enough 1X Grinding Buffer (with BSA) to cover the tissue (usually about 150-170 ml) in the blender cup. Homogenize the tissue, using three short bursts of approximately 3 sec each, on low speed. Do not over-grind.

4. Filter the homogenate through a piece of Miracloth (purchased from Calbiochem) that has been folded in half and used to line the inside of a funnel (placed over a beaker on ice). Collect the filtered homogenate in the beaker below the funnel. Squeeze the macerated tissue inside the Miracloth 'bag' gently to extract all the liquid. Discard the remaining tissue and used Miracloth.

5. Distribute the filtrate evenly between four 50 ml centrifuge tubes and centrifuge it in a swinging bucket rotor at 4,250 rpm (3,000xg) at 4°C for 10 minutes

6. The resulting supernatant will have a thick lipid layer floating on top. Remove this with a Kimwipe wrapped around the wide end of a 1,000 µl plastic pipette tip. Decant the supernatant into a second set of clean 50 ml centrifuge tubes.

7. Centrifuge this supernatant in a swinging bucket rotor at 8,000 rpm (10,500xg) at 4°C for 20 minutes. Carefully decant the supernatant and discard it.

8. Using a small paintbrush, gently resuspend each pellet in 250 µL 1X Resuspension Buffer. Pool the resulting suspension in one tube and swirl gently to mix. Carefully load the pooled suspension onto the top of the prepared Percoll gradient.

9. Centrifuge the supernatant in a swinging bucket rotor at 10,500 rpm (18,000xg) at 4°C for 30 minutes without the brake. Using the brake on this step will disturb the gradient and greatly diminish the final glyoxysome yield.

10. Glyoxysomes will be in a visible yellowish band at the Percoll/sucrose interface as shown in figure A.2. Carefully remove the upper layers of lipid and broken organelles in the gradient with a Pasteur pipette. Finally, collect and transfer the glyoxysomes with a clean pipette to a 15 ml Corex tube.

NOTE: This step is the most critical - taking too much Percoll or sucrose cushion will reduce the purity of the glyoxysomes while removing too little will decrease the overall yield.

11. Dilute the glyoxysomes 3 to 5 fold with 1X Resuspension Buffer, usually about 8 ml.

12. Pellet the glyoxysomes by centrifugation in a swinging bucket rotor at 6500rpm (7,000xg) at 4^{o}C for 14-20 minutes (with the brake). A shorter (14 min.) spin will result in a soft organelle pellet, making it harder to remove all of the supernatant. A longer spin (20 min) will yield a tighter pellet.

13. Carefully remove the supernatant and discard. Gently resuspend the pellet of purified glyoxysomes in 100 µl 1X Resuspension Buffer.

14. To approximate the yield, measure the absorbance of a 1/500 dilution (with 1X Resuspension Buffer) at A_{280} and A_{235}. Use these values in the equation below

Approx. Concentration: $[(A_{235}-A_{280})/2.51] \times 500$ = mg protein/ml

Approx. Yield:(mg protein/ml) x (final resuspension volume, ml) = mg total protein

These numbers are only approximate, but they are quick and easy to get and are consistent between organelle preparations. We use this calculation to standardize the amount of glyoxysomes used in each experiment. If more accurate protein concentrations are needed, one can do a biochemical protein assay, such as Pierce's BCA assay or any other protein assay of choice. An electron micrograph of purified glyoxysomes is shown in Figure A.3.

Determining integrity of the organelles

There are many enzymatic assays that can be used to verify the presence of intact glyoxysomes including catalase [23,24] and isocitrate lyase [24] assays. Mitochondrial contamination can be assessed by performing fumarase assays [24,25]**.** Organelle latency can be determined by performing the enzyme assays in the presence and absence of 0.5% Triton X-100 to disrupt the membrane. Though substantially enriched for glyoxysomes, the final organelle pellet usually contains some mitochondrial contamination.

Critical Parameters and Troubleshooting

There are several critical points for consideration during the purification procedure.

- Care must be taken to ensure that plants are grown in the dark, are about 5-8 cm tall, and that exposure to light during harvesting is minimized to get a good yield of glyoxysomes. This is because when seedlings begin greening and producing the first true leaves, some glyoxysomes transition into leaf peroxisomes while others are probably degraded (there are fewer peroxisomes found in leaves than glyoxysomes present in cotyledons).
- The tissue must remain cold throughout the protocol to help reduce endogenous protease activities that can cause the degradation of glyoxysomes and glyoxysomal peripheral membrane proteins.
- The tissue should not be over-ground during the homogenization step. Instead subject the tissue to just enough homogenization needed to break up the majority of the tissue. When done correctly there should be no large chunks of intact tissue evident after homogenization, though smaller pieces of ground tissue should be present.

Anticipated Results

A preparation of 35 g of pumpkin cotyledons should yield 100 µl of glyoxysomes with an approximate protein concentration of 50-75 mg/ml. The yield largely depends on the successful removal of the glyoxysome layer from the Percoll gradient.

Time Considerations

An efficient glyoxysome preparation should be completed within 2-2.5 hours. Purified glyoxysomes can be stored on ice, but will lose structural and metabolic integrity within hours. Intact glyoxysomes do not survive freezing, though many glyoxysomal enzymes will continue to have measurable activity.

Reagents and Solutions

All solutions should be filtered and stored at 4°C.

2X Grinding Buffer (1 Liter)

	Weight	Conc (2X)	Final Conc (1X)
Tetrasodium Pyrophosphate (PPi)	17.844 g	40 mM	20 mM
EDTA	0.744 g	2 mM	1 mM
D-Mannitol	109.32 g	0.6 M	0.3 M

Add distilled water to near volume. Adjust the pH to 7.5 using glacial acetic acid. Take to final volume of 1 L with distilled water. Filters sterilize (45µm) the solution and store it at 4°C. 1X Grinding Buffer with added BSA (1 mg/ml final concentration) needs to be prepared before each glyoxysome preparation.

2X Resuspension Buffer (1 Liter)

	Weight	Conc (2X)	Final Conc (1X)
Hepes	4.776 g	20 mM	10 mM
D-Mannitol	109.32 g	0.6 M	0.3 M

Add distilled water to near volume. Adjust pH to 7.2 with KOH and take to final volume with distilled water. Filter sterilize (45 µm) the solution and store it at 4°C.

28% Percoll/1X Resuspension Buffer (for the gradient)

		Volume
Percoll		28 ml
2X Resuspension Buffer		50 ml
distilled water		22 ml
	total	100 ml

Store at 4°C.

2M Sucrose (125ml) cushion for gradient

	Weight	Concentration
Sucrose	85.575 g	2 M

This solution needs to be filtered (45 µM) which can be tricky due to the viscosity of the liquid. It also should be stored at 4°C.

Acknowledgements

This appendix was published as an invited chapter in Current Protocols in Cell Biology [26].

Figure A.1: Five-day-old dark-grown pumpkin seedlings
Anatomical terms included in the text are indicated on the diagram as follows: 1, seed coat; 2, cotyledons; 3, hypocotyls; 4, radicle.

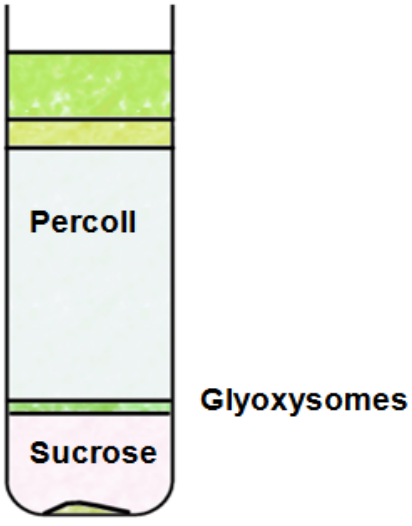

Figure A.2: The final gradient. Glyoxysomes are present as a discrete band at the percoll and sucrose interface. Care should be taken to minimize the volume of sucrose removed from the gradient.

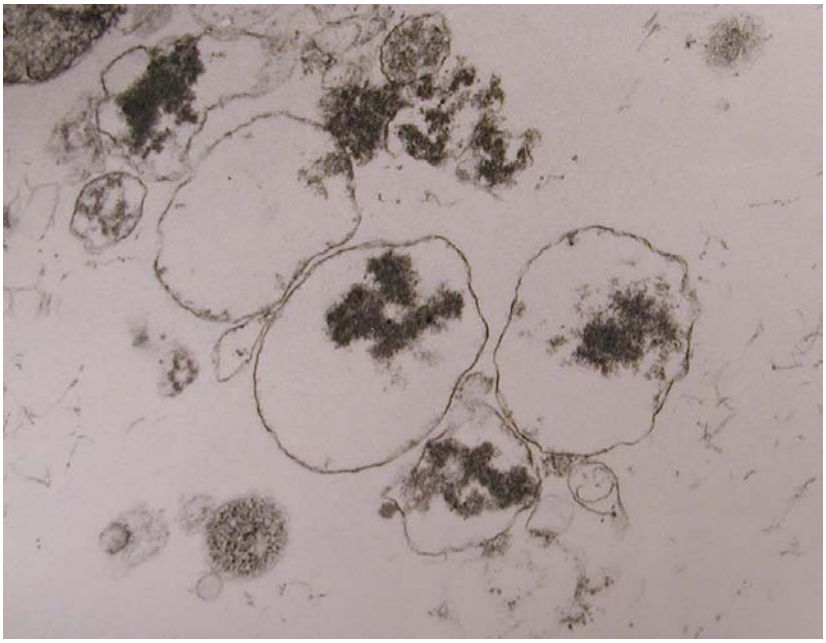

Figure A.3: Electron micrograph of purified pumpkin glyoxysomes.

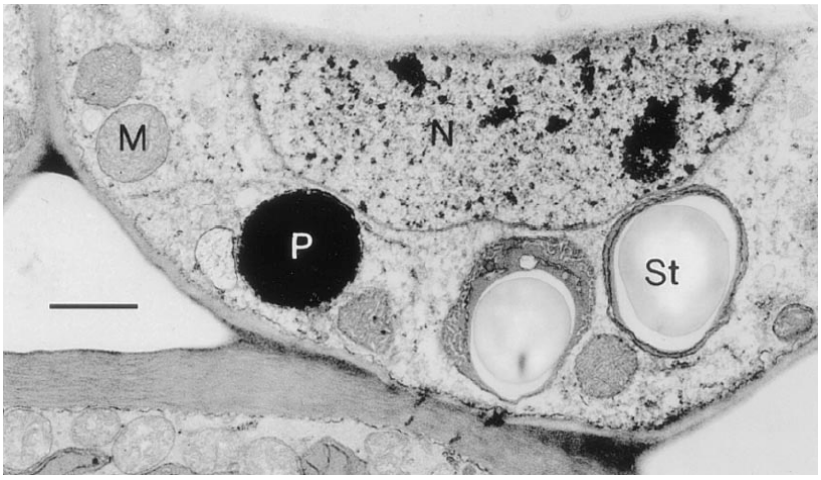

Figure A.4: Electron micrograph showing the cytochemical localization of uricase in a peroxisome in mature cowpea nodules (from Fig. 3 in Webb MA and Newcomb EH. 1987. Planta 172:162–175; reprinted with permission as Figure 1 in Johnson TL and Olsen LJ. 2001. Plant Physiol. 127:731–739). The intense staining of the peroxisome in the uninfected cell is the result of treatment with 3,3'-diaminobenzidine plus urate. X13,000; bar = 1 µm. M, Mitochondrion; N, nucleus; P, peroxisome; St, starch-containing plastid.

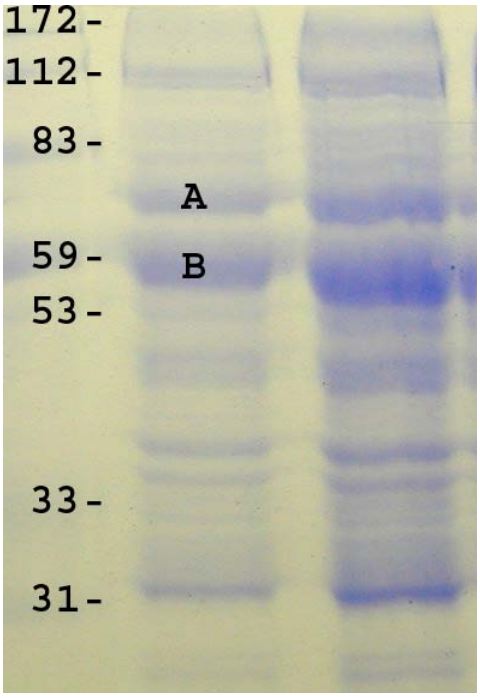

Figure A.5: Coomassie-stained gel of proteins from purified glyoxysomes. Proteins from freeze-thawed, lysed glyoxysomes were separated by 10% SDS-PAGE; left lane, 25 µg; right lane 50 µg. The identity of the major glyoxysomal protein bands indicated in the figure are A, isocitrate lyase (64kDa) and B, catalase (55 kDa).

Literature Cited

1. Tolbert, N., 1971, Microbodies, peroxisomes and glyoxysomes. Annu Rev Plant Physiol.
2. Heinze, M., R. Reichelt, S. Kleff, and K. Eising, 2000, High rsolution scanning electron microscopy of protein inclusions (Cores) purified from peroxisomes of sunflower (*Helianthus annuus L.*) cotyledons. Crys Res Tech. **35**: 877-886.
3. Beevers, H., ed. 2002, Early research on peroxisomes in plants. in plant peroxisomes. Biochemistry, cell biology and biotechnological applications, ed. A. Baker and I. Graham, Kluwer Academic Publishers.
4. Olsen, L.J. and J.J. Harada, 1995, Peroxisomes and their assembly in higher-plants. Ann Rev Plant Physiol. **46**: 123-146.
5. Olsen, L., 1998, The surprising complexity of peroxisome biogenesis. Plant Mol Biol. **38**: 163-189.
6. Brickner, D., J. Harada, and L. Olsen, 1997, Protein transport into higher plant peroxisomes. In vitro import assay provides evidence for receptor involvement. Plant Physiol. **113**: 1213-1221.
7. Purdue, P. and P. Lazarow, 2001, Peroxisome biogenesis. Ann Rev Cell Dev Biol. **17**: 701-752.
8. Brown, L. and A. Baker, 2003, Peroxisome biogenesis and the role of protein import. J Cell Mol Med. **7**: 388-400.
9. Johnson, T.L. and L.J. Olsen, 2003, Import of the peroxisomal targeting signal type 2 protein 3-ketoacyl-coenzyme A thiolase into glyoxysomes. Plant Physiol. **133**: 1991-1999.
10. Subramani, S., 1996, Protein translocation into peroxisomes. J Biol Chem. **271**: 32483-32486.
11. Behari, R. and A. Baker, 1993, The carboxyl terminus of isocitrate lyase is not essential for import into glyoxysomes in an in vitro system. J Biol Chem. **268**: 7315-7322.
12. Brickner, D. and L. Olsen, 1998, Nucleotide triphosphates are required for the transport of glycolate oxidase into peroxisomes. Plant Physiol. **116**: 309-317.
13. Crookes, W. and L. Olsen, 1998, The effects of chaperones and the influence of protein assembly on peroxisomal protein import. J Biol Chem. **273**: 17236-17242.
14. Mori, H. and M. Nishimura, 1989, Glyoxysomal malate synthase is specifically degraded in microbodies during greening of pumpkin cotyledons. FEBS letters. **244**: 163-166.
15. Goyer, A., T.L. Johnson, L.J. Olsen, E. Collakova, Y. Shachar-Hill, D. Rhodes, and A.D. Hanson, 2004, Characterization and metabolic function of a peroxisomal sarcosine and pipecolate oxidase from Arabidopsis. J Biol Chem. **279**: 16947-16953.

16. Liepman, A.H. and L.J. Olsen, 2001, Peroxisomal alanine: glyoxylate aminotransferase (AGT1) is a photorespiratory enzyme with multiple substrates in *Arabidopsis thaliana*. Plant J. **25**: 487-498.
17. Liepman, A.H. and L.J. Olsen, 2003, Alanine aminotransferase homologs catalyze the glutamate : glyoxylate aminotransferase reaction in peroxisomes of Arabidopsis. Plant Physiol. **131**: 215-227.
18. Zolman, B.K. and B. Bartel, 2004, An Arabidopsis indole-3-butyric acid-response mutant defective in PEROXIN6, an apparent ATPase implicated in peroxisomal function. Proc Natl Acad Sci U S A. **101**: 1786-1791.
19. Zolman, B.K., M. Monroe-Augustus, B. Thompson, J.W. Hawes, K.A. Krukenberg, S.P.T. Matsuda, and B. Bartel, 2001, chy1, an Arabidopsis mutant with impaired beta-oxidation, is defective in a peroxisomal beta-hydroxyisobutyryl-CoA hydrolase. J Biol Chem. **276**: 31037-31046.
20. Zolman, B.K., A. Yoder, and B. Bartel, 2000, Genetic analysis of indole-3-butyric acid responses in *Arabidopsis thaliana* reveals four mutant classes. Genetics. **156**: 1323-1337.
21. Sanders, P.M., P.Y. Lee, C. Biesgen, J.D. Boone, T.P. Beals, E.W. Weiler, and R.B. Goldberg, 2000, The Arabidopsis DELAYED DEHISCENCE1 gene encodes an enzyme in the jasmonic acid synthesis pathway. Plant Cell. **12**: 1041-1061.
22. Stintzi, A. and J. Browse, 2000, The Arabidopsis male-sterile mutant, opr3, lacks the 12-oxophytodienoic acid reductase required for jasmonate synthesis. Proc Natl Acad Sci U S A. **97**: 10625-10630.
23. Aebi, H., 1984, Catalase in vitro. Methods Enzymol. **105**: 121-126.
24. Cooper, T.G. and H. Beevers, 1969, Mitochondria and glyoxysomes from castor bean endosperm - enzyme constituents and catalytic capacity. J Biol Chem. **244**: 3507-3512.
25. Hatch, M.D., 1978, Simple spectrophotometric assay for fumarate hydratase in crude tissue extracts. Anal Biochem. **85**: 271-275.
26. Harrison-Lowe, N.J. and L.J. Olsen, 2005, Isolation of glyoxysomes from pumpkin cotyledons. Curr Protoc Cell Biol: 3.19.11-3.19.18.